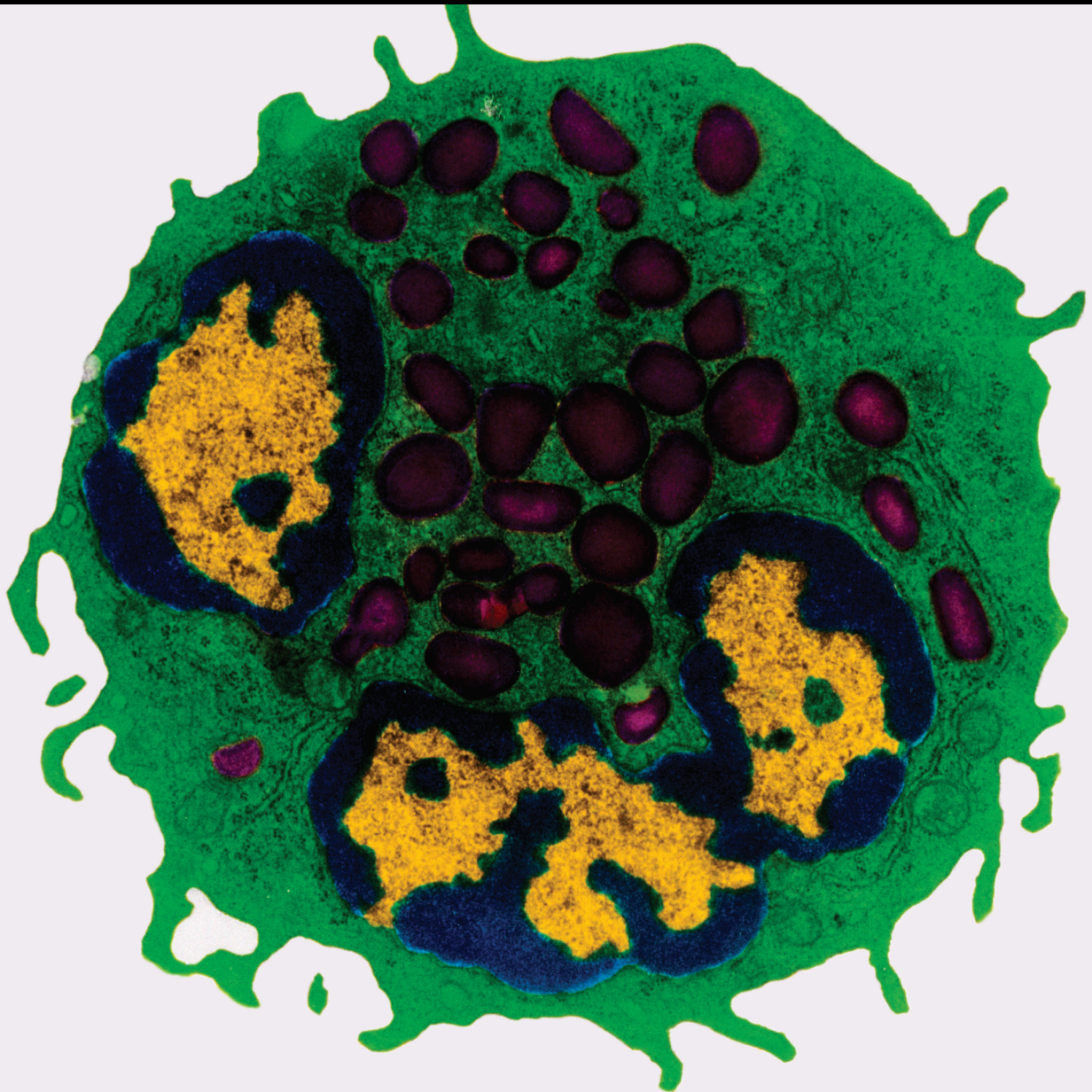


Mediators of Inflammation in Bone Physiology and Diseases

Lead Guest Editor: Drenka Trivanović

Guest Editors: Michaela Tencerova, Marietta Herrmann, Alanna Green, and Petar Milovanovic





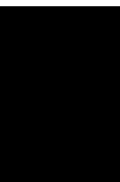
Mediators of Inflammation in Bone Physiology and Diseases

Mediators of Inflammation

**Mediators of Inflammation in Bone
Physiology and Diseases**

Lead Guest Editor: Drenka Trivanović

Guest Editors: Michaela Tencerova, Marietta
Herrmann, Alanna Green, and Petar Milovanovic



Copyright © 2022 Hindawi Limited. All rights reserved.

This is a special issue published in “Mediators of Inflammation.” All articles are open access articles distributed under the Creative Commons Attribution License, which permits unrestricted use, distribution, and reproduction in any medium, provided the original work is properly cited.

Chief Editor

Anshu Agrawal, USA

Editorial Board

Amedeo Amedei, Italy
Oleh Andrukhov, Austria
Emiliano Antiga, Italy
Zsolt J. Balogh, Australia
Adone Baroni, Italy
Jagadeesh Bayry, France
Tomasz Brzozowski, Poland
Elisabetta Buommino, Italy
Daniela Caccamo, Italy
Luca Cantarini, Italy
Raffaele Capasso, Italy
Calogero Caruso, Italy
Maria Rosaria Catania, Italy
Carlo Cervellati, Italy
Cristina Contreras, Spain
Robson Coutinho-Silva, Brazil
Jose Crispin, Mexico
Fulvio D'Acquisto, United Kingdom
Eduardo Dalmarco, Brazil
Carlos Dieguez, Spain
Agnieszka Dobrzyn, Poland
Elena Dozio, Italy
Emmanuel Economou, Greece
Ulrich Eisel, The Netherlands
Mirvat El-Sibai, Lebanon
Giacomo Emmi, Italy
Claudia Fabiani, Italy
Fabiola B Filippin Monteiro, Brazil
Antonella Fioravanti, Italy
Jan Fric, Czech Republic
Tânia Silvia Fröde, Brazil
Julio Galvez, Spain
Mirella Giovarelli, Italy
Denis Girard, Canada
Ronald Gladue, USA
Markus H. Gräler, Germany
Oreste Gualillo, Spain
Qingdong Guan, Canada
Elaine Hatanaka, Brazil
Tommaso Iannitti, United Kingdom
Byeong-Churl Jang, Republic of Korea
Yasumasa Kato, Japan
Yona Keisari, Israel
Alex Kleinjan, The Netherlands






Elzbieta Kolaczowska, Poland
Vladimir A. Kostyuk, Belarus
Dmitri V. Krysko, Belgium
Esra Küpeli Akkol, Turkey
Martha Lappas, Australia
Francesca Lembo, Italy
Eduardo López-Collazo, Spain
Andreas Ludwig, Germany
Ariadne Malamitsi-Puchner, Greece
Joilson O. Martins, Brazil
Donna-Marie McCafferty, Canada
Barbro N. Melgert, The Netherlands
Paola Migliorini, Italy
Vinod K. Mishra, USA
Eeva Moilanen, Finland
Alexandre Morrot, Brazil
Nadra Nilsen, Norway
Daniela Novick, Israel
Marja Ojaniemi, Finland
Sandra Helena Penha Oliveira, Brazil
Carla Pagliari, Brazil
Martin Pelletier, Canada
Vera L. Petricevich, Mexico
Sonja Pezelj-Ribarić, Croatia
Rituraj Purohit, India
Michal A. Rahat, Israel
Zoltan Rakonczay Jr., Hungary
Marcella Reale, Italy
Emanuela Roscetto, Italy
Carlos Rossa, Brazil
Settimio Rossi, Italy
Bernard Ryffel, France
Domenico Sergi, Italy
Elena Silvestri, Italy
Carla Sipert, Brazil
Helen C. Steel, South Africa
Saravanan Subramanian, USA
Veendamali S. Subramanian, USA
Jacek Cezary Szepietowski, Poland
Taina Tervahartiala, Finland
Alessandro Trentini, Italy
Kathy Triantafilou, United Kingdom
Fumio Tsuji, Japan
Maria Letizia Urban, Italy



Giuseppe Valacchi, Italy
Luc Vallières, Canada
Kerstin Wolk, Germany
Suowen Xu, USA
Guangtao Xu, China
Soh Yamazaki, Japan
Young-Su Yi, Republic of Korea
Shin-ichi Yokota, Japan
Teresa Zelante, Singapore
Francesca Zimetti, Italy




Contents

Mediators of Inflammation in Bone Physiology and Diseases

Drenka Trivanović , Michaela Tencerova , Marietta Herrmann , Alanna C. Green , and Petar Milovanović 

Editorial (2 pages), Article ID 9767408, Volume 2022 (2022)

Investigation of Cytotoxicity, Oxidative Stress, and Inflammatory Responses of Tantalum Nanoparticles in THP-1-Derived Macrophages

Li Zhang , El-Mustapha Haddouti, Hannes Beckert, Ralf Biehl, Shyam Pariyar, Julian M. R uwald, Xian Li, Max Jaenisch, Christof Burger, Dieter C. Wirtz, Koroush Kabir , and Frank A. Schildberg 






Research Article (14 pages), Article ID 3824593, Volume 2020 (2020)

Tetrandrine Inhibits Titanium Particle-Induced Inflammatory Osteolysis through the Nuclear Factor- κ B Pathway

Zige Liu , Yan Li , Fengying Guo , Chen Zhang , Guorui Song , Jiahao Yang , and Desheng Chen 


Research Article (16 pages), Article ID 1926947, Volume 2020 (2020)

Negligible Effect of Estrogen Deficiency on Development of Skeletal Changes Induced by Type 1 Diabetes in Experimental Rat Models

Aleksandra Janas , Ewa Kruczek, Piotr Londzin , Sławomir Borymski , Zenon P. Czuba , and Joanna Folwarczna 


Research Article (21 pages), Article ID 2793804, Volume 2020 (2020)

Hypertryptasemia and Mast Cell-Related Disorders in Severe Osteoporotic Patients

Giulia Carosi, Gregorio Guabello, Matteo Longhi, Federica Grifoni, Elena Passeri, and Sabrina Corbetta 

Research Article (8 pages), Article ID 5785378, Volume 2020 (2020)

CD4+ T Cell Profile and Activation Response in Sickle Cell Disease Patients with Osteonecrosis

Paula B. Daltro , Tiago O. Ribeiro, Gildásio C. Daltro , Roberto J. Meyer , and Vitor Fortuna 

Research Article (12 pages), Article ID 1747894, Volume 2020 (2020)

Editorial

Mediators of Inflammation in Bone Physiology and Diseases

Drenka Trivanović ¹, **Michaela Tencerova** ², **Marietta Herrmann** ¹, **Alanna C. Green** ³,
and Petar Milovanović ⁴

¹*IZKF Group Tissue Regeneration in Musculoskeletal Diseases, University Hospital Wuerzburg & Bernhard-Heine-Center for Locomotion Research, University of Wuerzburg, Wuerzburg, Germany*

²*Institute of Physiology of the Czech Academy of Sciences, Prague, Czech Republic*

³*Department of Oncology & Metabolism, University of Sheffield, Sheffield, UK*

⁴*Institute of Anatomy, Faculty of Medicine, University of Belgrade, Belgrade, Serbia*

Correspondence should be addressed to Drenka Trivanović; d-trivanovic.klh@uni-wuerzburg.de

Received 19 March 2022; Accepted 19 March 2022; Published 13 April 2022

Copyright © 2022 Drenka Trivanović et al. This is an open access article distributed under the Creative Commons Attribution License, which permits unrestricted use, distribution, and reproduction in any medium, provided the original work is properly cited.

Complex crosstalk between immune cells and cells involved in skeletal renewal is essential for bone health. Bone tissue formation and resorption are governed by the inflammation initiated by endogenous or exogenous stimuli, as well as local and systemic metabolism and the aging process. This special issue is focused on the topic of inflammation in bone physiology contributing to the novel findings in the osteoimmunology field. It brings several research articles in which the immune background of bone tissue disorders, as well as the behavior of orthopedic implants important for the locomotor system, was investigated.

Osteoporosis is the most prevalent metabolic skeletal disease and public health problem, characterized by decreased bone mass and increased risk of fractures. Basically, osteoporosis reflects a state of imbalance between structural and biological demands for calcium and phosphate during inflammatory state. The aging-associated chronic low-grade inflammatory state affects osteoporotic bone development. A temporal framework between inflammation and osteoporosis appears to be important in aging, menopause, pregnancy, transplantation, and steroid applications. Importantly, the concordance of osteoporosis and inflammation is regulated by inflammatory mediators [1]. In this special issue, one of the aims was to reveal the prevalence of rare hematologic disease, systemic mastocytosis in patients with unexplained osteoporosis to identify whether mastocytosis is a plausible cause of secondary osteoporosis.

Unlike primary osteoporosis, associated with aging, secondary osteoporosis is usually related to other diseases and drugs. Systemic mastocytosis was characterized by a clonal proliferation of neoplastic mast cells which can occur in the bone marrow. It is suggested that hypertryptasemia (high serum levels of mastocyte cell-specific serine protease tryptase) can be a useful marker of mastocyte-cell related diseases, such as bone fragility and secondary osteoporosis.

In the manuscript published in this special issue, a rat model was utilized to reveal the significance of the interaction of estrogen deficiency and hyperglycemia in the skeletal system. In this work, bilateral ovariectomy was applied to induce estrogen deficiency, while diabetes mellitus was established by single streptozotocin administration. Interestingly, measurement of several cytokines in the circulation revealed only one bioactive molecule, the chemokine regulated upon activation, normal T cell expressed and presumably secreted (RANTES), which is found to be significantly affected by both ovariectomy and diabetes mellitus in rats. Serum levels of chemokine RANTES, secreted by osteoblasts and osteoclasts in bone, were increased mainly in the ovariectomized diabetic rats. Results of this study suggest that the effects on bone microarchitecture and inflammation induced by hyperglycemia in rats were only slightly moderated by estrogen deficiency [2].

Osteonecrosis occurs when reduced blood flow to bone causes death of bone and marrow cells. Glucocorticoid and

alcohol usage may result in osteonecrosis which can affect almost any bone of the body, where the hips, knees, and shoulders are the most common affected sites. Vascular occlusions, low-grade chronic inflammation, poor oxygen, and nutrient supply to the affected bone region are considered as major etiological indicators. Osteonecrosis-related chronic inflammation, including accumulation of activated neutrophils, macrophages, and T cells, is followed by the increased production of inflammatory mediators. Macrophages and neutrophils produce reactive oxygen and nitrogen species with proinflammatory activities. Another work published in this special issue explored the association of T cell populations (and their phenotype) in the pathophysiology of osteonecrosis that affects patients with sickle cell disease. Sickle cell disease is caused by a point mutation in the β -globin gene, resulting in the production of abnormal hemoglobin, deformed erythrocytes, and finally, inflammation-associated hemolysis and vascular occlusions. Since osteonecrosis is clinical complication of sickle cell disease, in this study, T cells were analyzed in human peripheral blood and bone marrow aspirates of healthy and sickle cell disease patients. This study reported the increased proportion of proinflammatory cytokine-producing CD4⁺ T cells in the bone marrow of sickle disease patients. From collected observations, it is suggested that these T cell populations may contribute to chronic inflammation and the pathophysiology of osteonecrosis in sickle cell disease [3].

Artificial joint replacement is the current clinical gold standard treatment for destructive joint diseases. Previous *in vitro* and *in vivo* experiments, as well as clinical studies reported that byproducts from joint replacements can induce chronic low-grade inflammation resulting in periprosthetic osteolysis, aseptic loosening, and prosthesis failure. Inflammatory insults in peri-implant areas, caused by the wear particles, provoke osteoclast activation at the bone-implant interface and initiate bone resorption. In awareness of the need of improved approaches for the treatment of aseptic loosening, the effect of tetrandrine on inflammatory osteolysis in a titanium particle-induced inflammatory osteolysis mouse model was investigated as well. It is found that tetrandrine inhibits the expression of proinflammatory cytokines, TNF- α , IL-1 β , and IL-6, as well as receptor activator for nuclear factor- κ B ligand- (RANKL-) induced osteoclast formation and bone resorption [4]. Observed data suggest tetrandrine as reasonable treatment option for osteolytic peri-implant regions. Another study explored *in vitro* effects of tantalum and titanium dioxide nanoparticles on a macrophage cell line model. Although the therapeutic potential of tantalum-based implants for total joint replacement is well described, the effects of wear particles of tantalum implants on peri-implant cells and their potential contribution to aseptic implant loosening are not revealed. This is of particular importance since macrophage polarization initiated inflammatory signaling and osteoclastogenesis represents the main control point for cell death in peri-implant regions. This study reported a reduced potential of tantalum nanoparticles to induce TNF α and IL-1 β as well as reactive oxygen species by macrophages when compared to titanium dioxide particles, suggesting that

tantalum-based implants might be a more rational therapy option with lower risk to provoke aseptic loosening, as previously described [5].

We hope that this special issue provides new interesting insights on the complex immune background of bone diseases, as well as their significance in designing optimal biomaterials for orthopedic implants. In addition, we believe that this issue opens new questions which will be resolved in future fundamental and clinical studies.

Conflicts of Interest

The editors declare that there is no conflict of interest regarding the publication of this special issue.

Acknowledgments

We appreciate all authors who submitted their research articles and all reviewers for their great contributions to this special issue.




Drenka Trivanović
 Michaela Tencerova
 Marietta Herrmann
 Alanna C. Green
 Petar Milovanović

References

- [1] M. N. Weitzmann, "Bone and the immune system," *Toxicologic Pathology*, vol. 45, no. 7, pp. 911–924, 2017.
- [2] R. Zhou, Q. Guo, Y. Xiao et al., "Endocrine role of bone in the regulation of energy metabolism," *Bone Research*, vol. 9, no. 1, p. 25, 2021.
- [3] S. B. Goodman and M. Maruyama, "Inflammation, bone healing and osteonecrosis: from bedside to bench," *Journal of Inflammation Research*, vol. 13, pp. 913–923, 2020.
- [4] N. S. Adapala, G. Swarnkar, M. Arra et al., "Inflammatory osteolysis is regulated by site-specific ISGylation of the scaffold protein NEMO," *eLife*, vol. 9, article e56095, 2020.
- [5] S. B. Goodman and J. Gallo, "Periprosthetic osteolysis: mechanisms, prevention and treatment," *Journal of Clinical Medicine*, vol. 8, no. 12, p. 2091, 2019.

Research Article

Investigation of Cytotoxicity, Oxidative Stress, and Inflammatory Responses of Tantalum Nanoparticles in THP-1-Derived Macrophages

Li Zhang ¹, El-Mustapha Haddouti,¹ Hannes Beckert,² Ralf Biehl,³ Shyam Pariyar,⁴ Julian M. Rüwald,¹ Xian Li,⁵ Max Jaenisch,¹ Christof Burger,¹ Dieter C. Wirtz,¹ Koroush Kabir ¹ and Frank A. Schildberg ¹

¹Clinic for Orthopedics and Trauma Surgery, University Hospital Bonn, 53127 Bonn, Germany

²Microscopy Core Facility, Medical Faculty, Bonn Technology Campus Life Sciences, University of Bonn, 53127 Bonn, Germany

³Jülich Centre for Neutron Science (JCNS-1) & Institute of Biological Information Processing (IBI-8), Forschungszentrum Jülich, 52425 Jülich, Germany

⁴Department of Horticultural Sciences, University of Bonn, 53121 Bonn, Germany

⁵Department of Orthopedic and Trauma Surgery, Xiyuan Hospital, China Academy of Chinese Medical Science, 100091 Beijing, China

Correspondence should be addressed to Koroush Kabir; koroush.kabir@ukbonn.de and Frank A. Schildberg; frank.schildberg@ukbonn.de

Received 31 July 2020; Revised 29 October 2020; Accepted 2 November 2020; Published 3 December 2020

Academic Editor: Marietta Herrmann

Copyright © 2020 Li Zhang et al. This is an open access article distributed under the Creative Commons Attribution License, which permits unrestricted use, distribution, and reproduction in any medium, provided the original work is properly cited.

Tantalum (Ta) is gaining attention as a biomaterial in bone tissue engineering. Although the clinical advantage of Ta-based implants for primary and revision total joint replacement (TJA) has been well documented, few studies investigated the effect of wear products of Ta implants on peri-implant cells, and their potential contribution to aseptic implant loosening. This study is aimed at examining the cytotoxicity, oxidative stress, and proinflammatory potential of Ta and TiO₂ nanoparticles (NPs) on macrophages *in vitro*. NPs were characterized using scanning electron microscopy, dynamic light scattering, and energy-dispersive X-ray. To test the NP-mediated cellular response in macrophages, THP-1-derived macrophages were challenged with both NPs, and cytotoxicity was analyzed using CCK-8 and LDH assays. Flow cytometry was used to investigate particle uptake and their internalization routes. NP-mediated oxidative stress was investigated by measuring the production of reactive oxygen species, and their proinflammatory potential was determined by quantifying the production of TNF α and IL-1 β in cell culture supernatants using ELISA. We found that both Ta and TiO₂ NPs were taken up through actin-dependent phagocytosis, although TiO₂ NPs did also show some involvement of macropinocytosis and clathrin-mediated endocytosis. Ta NPs caused no apparent toxicity, while TiO₂ NPs demonstrated significant cytotoxicity at a concentration of over 100 μ g/mL at 24 h. Ta NPs induced negligible ROS generation and proinflammatory cytokines (TNF α , IL-1 β) in macrophages. In contrast, TiO₂ NPs markedly induced these effects in a dose-dependent manner. Our findings indicate that Ta NPs are inert, nontoxic, and noninflammatory. Therefore, Ta could be considered an excellent biomaterial in primary and revision joint arthroplasty implants.

1. Introduction

Aseptic loosening is the leading cause of revision surgery and plays a predominant role in limiting the longevity of current total joint arthroplasty (TJA). Wear particles have been recognized as one of the major factors responsible for aseptic

implant loosening [1]. After implantation, orthopedic prosthesis becomes an internal source of wear particles [2–5]. Upon corrosion and abrasion, nondegradable biomaterial wear particles are inevitably released in adjacent peri-implant tissues or systemically disseminated, inducing local and systemic reactions [6–8]. They represent a long-term

hazard that interacts with peri-implant cell lineages such as macrophages, fibroblasts, osteoblasts, osteoclasts, and mesenchymal stem cells (MSCs). This process may disrupt local cellular functions; create chronic inflammation, which favors periprosthetic osteolysis; and eventually leads to aseptic implant loosening with subsequent revision surgery. Clinically, as the only established treatment for periprosthetic aseptic loosening, revision TJA is technically demanding and associated with high complication rates, high morbidity, and poor clinical and functional outcomes. Moreover, because of the complexity of the procedure, compromised soft tissue, and bone defects, revision TJA has a greater failure rate than primary TJA [9]. Therefore, choosing the appropriate implant biomaterial is critical for the long-term survival of both primary and revision TJAs.

Tantalum (Ta) is described as an “extremely bioinert” material and has been widely applied as artificial joints, endovascular stents, and coating [10–12]. As biomaterial for implant components in primary and revision TJA, Ta can be formed with a highly porous structure that could mimic the structure of cancellous bone. Similar to titanium (Ti), Ta provides outstanding biocompatibility and corrosion resistance [13, 14]. Moreover, porous Ta components offer lower elastic modulus and higher surface frictional characteristics than conventional Ti implants, thus reducing shielding and improving early stability. These properties make Ta an ideal choice in TJA revision surgery [15, 16]. Recent studies on failed Ta implant revision hip arthroplasty described nanoscale Ta fragments (diameters ranging from 9.6 to 243.5 nm) released from the implant surface [17, 18]. Because of this phagocytosable size range and spatial proximity, Ta nanoparticles (NPs) could be internalized by peri-implant cells, e.g., macrophages, fibroblasts, and MSCs, and provoke hazardous cellular responses. However, the difficulties in purifying and characterizing NPs until today result in an underestimation of the adverse impact of Ta NPs. Therefore, particular attention must be paid to nanoscale Ta wear particles’ potentially hazardous effect on peri-implant cells and their potential contribution to repeated prosthetic loosening and subsequent rerevision [19]. However, to date, this topic remains largely unknown.

Macrophages are the critical cells associated with wear particle-induced aseptic loosening. As sentinels of the innate immune system, macrophages are the first immune cells involved in aseptic loosening by recognizing, internalizing, and getting activated upon wear particle exposure [20, 21]. Once activated, macrophages exert an increased proinflammatory phenotype and initiate a chronic inflammatory response characterized by the release of proinflammatory mediators, such as TNF α , IL-1 β , monocyte chemoattractant protein-1 (MCP-1), and IL-8 [21, 22]. These reactions create an inflammatory microenvironment that facilitates elevated osteoclastic bone destruction, suppressed bone formation, and ultimately lead to aseptic implant loosening. Therefore, an attempt to elucidate macrophages’ response to biomaterial wear debris is critical to understanding the pathology of implant loosening.

The biological response of peri-implant cells to implants is critical for early and late implant success. Recently, emerg-

ing *in vitro* and *in vivo* studies on osteoblasts and MSCs have demonstrated the Ta-based implants’ advantages over commonly used Ti-based implants [23–25]. However, limited research investigated the interaction between Ta implants and other peri-implant cells, such as macrophages. In particular, the biological response of macrophages to Ta implants’ wear products, such as nanoscale Ta particles and ions, has never been elucidated. Therefore, this study is aimed at analyzing the effects of Ta NPs on macrophage biology using the THP-1 cell line, an *in vitro* cell model that is well known, reproducible, and readily available to different labs. To this end, we investigated Ta NPs’ uptake routes, cytotoxicity, oxidative stress, and proinflammatory potential on THP-1-derived macrophages *in vitro*.

2. Materials and Methods

2.1. Cell Culture and Differentiation. THP-1 cells (American Type Culture Collection, Manassas, VA, USA), a human monocytic leukemia-derived cell line, were cultured in RPMI 1640 medium supplemented with 10% fetal bovine serum and 1% penicillin/streptomycin at 37°C in a humidified atmosphere with 5% CO₂. For macrophage differentiation, the THP-1 cells were stimulated with 50ng/mL phorbol 12-myristate 13-acetate (PMA) (Sigma-Aldrich, Taufkirchen, Germany) overnight.

2.2. Particle Preparation. Ta (NM-0036-HP) and TiO₂ (NO-0046-HP) nanosized particles were obtained from IoLiTec (Heilbronn, Germany), weighed into autoclaved tubes, and then sterilized by radiation. Stock dispersions (50 mg/mL) were prepared in phosphate-buffered saline (PBS) solution, followed by 20min of continuous sonication using the Emmi-12HC (EMAG AG, Germany) bath sonicator operating at 45kHz at 30°C. Then, the stock solution was stored at 4°C in the dark. Final dispersions were prepared from a serial dilution of the stock in full cell culture medium followed by another 20min sonication at 30°C and vigorous vortexing for 5s immediately before adding them to the cells.

2.3. Characterization of Particles. The physicochemical properties of particles were analyzed with scanning electron microscopy (SEM) and dynamic light scattering (DLS). The particle morphology and size distribution were determined with SEM. Samples dispersed in ddH₂O were vortexed before applying 2 μ L of the mixture onto a silicon wafer. After drying the sample, the wafer was sputtered with an ~2nm platinum layer in a Leica ACE600 sputter coater in an argon atmosphere to prepare it for high-resolution field-emission scanning electron microscopy (FESEM) (Crossbeam 550, Zeiss). A Schottky emitter-based field emission Gemini II electron column (Zeiss) was used with 0.8kV acceleration voltages and currents between 150pA and 250pA for imaging. The samples were imaged with the InLens SE (secondary electrons) detector (Zeiss) for topographic imaging (working distance < 3 mm). ImageJ (NIH) software was used to determine the size distribution of NPs by randomly selecting 100 particles from the SEM images. The size distribution of NPs was fitted using a Gaussian

distribution in GraphPad Prism 7 software (GraphPad, La Jolla, CA, USA).

The DLS experiment was carried out with Zetasizer Nano-ZS (Malvern, Worcestershire, Great Britain), which estimates the size distribution from the measured correlation function by nonnegative least square (NNLS) analysis. TiO₂ and Ta NPs were dispersed in ddH₂O, PBS, RPMI 1640, and RPMI 1640 containing 10% FBS. Then, samples of NPs were mixed thoroughly via sonication and vortexing before measuring them at 250 μg/mL. The scattered light is monitored at an angle of 173° with a wavelength of 633 nm. Measurements were done at 20°C at an average of 10-20 short frames of 10 s. The observed decay rate is $I = q^2 D_0$ with scattering vector q . The hydrodynamic radius R_h is related to the diffusion coefficient D_0 according to the Stokes-Einstein equation $D_0 = k_B T / 6\pi\eta R_h$ with the Boltzmann constant k_B , temperature T (in K), and viscosity η of the solvent.

The energy-dispersive X-ray (EDX) analysis was performed using the EDX system (EDAX, Ametek GmbH, Meerbusch, Germany). The EDX system is fitted with a Super Ultrathin Window Si-(Li) detector with a resolution < 138 eV (MnK α at 1000 cps), configured with a take-off angle of 45° relative to the microscope stage. The Genesis 4000 software (version 3.61) was used to display and evaluate the collected spectra. Measuring adjustments (dwell time = 100 μs; amplifier integration time = 100 μs; reads = 100; and map resolution = 512 × 256 pixels) remained constant during the measurements. The time required for the analysis of each sample was 655 live seconds. Al, Ta, Si, Ti, Fe, Co, and Ni, were chosen for quantification, whereas the other elements such as carbon, oxygen, nitrogen, potassium, and magnesium were not considered (Supplementary Figure 2). Quantification of the elements was standardless using the ZAF-algorithm and selecting the automatic integration of the obtained spectra. The evaluated parameters were the standardized amounts of Ta and Ti.

2.4. Endotoxin Test. Endotoxin levels in nanoparticle samples were quantified with the Limulus amoebocyte lysate (LAL) assay using the ToxinSensor™ Chromogenic LAL Endotoxin Assay Kit (Genscript) according to the manufacturer's instructions with modifications. This kit has a minimum endotoxin detection limit of 0.01 EU/mL and a measurable concentration range of 0.01 to 1 EU/mL. 100 μg raw NPs were suspended in 1 mL endotoxin-free water at 100 μg/mL. A volume of 100 μL NP suspension and 100 μL of endotoxin standard samples derived from *Escherichia coli* (0.01-0.1 unit/mL) were incubated with 100 μL reconstituted LAL reagent for 30 min at 37°C and a volume of 100 μL endotoxin-free water as control. After the initial incubation, 100 μL reconstituted chromogenic substrate solution was added into each vial, and the incubation continued for an additional 6 min. The reaction was stopped by adding 500 μL of reconstituted color-stabilizer #1 (stop solution). Then, 500 μL of reconstituted color-stabilizer #2 and #3 were added. Importantly, particles were removed by two rounds of centrifugation (2500 rpm for 15 min) as they may interfere with the absorbance value [26]. Finally, the absorbance value of each reaction was determined at 545 nm using a microplate

reader. Distilled water was used as a blank to adjust the photometer to zero absorbance. All samples (100 μL) were analyzed in duplicate. Only tests producing a correlation coefficient for the standard curve of 0.98 or greater were accepted. Because NPs may interfere with the endotoxin measurement, all NP samples were measured with and without aliquots of a test sample containing a known amount of the endotoxin (0.005 EU/mL). The assays were considered reliable if the recovery of spikes was 80-120%.

2.5. Cell Viability Assay. The CCK-8 Cell Counting Kit (Dojindo, Japan) was used to evaluate the viability of macrophages that were treated with TiO₂ and Ta NPs. Briefly, THP-1 cells were seeded in 96-well cell culture plates (0.8 × 10⁵ cells/well) with PMA and incubated overnight for differentiation. Cells were then challenged with a series of concentrations of NPs (20, 50, 100, 200, and 500 μg/mL and 0.2 mL/well) for 1h, h, 6h, 1d, 3d, and 7d. At the end of each time point, the medium was replaced with fresh culture medium containing CCK-8 solution (1:10 in culture medium), and further incubated for another hour at 37°C and 5% CO₂. The supernatant was collected and transferred to another 96-well plate to avoid the interference of NPs on optical density (OD) reading. Finally, absorbance was measured at 450 nm using a microplate reader (Tecan, Männedorf, Switzerland). The viability of the nonchallenged cells was considered 100%.

2.6. Lactate Dehydrogenase Release Assay. Cell culture supernatants from THP-1-derived macrophages were collected after 1, 3, and 7 days after NP exposure. Resulting supernatants were evaluated for LDH activity using the Cytotoxicity LDH Assay Kit-WST (Dojindo, Japan). The absorbance of all samples at a wavelength of 490 nm was recorded using a microplate reader. Low controls (untreated cells) and high controls (cells treated with lysis buffer) were used to calculate the cell mortality:

$$\text{Cytotoxicity (\%)} = \frac{\text{test substance} - \text{low control}}{\text{high control} - \text{low control}} \times 100. \quad (1)$$

2.7. Measurement of Nanoparticle Uptake by Flow Cytometry. Particle uptake by macrophages was measured via flow cytometry. THP-1 cells were seeded into 24-well cell culture plates at 2 × 10⁵ cells per well with PMA overnight. Then, THP-1 cells were preincubated for 30 min with the following uptake inhibitors: 25 μM cytochalasin D (CytD), used to disrupt actin-dependent phagocytosis [27]; 100 μM amiloride (Ame), applied as an inhibitor of micropinocytosis [28]; and 25 μM genistein (Gen) and 25 μM chlorpromazine hydrochloride (Cpz), used to inhibit caveolae- and clathrin-mediated endocytosis, respectively [29]. Cells were subsequently exposed to TiO₂ or Ta NPs at concentrations of 100 and 500 μg/mL (0.5 mL/well) for 1 and 6h. The inhibitors were not removed during the uptake experiments. At the end of each time point, cells were trypsinized and centrifuged. The resulting cell pellet was resuspended in 200 μL ice-cold PBS and analyzed with flow cytometry. Flow cytometry data were acquired using FACSCanto II using FACS-Diva

software and analyzed using FlowJo software (all from BD Biosciences). Cell profiles were investigated through forward scatter (FSC) vs. side scatter (SSC) to exclude cell debris and free particles. Mean SSC was used as a measure of particle uptake. The increase in SSC, which was directly related to the cellular granularity, was analyzed as described previously [30]. SSC increases at 4°C, which indicates the passive, energy-independent entrance of particles into cells, and a portion of particles adherent to macrophages' outer membranes were analyzed and subtracted from the data acquired at 37°C.

2.8. Bright-Field Microscopy. THP-1 cells were differentiated as described above in a 12-well chamber slide (35mm) (ibidi, Germany) and treated for 24 h with standard culture medium, TiO₂, and Ta NPs. Bright-field microscope images were taken using an IX81 microscope (Olympus).

2.9. Measurement of Intracellular ROS Generation. The generation of intracellular ROS was measured using 2',7'-dichlorodihydrofluorescein diacetate (DCFH-DA, Sigma-Aldrich). PMA-differentiated THP-1 cells (0.8×10^5 cells/well in 96-well plates) were washed with warm PBS and then treated with TiO₂ or Ta NPs at 50 to 500 µg/mL for 1, 3, 6, and 24 h. N-Acetyl-L-cysteine (NAC) was applied in some experiments to inhibit ROS production. For these tests, PMA-differentiated THP-1 cells were pretreated with 10 mM NAC for 30 min and then stimulated with 100 or 500 µg/mL NPs for another 6 or 24 h in the presence of 10 mM NAC. Then, serum-free RPMI medium containing 20 µM DCFH-DA was added to the samples and controls for another 30 min under standard culturing conditions. Untreated controls were maintained for each time interval. Subsequently, cells were carefully washed twice with prewarmed PBS. The fluorescence intensity of the resulting fluorescent product dichlorofluorescein (DCF) was measured with a microplate reader at the excitation and emission wavelengths of 485 and 530 nm, respectively.

2.10. Enzyme-Linked Immunosorbent Assay (ELISA). PMA-differentiated THP-1 cells (0.8×10^5 cells/well of a 96-well plate) were firstly primed with 200 ng/mL LPS (LPS-EK Ultrapure, InvivoGen) or incubated with standard culture medium for 3 h. Then, LPS was removed, and macrophages were treated with particles for 1 h, 3 h, 6 h, 1 d, 3 d, and 7 d. NAC was applied in some experiments to inhibit ROS in THP-1 macrophages. For these tests, PMA-differentiated THP-1 cells were pretreated with 10 mM NAC for 30 min following LPS priming and then stimulated with 100 or 500 µg/mL NPs for another 6 h in the presence of 10 mM NAC. Cell-free supernatants were collected and centrifuged ($200 \times g$, 10 min, 4°C), and aliquots were stored at -80°C. TNFα and IL-1β were determined with an ELISA kit (R&D Systems, Wiesbaden, Germany) according to the manufacturer's protocol, using a microplate ELISA reader.

2.11. Statistical Analysis. GraphPad Prism 7 software was used for statistical analysis. All values were expressed as the mean + SD. Student's *t*-test was used for comparisons

between two groups, and one-way ANOVA was used to determine statistical differences between several groups. Differences were considered significant at **p* < 0.05, ***p* < 0.01, and ****p* < 0.001.

3. Results

3.1. Nanoparticle Characterization. SEM images of TiO₂ NPs (Figure 1(a)) and Ta NPs (Figure 1(b)) exhibited a spherical shape. TiO₂ NPs were slightly more plate-like, with less rounded features. The average size of the TiO₂ and Ta particles estimated from SEM images was 54.3 ± 14.6 nm (Figure 1(c)) and 67.9 ± 22.1 nm (Figure 1(d)), respectively. To further characterize the size distribution of particles in the liquid phase, TiO₂ and Ta NPs were analyzed using dynamic light scattering (DLS). The hydrodynamic sizes of TiO₂ and Ta NPs in ddH₂O, PBS, RPMI 1640 growth medium, and RPMI 1640 growth medium containing 10% FBS are summarized in Supplementary Table 1. The DLS results demonstrated that both NPs had the tendency to form aggregates in different solutions. In addition, endotoxin levels were also tested in both groups by employing the LAL chromogenic assay. All NP samples did not show any contamination with endotoxins (Supplementary Figure 1), confirming that all particle samples could be considered endotoxin-free. To confirm NP purity, energy-dispersive X-ray (EDX) analyses were performed. The resulting EDX spectra of NPs indicated the presence of Ti and Ta as the main elements, with no indication of other selected elements (Supplementary Figure 2). Notably, our EDX data revealed some extent of oxidation of Ta NPs, which may be attributed to the formation of an oxide layer on the surface of Ta NPs during sample preparation.

3.2. Bright-Field Microscopy of THP-1-Derived Macrophages Exposed to TiO₂ and Ta NPs. To observe the interaction between THP-1-derived macrophages and NPs, THP-1-derived macrophages were exposed to culture medium (Figure 2(a)), TiO₂ NPs (Figure 2(b)), and Ta NPs (Figure 2(c)) for 24 h, and bright-field images were taken. Bright-field images showed the presence of TiO₂ and Ta NP agglomerates in the presence of THP-1-derived macrophages.

3.3. Analysis of the Cytotoxic Effect of TiO₂ and Ta NPs in THP-1-Derived Macrophages. THP-1-derived macrophages were exposed to TiO₂ and Ta NPs using a concentration range of 20-500 µg/mL. Cell viability was evaluated by CCK-8 assay. TiO₂ NPs demonstrated no dose-dependent cytotoxicity until they reached a threshold of 200 µg/mL at 24 hours (Figure 3(a)). Beyond this limit, TiO₂ NPs significantly decreased macrophage viability in a dose- and time-dependent manner compared to untreated cells (Supplementary Figure 3(a)). In contrast, exposure of macrophages to 20-500 µg/mL Ta NPs did not result in a significant decrease in cell viability (Figure 3(b), Supplementary Figure 3(b)) until 7 days. Notably, at 24 and 48 h using 20 µg/mL, cell viability was even slightly increased (Supplementary Figure 3(b)). As Ta's density is higher than that of TiO₂, we also compared 100 µg/mL TiO₂ with 500 µg/mL Ta

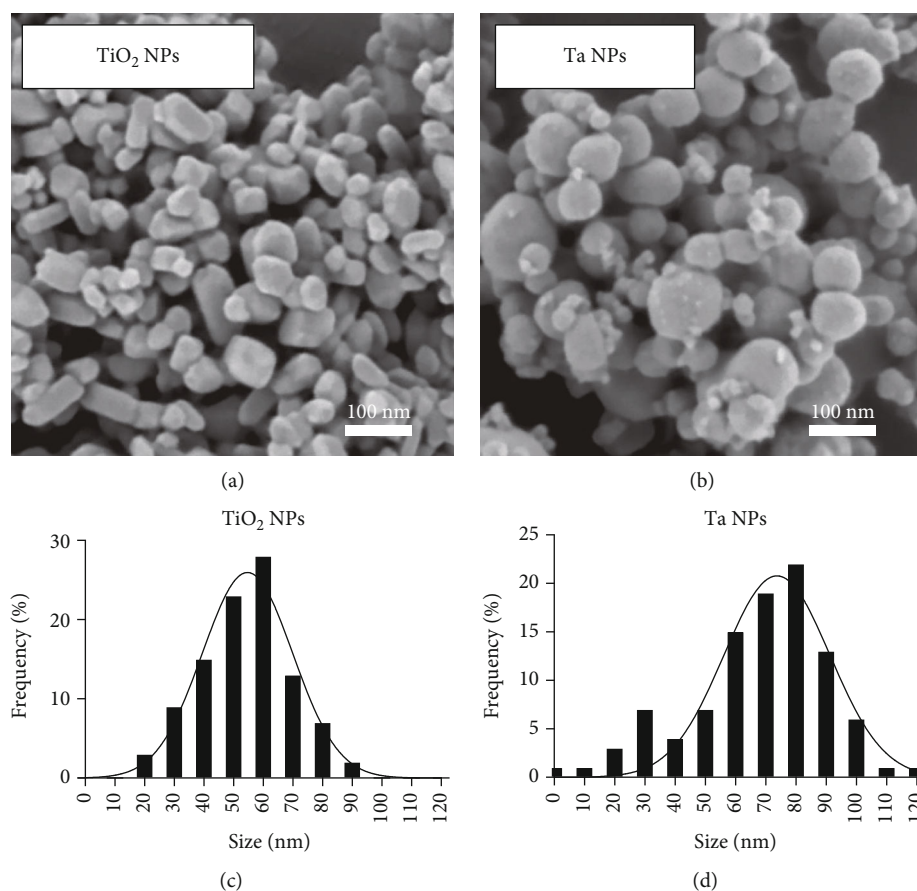


FIGURE 1: Characterization of TiO₂ and Ta NPs. (a, b) Scanning electron microscopic (SEM) images of TiO₂ NPs and Ta NPs. (c, d) Particle size distribution with Gaussian fitting of TiO₂ NPs and Ta NPs was determined by randomly selecting 100 particles from the SEM images.

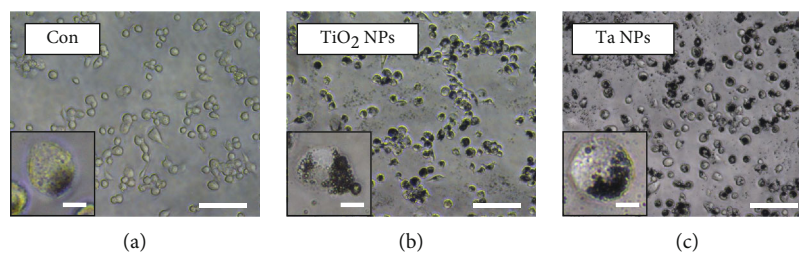


FIGURE 2: Bright-field microscope images of THP-1-derived macrophages treated with TiO₂ and Ta NPs. THP-1-derived macrophages were cultured in the presence of (a) standard culture medium (Con: control), (b) TiO₂ NPs, and (c) Ta NPs for 24 h. Bright-field images were taken 24h after exposure. Scale bar: 100 μm (overview) and 10 μm (enlarged insert).

to compensate a potential bias by NP density. Similar to the direct comparison between the same NP concentrations, cells were still less viable in the presence of 100 μg/mL TiO₂ than in the presence of 500 μg/mL Ta NPs.

LDH is being released by cells as a consequence of cell membrane damage, and therefore, it is an indicator of irreversible cell death. As expected, the LDH release assay congruently supported our CCK-8 cell viability results. Compared to untreated cells, in the TiO₂ NP group, there was no appreciable cell death until 24 hours. Then, increasing cell death was observed in a dose- and time-dependent manner (Figure 3(c), Supplementary Figure 3(c)). In contrast, expo-

sure of macrophages to 20-500 μg/mL Ta NPs for up to 7 days did not result in a significant increase in cell death (Figure 3(d), Supplementary Figure 3(d)). Overall, TiO₂ and Ta NPs demonstrated good biocompatibility at low concentrations. At high concentrations, however, only TiO₂ NPs led to cytotoxicity.

3.4. Cellular Uptake and Internalization Routes of TiO₂ and Ta NPs. Macrophages are phagocytic cells capable of sensing and internalizing particulate matters. To validate the uptake of TiO₂ and Ta NPs, THP-1 macrophages were exposed to TiO₂ and Ta NPs (100 and 500 μg/mL) for 1 and 6 h, and

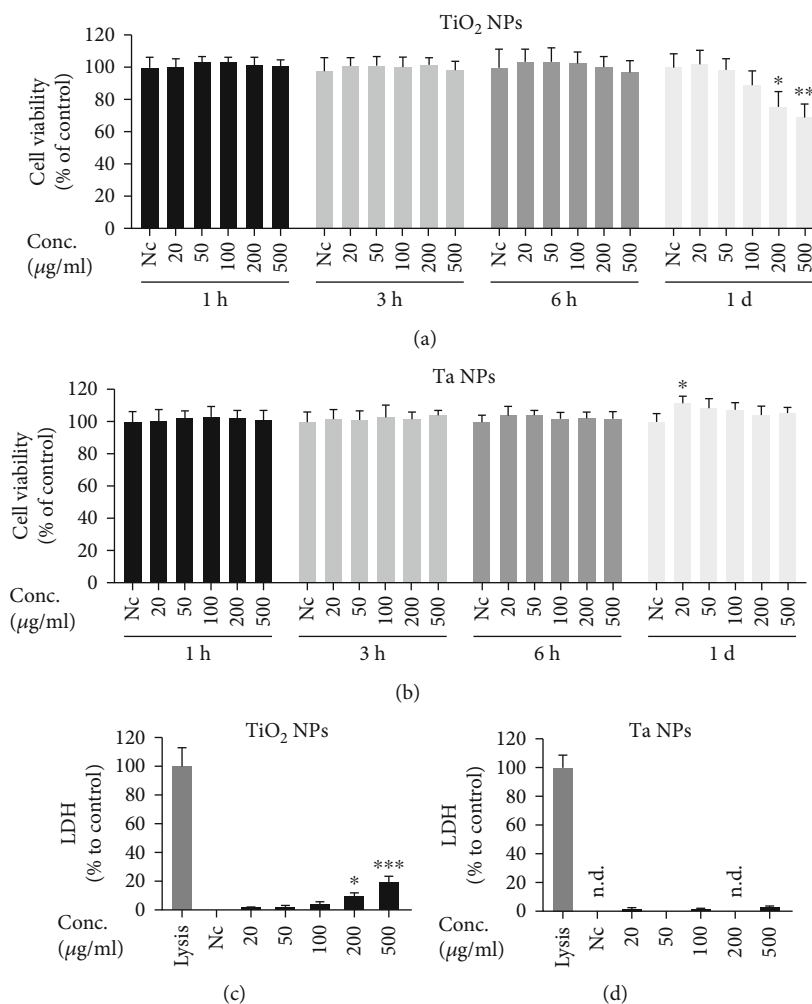


FIGURE 3: Analysis of cytotoxic effects of TiO₂ and Ta NPs on macrophages. (a, b) Cell viability was determined by CCK-8 assay at indicated time points. (c, d) Lactate dehydrogenase (LDH) leakage was evaluated by LDH assay after 24h. Viability and LDH release are normalized and expressed as mean + SD as percentage of untreated cells of three independent experiments (* $p < 0.05$, ** $p < 0.01$, and *** $p < 0.001$). n.d.: not detectable. Nc: nontreated control.

flow cytometry was used to quantify NP uptake. Flow cytometric analysis demonstrated that both TiO₂ and Ta NPs significantly enhanced cell granularity, which was detected by SSC signals and can be used as a readout for NP uptake. We observed significantly lower SSC signals in the Ta NP group in contrast to the TiO₂ group (Figure 4) at 1 and 6 h, suggesting that THP-1-derived macrophages took up more TiO₂ NPs than Ta NPs at the same concentration.

To determine possible uptake routes of TiO₂ and Ta NPs, THP-1-derived macrophages were preincubated with different uptake inhibitors before NP exposure. Comparison of the FACS analysis data at 1 and 6 h demonstrated that the majority of the particles were internalized within the first hour (Figure 4). To ensure that the uptake inhibitors did not affect cell viability, cell viability was tested in the presence of different inhibitor concentrations up to 6 hours (Supplementary Figure 4).

As shown in Figures 4(a) and 4(b), the uptake of TiO₂ and Ta NPs was significantly reduced after preincubation with CytD, Ame, and Cpz, but not Gen, suggesting that mac-

rophages take up TiO₂ NPs via phagocytosis, macropinocytosis, and clathrin-dependent endocytosis. Similarly, Ta NPs were internalized through phagocytosis (Figures 4(c) and 4(d)). However, macropinocytosis and clathrin- and caveolin-mediated endocytosis inhibitors did not significantly reduce Ta uptake, indicating the absence of these mechanisms. In summary, the active internalization of TiO₂ and Ta NPs were dominated by phagocytosis. TiO₂ NP uptake also involved macropinocytosis as well as clathrin-mediated endocytosis, but to less extent. Caveolae-mediated endocytosis seems not to be involved in the uptake of both particles.

3.5. Ta NPs Trigger Less ROS Production than TiO₂ NPs. NP-induced oxidative stress contributes to nanopathology [31]. In this study, the overall intracellular ROS elevation after NP challenge was examined using the probe 2',7'-dichlorodihydrofluorescein diacetate (DCFH-DA). In our setup, as shown in Figure 5(a), TiO₂ NPs dose-dependently induced robust intracellular ROS generation at different time points.

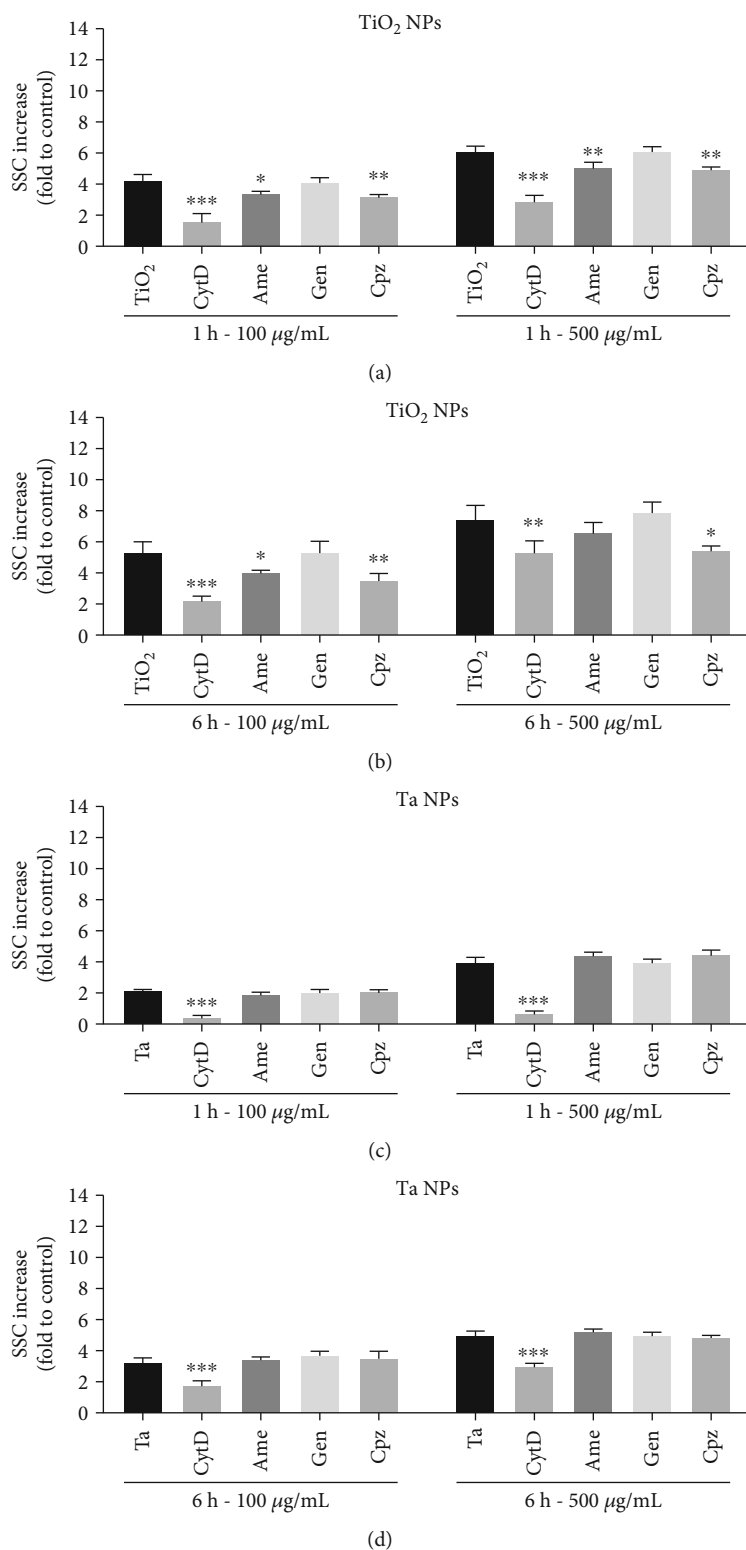


FIGURE 4: TiO₂ and Ta NP internalization and their particle-specific uptake routes. THP-1-derived macrophages were pretreated with different uptake inhibitors for 30min and then exposed to (a) TiO₂ and (b) Ta NPs at 100 and 500µg/mL for 1 and 6 h. Changes in side scatter (SSC) were analyzed with flow cytometry. SSC changes at 4°C were subtracted, and data were expressed as mean + SD as fold of NP-untreated cells (Nc) of three independent experiments. Statistical differences were shown as **p* < 0.05, ***p* < 0.01, and ****p* < 0.001 for inhibitor-treated groups vs. cells treated with particles only.

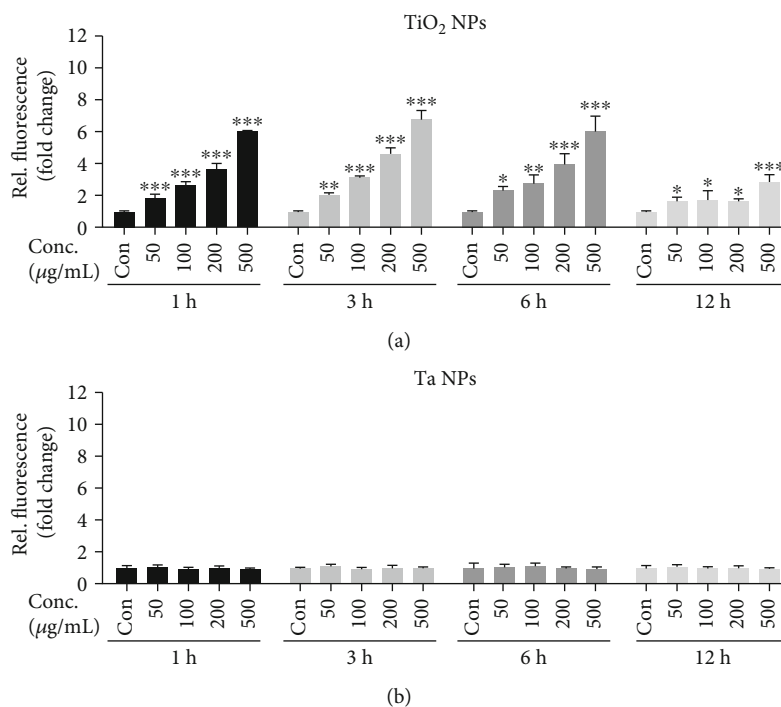


FIGURE 5: Endogenous ROS generation in THP-1-derived macrophages after TiO₂ and Ta NP exposure. THP-1-derived macrophages were stimulated with (a) TiO₂ and (b) Ta NPs (50-500 µg/mL) for 1, 3, 6, and 24 h. Cells were stained with DCFH-DA (20 µM) for 30 min, and then fluorescence intensity was analyzed with a microplate reader. Fluorescence values are normalized and expressed as mean + SD as fold of untreated cells of three independent experiments (* $p < 0.05$, ** $p < 0.01$, and *** $p < 0.001$).

Comparison of these data showed that the majority of ROS was produced within the first hour after NP treatment. Notably, a reduction of endogenous ROS production was observed at 24 hours. This may result due to a decrease in cell viability (Figure 3(a)) at this time point. In contrast, Ta NPs induced negligible intracellular ROS elevation at different concentrations and incubation periods (Figure 5(b)). These results indicated that, compared to TiO₂ NPs, Ta NPs are “inert” in generating ROS.

3.6. Ta NPs Exert Less Proinflammatory Activity than TiO₂ NPs In Vitro. The wear particle-induced inflammatory response, mainly driven by macrophages, underlies the pathology of periprosthetic osteolysis and aseptic loosening [32]. Among all the proinflammatory mediators, TNF α and IL-1 β are the primary initiators and significant mediators of the wear particle-induced inflammatory cascade. Therefore, we investigated the proinflammatory effect of TiO₂ and Ta NPs by evaluating their induction of TNF α and IL-1 β with or without LPS priming.

As shown in Figure 6, the production of TNF α is only weakly stimulated by TiO₂ NPs alone (Figure 6(a)), whereas, in LPS-primed macrophages, TNF α release was markedly increased (Figure 6(b)). Further, simultaneous exposure of macrophages to TiO₂ NPs and LPS dose-dependently enhanced TNF α production (Figure 6(b)), which is well beyond the levels observed with TiO₂ NPs or LPS prime alone. Notably, TiO₂ NPs at low concentration (100 µg/mL) induced significantly more TNF α production than Ta NPs

at high concentration (500 µg/mL) in LPS-primed macrophages. This suggests that TiO₂ NPs synergized with LPS to stimulate the production of TNF α . Whereas, Ta NPs did not exert such synergistic effect (Figure 6(b)).

Similar to TNF α , little IL-1 β secretion was detected in macrophages challenged with Ta NPs alone up to 24 hours. TiO₂ NPs (500 µg/mL) stimulated a significantly higher IL-1 β level than Ta NPs in unprimed macrophages, starting at 3 h (Figure 6(c)). After LPS priming, much higher IL-1 β levels were detected in TiO₂-treated macrophages. TiO₂ NPs further elevated IL-1 β release in a time- and dose-dependent manner (Figure 6(d)), higher than LPS or TiO₂ NPs alone. In contrast to the TNF α result, the Ta NP groups stimulated a negligible IL-1 β increase after LPS priming (Figure 6(d)) compared to the untreated group. This indicated that the IL-1 β level was not entirely dependent on LPS. In summary, these results suggest that LPS aggravates inflammation in macrophages. Also, TiO₂ NPs synergized with the LPS effect to increase the production of TNF α and IL-1 β while Ta NPs did not. Thus, TiO₂ NPs possess a more substantial proinflammatory effect than Ta NPs.

3.7. Scavenging of ROS Attenuates TiO₂-Induced Cell Death and Proinflammatory Cytokine Release. Intracellular ROS are key effectors in signal transduction and are proposed to be associated with cell death and inflammation. ROS generation has been proven crucial for NP-induced NLRP3 inflammasome activation and subsequent IL-1 β release [33, 34]. Therefore, we applied antioxidant NAC to prove the effect

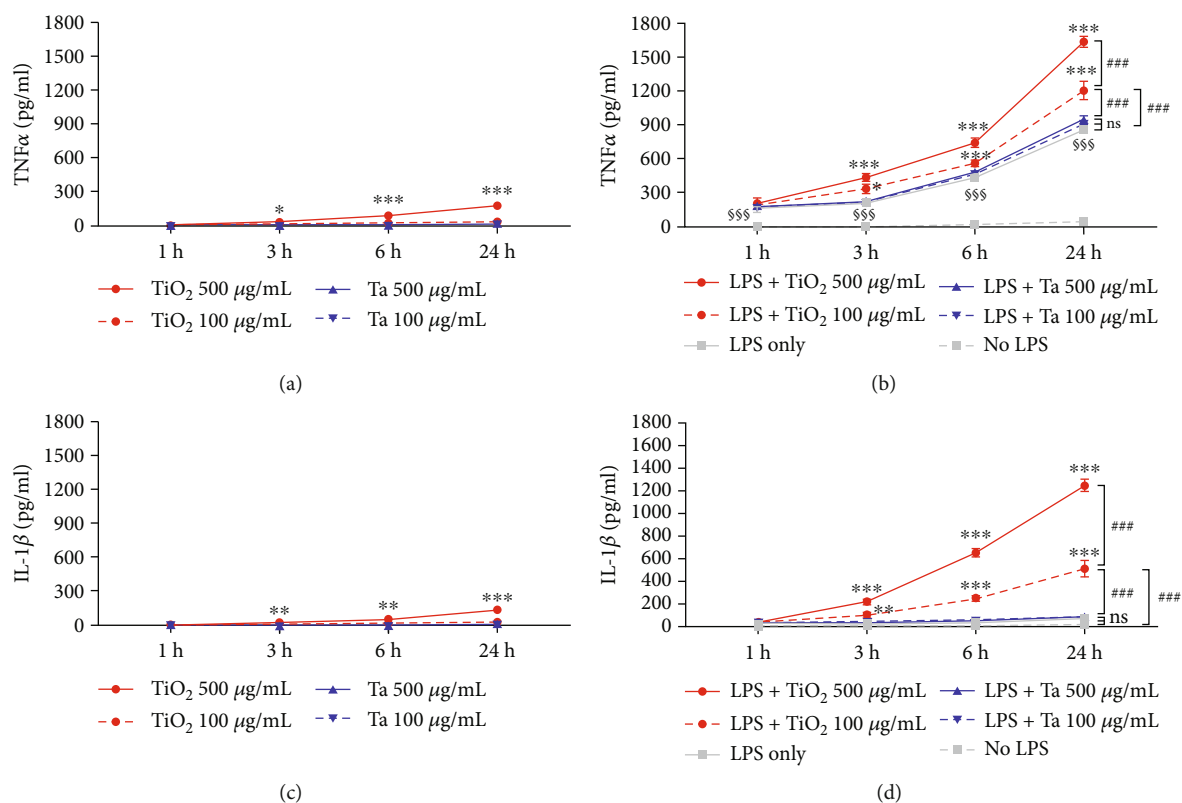


FIGURE 6: Proinflammatory potential of TiO₂ and Ta NPs on THP-1-derived macrophages. THP-1-derived macrophages were primed with 200 ng/mL LPS for 3 h, washed to remove the LPS, and then incubated with TiO₂ or Ta NPs using the indicated doses for up to 24 h. Release of (a, b) TNF α and (c, d) IL-1 β were measured by ELISA. THP-1-derived macrophages without LPS stimulation were used as controls. * indicates significant differences of different time points of the TiO₂ NP group compared to the TiO₂ NP 1 h group (* p < 0.05, ** p < 0.01, and *** p < 0.001). # indicates significant differences compared to the TiO₂ NP (100 μ g/mL) group at 24 h (### p < 0.001). \$ indicates significant LPS-mediated TNF α release compared to the untreated group (\$\$\$ p < 0.001).

of ROS on TiO₂ NP-induced cell death and IL-1 β release. NAC is a potent thiol-containing antioxidant that can act as a precursor of glutathione (GSH) and can also directly scavenge free radicals (e.g., H₂O₂ and OH⁻) [35]. As shown in Figures 7(a) and 7(b), the fluorescence intensity was lower in NAC-treated cells in comparison to cells treated with TiO₂ NPs alone at 6 and 24 h, indicating that NAC successfully antagonized ROS accumulation elicited by TiO₂ NPs in macrophages. Moreover, NAC treatment significantly mitigated cell death (Figure 6(c)) and potentially blocked IL-1 β release induced by TiO₂ NPs (Figure 6(d)) after LPS prime. These results indicated that ROS inhibition by NAC could rescue TiO₂ NP-induced nanotoxicity and mitigate IL-1 β production in macrophages.

4. Discussion

Ta-based implants have been widely used in primary and revision TJA. Nevertheless, knowledge about the possible effect of their wear products on peri-implant cells remains limited to date. Therefore, understanding the local cellular responses to nanoscale orthopedic wear particles will provide a new area for comprehension of aseptic loosening and offers new scientifically based recommendations to better design

suitable prosthetic interfaces and scaffolds. To the best of our knowledge, the present paper is the first *in vitro* analysis investigating Ta NPs and TiO₂ metallic NPs side by side in terms of their biological responses on macrophages. We provide scientific evidence that Ta NPs are inert, nontoxic, and noninflammatory NPs *in vitro*. The results of this study offer novel evidence-based insights to further substantiate the clinical application of Ta-based implants [36, 37].

We found a slight but significant increase in macrophage viability in the presence of 20 μ g/mL Ta NPs at 1 and 3 days. Similar results were found in the study by Wang et al. and Kang et al. showing that Ta NPs promote the proliferation of mouse MC3T3-E1 osteoblasts at low concentration (less than 20 μ g/mL) through the induction of autophagy [38, 39]. However, our CCK-8 and LDH results also demonstrated that Ta NPs, even when using higher concentrations (e.g., 50–500 μ g/mL) and longer incubation times (up to 7 days), still resulted in high cell viability, which ultimately supports their good biocompatibility. In contrast, TiO₂ NPs started to exhibit significant cytotoxicity at the 24-hour incubation time point. These aspects precisely show how important it is to fully characterize the cellular response of peri-implant cells to new implant materials and their resulting NPs. Therefore, the present study is of particular interest

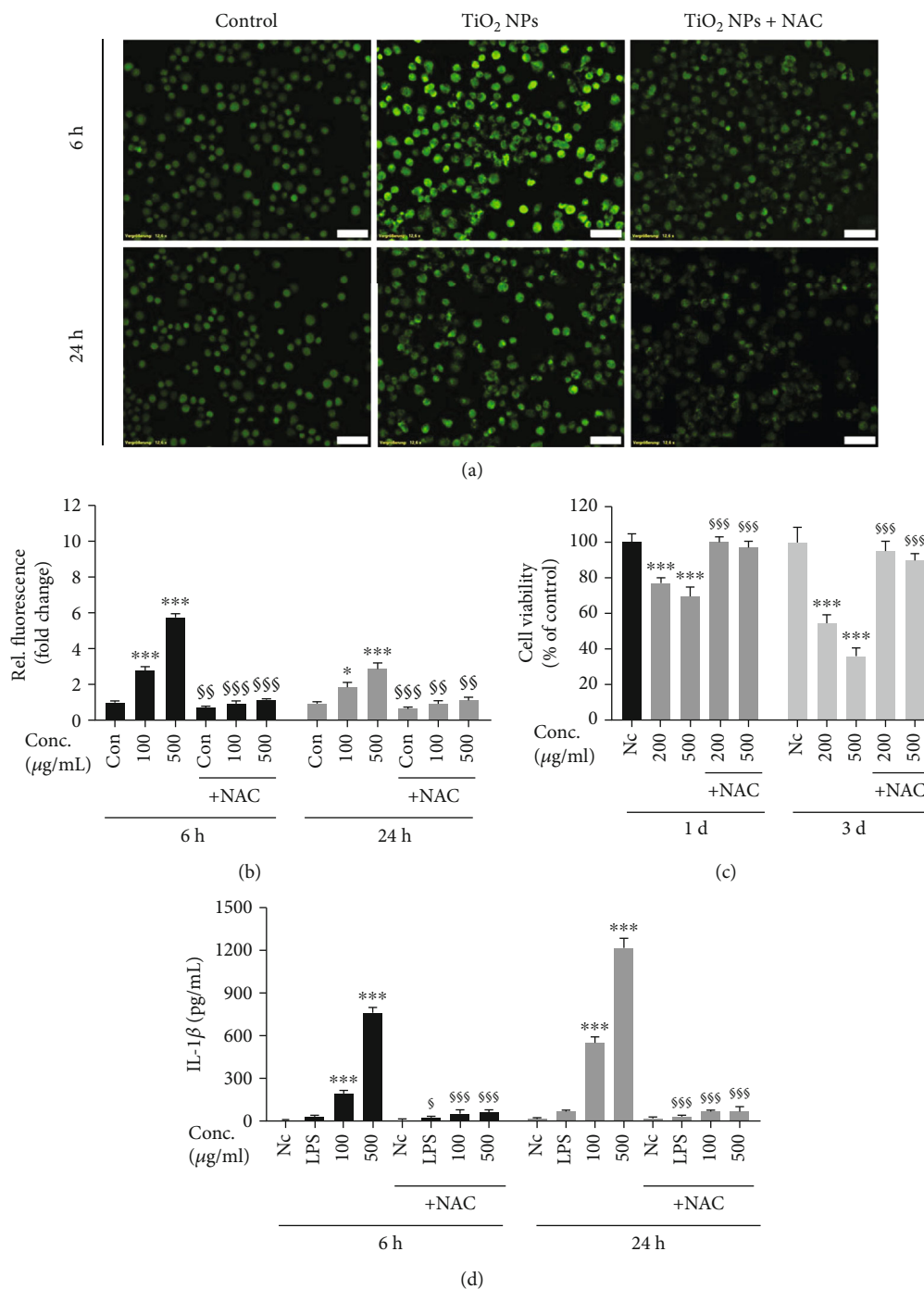


FIGURE 7: Protective role of ROS scavenger (NAC) on TiO₂ NP-induced cell death and IL-1β release. LPS-primed macrophages were preincubated for 30min with/without NAC (5mM), and then cotreated with TiO₂ NPs at the indicated doses for 6 and 24h. (a) Following exposure, cells were incubated with DCFH-DA (20μM) for 30 min at 37°C, and ROS production was detected by fluorescence microscopy (20x). Scale bar: 50μm. (b) Relative quantification of ROS generation (fold change). The protective role of NAC on (c) cell viability and release of (d) IL-1β were measured by CCK-8 and ELISA, respectively. Data are presented as mean + SD of three identical experiments performed in three replicates. * indicates significant difference as compared to the control (**p* < 0.05, ***p* < 0.01, and ****p* < 0.001); § indicates significant inhibitory effect of NAC on cell death and proinflammatory cytokine generation (§*p* < 0.05, §§*p* < 0.01, and §§§*p* < 0.001).

as it provides the first comparative analysis showing that Ta NPs induced less cytotoxicity in macrophages than NPs stemming from Ti implants.

Phagocytosis and endocytosis are responsible for the uptake and clearance of particles [27, 40]. However, to date, the mechanistic nature of TiO₂ and Ta NP internalization

in human macrophages remains obscure. Our study demonstrated that active Ta and TiO₂ NP internalization by macrophages is mainly driven by phagocytosis. Further, TiO₂ internalization is also mediated, to a lesser extent, by clathrin-dependent endocytosis and micropinocytosis. These results are supported by previous studies, which have shown that TiO₂ particle internalization is mediated by phagocytosis and endocytosis in glial cells [28], H9c2 rat cardiomyoblasts [27], and rodent macrophages [41, 42]. The multiple uptake pathways of TiO₂ NPs may partially explain why they were internalized more efficiently and why they induce more robust cytotoxicity, oxidative stress, and inflammatory cytokines compared to Ta NPs under the same conditions.

Increased bone resorption due to chronic inflammatory responses from wear particle-challenged macrophages underlies the pathogenesis of periprosthetic osteolysis [21]. TNF α is a master cytokine during inflammation and a potent inducer of other proinflammatory chemokines and cytokines. When focussing on inflammatory cytokines, the Ta-based surface seems to exert an anti-inflammatory effect compared to the Ti-based surface [43], suggesting that Ta substrates are more biologically inert and may provide a more favorable environment when applied as biomaterial. However, other studies reported that Ta-based surfaces could be more inflammatory than Ti-based [44] surfaces. This discrepancy may be attributed to the difference in surface elemental composition, modification methods, and culturing model (*in vitro*, *in vivo*, and *ex vivo*).

Our results demonstrated that Ta and TiO₂ NPs induced slight TNF α production without LPS priming. After exposure to LPS, which mimicked the situation of a low-grade infection in addition to the presence of wear particles, TNF α secretion increased over time in both NP groups. This is mainly because LPS can stimulate TNF α production through binding to Toll-like receptor-4 and subsequent activation of transcription factor NF- κ B. It is important to note that the TNF level elevation over time in the LPS plus Ta NP group is insignificant compared to that of the LPS-only group. In contrast, TiO₂ NPs act synergistically with LPS and further elevate TNF α production. This synergistic effect directly leads to a significantly higher amount of TNF α in the TiO₂ NP group (100 μ g/mL) compared to the Ta NP group (100 and 500 μ g/mL), indicating that, in the form of nanoscale particles, Ta is less proinflammatory than Ti particles.

IL-1 β is considered an essential proinflammatory mediator driving osteolysis at the bone-implant interface. Recent studies demonstrated that orthopedic wear particles mediate IL-1 β release via activation of the NLRP3 inflammasome [45, 46], whose activation is a two-step process requiring both priming (e.g., bacterial LPS) and activation signals (e.g., nigericin, silica crystal, and wear particles). Supporting these data, dramatic elevation of IL-1 β secretion was only observed after LPS priming and TiO₂ NPs. This indicated that both LPS priming and wear particles are required to license NLRP3 inflammasome activation [47]. Infection (in our case simulated by LPS) thus could be a potent inducer of inflammation, dramatically amplifying wear particle-induced inflammation and, therefore, could be a risk factor for implant loosening. The current results are in line with previ-

ous data which showed that LPS contributes to the biological activity of wear particles by increasing the proinflammatory cytokine production in macrophages [46, 48]. It is important to note that 500 μ g/mL Ta NPs induced similar SSC elevation to that of 100 μ g/mL TiO₂ NPs at 6 hours. However, Ta NPs stimulated almost no elevation of IL-1 β in the supernatant over time, even after priming with LPS. This, again, supported the noninflammatory property of Ta NPs compared to TiO₂ NPs. It also suggests that, in the context of peri-implant infection, Ta-based implants may help limit the peri-implant inflammation, or could be a proper choice in revision surgery due to periprosthetic joint infection (PJI).

Interestingly, TiO₂ NPs alone induced a low but significant elevation of IL-1 β over time. Given that all our particle samples were endotoxin-free, this effect may be due to other priming signals, such as TNF α [49] (Figure 6(a)). This fits the clinical picture in which increased values of IL-1 β are detected together with TNF α in chronic low-grade peri-implant inflammation without any sign of infection.

Oxidative stress has been proposed to play a role in nanotoxicology and inflammatory reactions [31, 50]. Previous studies have revealed that, compared to Ti substrates, Ta substrates demonstrate lower ROS generation in osteoblasts and bone marrow stromal cells and, therefore, exhibit better cellular viability and osteoinductivity [23, 51]. In our study, we found that TiO₂ NPs induced robust ROS elevation while Ta NPs induced negligible amounts of ROS. This distinct difference in ROS-generating potential could be mainly attributed to the difference in particle type. Nevertheless, we cannot exclude that there are other potential influential factors, e.g., uptake efficiency, size, morphology, and oxidation extent. Furthermore, TiO₂ NPs demonstrated higher cytotoxicity and induced higher inflammatory cytokines than Ta NPs. Thus, it is feasible to speculate that the difference in cytotoxicity and IL-1 β release is due to differences in NPs' oxidative potential. We further proved this notion using NAC, a general ROS scavenger. Our study demonstrated that scavenging ROS with NAC abrogated TiO₂ NP-induced ROS production in macrophages. Furthermore, NAC mitigated TiO₂ NP-induced cell death and abrogated IL-1 β release. Similar results were found in previous studies in which ROS suppression by NAC protected cells from cell death [52, 53] and IL-1 β release [54–57] in response to ROS-generating NPs. This further proved that ROS depression can mitigate NP-induced cell death and IL-1 β production and, therefore, may alleviate peri-implant tissue and inflammation. Although NAC has been successfully applied in previous studies as a ROS scavenger, it has multiple effects on cells [58, 59], which complicates the interpretation of the results. More specific ROS inhibitors are needed in the future to identify the ROS source. Collectively, the differences in inducing oxidative stress could explain why Ta NPs are relatively inert opposed to promoting cell death and inflammation as previously described for TiO₂, or other widely used NPs such as silica NPs [60]. Furthermore, targeting ROS may serve as a therapeutic way to mitigate wear particle-induced chronic inflammation and prosthetic loosening. However, the exact source of ROS, e.g., mitochondrial and NADPH oxidase, and their relative contribution to NP-induced inflammation, need further characterization.

5. Conclusions

For the first time in this study, we examined macrophages' cellular response to nanoscale Ta and Ti particles *in vitro*. We found that Ta, in the form of nanoscale particles, was "bioinert" and induced less cytotoxicity, ROS production, and inflammatory response compared to TiO₂ NPs. Thus, when applied as TJA biomaterials, Ta-based implants may provide a more favorable peri-implant biological environment and less potential to contribute to aseptic loosening than Ti implants. Considering that multiple biomaterials have been applied in the TJA field, comparing Ta particles with additional other particle types (e.g., polyethylene, cobalt, and chromium) should be included in future studies to assess the value of switching from conventional implants to Ta-based implants.

Data Availability

The data used to support the findings of this study are available from the corresponding authors upon request.

Conflicts of Interest

The authors declare that there is no conflict of interest regarding the publication of this article.

Authors' Contributions

Korosh Kabir and Frank A. Schildberg contributed equally to this work.

Acknowledgments

We appreciate the technical assistance from Ms. Cécilia Hilgers, Mr. Werner Masson, and Mr. Knut Wichterich. Furthermore, we would like to acknowledge the assistance of the Flow Cytometry Core Facility at the Institute of Experimental Immunology, Medical Faculty at the University of Bonn. We would also like to acknowledge the assistance of the Microscopy Core Facility of the Medical Faculty within the Bonn Technology Campus Life Sciences, University of Bonn as well as the EDX-Facility at the Department of Horticultural Sciences, Faculty of Agriculture, University of Bonn. Furthermore, we thank Dr. Shu Chen for her support and help in this project. We thank the China Scholarship Council (CSC) for the financial support of this work.

Supplementary Materials

Supplementary Table 1: hydrodynamic radius measured by DLS. TiO₂ and Ta nanoparticles (NPs) were dispersed in ddH₂O, PBS, RPMI 1640, and RPMI 1640 containing 10% FBS at 250 µg/mL. Hydrodynamic radius (nm) was determined by DLS, and data from major peaks were presented. Supplementary Figure 1: endotoxin contamination of TiO₂ and Ta NPs. Quantitative evaluation of endotoxin contamination was determined by an LAL endotoxin assay kit. Data were representative of three independent experiments. The endotoxin level was calculated according to the standard

curve. n.d.: not detectable. Supplementary Figure 2: spectral intensities of the Ta (a) and TiO₂ (b) samples observed in the energy-dispersive X-ray (EDX) analysis system. The spectra were analyzed in high vacuum (accelerating voltage: 20kV; spot size: 5.5). No contamination of other elements were observed. Supplementary Figure 3: cytotoxic effects of TiO₂ and Ta NPs on macrophages from 1 day to 7 days. (a, b) Cell viability was determined by CCK-8 assay at indicated time points. (c, d) Lactate dehydrogenase (LDH) leakage was evaluated by LDH assay after 24h. Viability and LDH release are normalized and expressed as mean + SD as percentage of untreated cells of three independent experiments (**p* < 0.05, ***p* < 0.01, and ****p* < 0.001). n.d.: not detectable. Nc: nontreated control. Supplementary Figure 4: cytotoxic effects of inhibitors on macrophages. Macrophages were incubated with different concentrations of uptake inhibitors, and cell viability was evaluated by CCK-8 assay. Viability is normalized and expressed as mean + SD as the percentage of untreated cells of three independent experiments. **p* < 0.05, compared with control. (*Supplementary Materials*)

References

- [1] O. N. Schipper, S. L. Haddad, P. Pytel, and Y. Zhou, "Histological analysis of early osteolysis in total ankle arthroplasty," *Foot & Ankle International*, vol. 38, no. 4, pp. 351–359, 2016.
- [2] T. Schmalzried, M. Jasty, and W. H. Harris, "Periprosthetic bone loss in total hip arthroplasty: polyethylene wear debris and the concept of the effective joint space," *The Journal of bone and joint surgery*, vol. 74, no. 6, pp. 849–863, 1992.
- [3] K. Hirakawa, T. W. Bauer, B. N. Stulberg, and A. H. Wilde, "Comparison and quantitation of wear debris of failed total hip and total knee arthroplasty," *Journal of Biomedical Materials Research*, vol. 31, no. 2, pp. 257–263, 1996.
- [4] K. J. Margevicius, T. W. Bauer, J. T. McMahon, S. A. Brown, and K. Merritt, "Isolation and characterization of debris in membranes around total joint prostheses," *JBJS*, vol. 76, no. 11, pp. 1664–1675, 1994.
- [5] D. J. Hall, R. Pourzal, J. J. Jacobs, and R. M. Urban, "Metal wear particles in hematopoietic marrow of the axial skeleton in patients with prior revision for mechanical failure of a hip or knee arthroplasty," *Journal of Biomedical Materials Research Part B: Applied Biomaterials*, vol. 107, no. 6, pp. 1930–1936, 2018.
- [6] I. Polyzois, D. Nikolopoulos, I. Michos, E. Patsouris, and S. Theocharis, "Local and systemic toxicity of nanoscale debris particles in total hip arthroplasty," *Journal of Applied Toxicology*, vol. 32, no. 4, pp. 255–269, 2012.
- [7] A. C. Paulus, K. Ebinger, X. Cheng et al., "Local biological reactions and pseudotumor-like tissue formation in relation to metal wear in a murine in vivo model," *BioMed Research International*, vol. 2019, 10 pages, 2019.
- [8] D. R. Bijukumar, A. Segu, J. C. Souza et al., "Systemic and local toxicity of metal debris released from hip prostheses: a review of experimental approaches," *Nanomedicine: Nanotechnology, Biology and Medicine*, vol. 14, no. 3, pp. 951–963, 2018.
- [9] N. A. Beckmann, R. G. Bitsch, M. Schonhoff, K.-A. Siebenrock, M. Schwarze, and S. Jaeger, "Comparison of the primary stability of porous tantalum and titanium acetabular revision constructs," *Materials*, vol. 13, no. 7, p. 1783, 2020.

- [10] H. Abdelaziz, R. Jaramillo, T. Gehrke, M. Ohlmeier, and M. Citak, "Clinical survivorship of aseptic revision total knee arthroplasty using hinged knees and tantalum cones at minimum 10-year follow-up," *The Journal of Arthroplasty*, vol. 34, no. 12, pp. 3018–3022, 2019.
- [11] M. T. Houdek, P. C. Ferguson, M. P. Abdel et al., "Comparison of porous tantalum acetabular implants and Harrington reconstruction for metastatic disease of the acetabulum," *Journal of Bone and Joint Surgery*, vol. 102, no. 14, pp. 1239–1247, 2020.
- [12] G. Mohandas, N. Oskolkov, M. T. McMahon, P. Walczak, and M. Janowski, "Porous tantalum and tantalum oxide nanoparticles for regenerative medicine," *Acta Neurobiologiae Experimentalis*, vol. 74, no. 2, pp. 188–196, 2014.
- [13] M. Stiehler, M. Lind, T. Mygind et al., "Morphology, proliferation, and osteogenic differentiation of mesenchymal stem cells cultured on titanium, tantalum, and chromium surfaces," *Journal of Biomedical Materials Research Part A*, vol. 86A, no. 2, pp. 448–458, 2008.
- [14] Q. Wang, H. Zhang, Q. Li et al., "Biocompatibility and osteogenic properties of porous tantalum," *Experimental and Therapeutic Medicine*, vol. 9, no. 3, pp. 780–786, 2015.
- [15] R. M. Meneghini, C. Meyer, C. A. Buckley, A. D. Hanssen, and D. G. Lewallen, "Mechanical stability of novel highly porous metal acetabular components in revision total hip arthroplasty," *The Journal of Arthroplasty*, vol. 25, no. 3, pp. 337–341, 2010.
- [16] D. R. Jenkins, A. N. Odland, R. J. Sierra, A. D. Hanssen, and D. G. Lewallen, "Minimum five-year outcomes with porous tantalum acetabular cup and augment construct in complex revision total hip arthroplasty," *The Journal of Bone and Joint Surgery*, vol. 99, no. 10, p. e49, 2017.
- [17] J. Schoon, S. Geißler, J. Traeger et al., "Multi-elemental nanoparticle exposure after tantalum component failure in hip arthroplasty: in-depth analysis of a single case," *Nanomedicine: Nanotechnology, Biology and Medicine*, vol. 13, no. 8, pp. 2415–2423, 2017.
- [18] G. C. Babis, N. A. Stavropoulos, G. Sasalos, M. Ochschenkuehn-Petropoulou, and P. Megas, "Metallosis and elevated serum levels of tantalum following failed revision hip arthroplasty—a case report," *Acta Orthopaedica*, vol. 85, no. 6, pp. 677–680, 2014.
- [19] A. Brüggemann, H. Mallmin, M. Bengtsson, and N. P. Hailer, "Safety of use of tantalum in total hip arthroplasty," *JBJS*, vol. 102, no. 5, pp. 368–374, 2020.
- [20] E. Ingham and J. Fisher, "The role of macrophages in osteolysis of total joint replacement," *Biomaterials*, vol. 26, no. 11, pp. 1271–1286, 2005.
- [21] C. Nich, Y. Takakubo, J. Pajarinen et al., "Macrophages—key cells in the response to wear debris from joint replacements," *Journal of biomedical materials research Part A*, vol. 101, no. 10, pp. 3033–3045, 2013.
- [22] N. J. Hallab and J. J. Jacobs, "Chemokines associated with pathologic responses to orthopedic implant debris," *Frontiers in Endocrinology*, vol. 8, p. 5, 2017.
- [23] M. Lu, P. Wu, X. Guo, L. Yin, H. Cao, and D. Zou, "Osteoinductive effects of tantalum and titanium on bone mesenchymal stromal cells and bone formation in ovariectomized rats," *European Review for Medical and Pharmacological Sciences*, vol. 22, no. 21, pp. 7087–7104, 2018.
- [24] X. Dou, X. Wei, G. Liu et al., "Effect of porous tantalum on promoting the osteogenic differentiation of bone marrow mesenchymal stem cells in vitro through the MAPK/ERK signal pathway," *Journal of Orthopaedic Translation*, vol. 19, pp. 81–93, 2019.
- [25] L.-Y. Shi, A. Wang, F.-Z. Zang, J.-X. Wang, X.-W. Pan, and H.-J. Chen, "Tantalum-coated pedicle screws enhance implant integration," *Colloids and Surfaces B: Biointerfaces*, vol. 160, pp. 22–32, 2017.
- [26] H. Ding, Z. Zhu, T. Tang, D. Yu, B. Yu, and K. Dai, "Comparison of the cytotoxic and inflammatory responses of titanium particles with different methods for endotoxin removal in RAW264.7 macrophages," *Journal of Materials Science: Materials in Medicine*, vol. 23, no. 4, pp. 1055–1062, 2012.
- [27] E. Huerta-García, M. D. P. Ramos-Godinez, A. López-Saavedra et al., "Internalization of titanium dioxide nanoparticles is mediated by actin-dependent reorganization and clathrin- and dynamin-mediated endocytosis in H9c2 rat cardiomyoblasts," *Chemical Research in Toxicology*, vol. 32, no. 4, pp. 578–588, 2019.
- [28] E. Huerta-García, S. G. Márquez-Ramírez, M. P. Ramos-Godinez et al., "Internalization of titanium dioxide nanoparticles by glial cells is given at short times and is mainly mediated by actin reorganization-dependent endocytosis," *Neurotoxicology*, vol. 51, pp. 27–37, 2015.
- [29] J. Linares, M. C. Matesanz, M. Vila et al., "Endocytic mechanisms of graphene oxide nanosheets in osteoblasts, hepatocytes and macrophages," *ACS Applied Materials & Interfaces*, vol. 6, no. 16, pp. 13697–13706, 2014.
- [30] J. Park, M. K. Ha, N. Yang, and T. H. Yoon, "Flow cytometry-based quantification of cellular Au nanoparticles," *Analytical Chemistry*, vol. 89, no. 4, pp. 2449–2456, 2017.
- [31] P. P. Fu, Q. Xia, H.-M. Hwang, P. C. Ray, and H. Yu, "Mechanisms of nanotoxicity: generation of reactive oxygen species," *Journal of Food and Drug Analysis*, vol. 22, no. 1, pp. 64–75, 2014.
- [32] S. B. Goodman and J. Gallo, "Periprosthetic osteolysis: mechanisms, prevention and treatment," *Journal of Clinical Medicine*, vol. 8, no. 12, p. 2091, 2019.
- [33] S. Feng, Z. Zhang, Y. Mo et al., "Activation of NLRP3 inflammasome in hepatocytes after exposure to cobalt nanoparticles: the role of oxidative stress," *Toxicology In Vitro*, vol. 69, p. 104967, 2020.
- [34] M. Zhu, L. Du, R. Zhao et al., "Cell-penetrating nanoparticles activate the inflammasome to enhance antibody production by targeting microtubule-associated protein 1-light chain 3 for degradation," *ACS Nano*, vol. 14, no. 3, pp. 3703–3717, 2020.
- [35] N. Daems, S. Penninckx, I. Nelissen et al., "Gold nanoparticles affect the antioxidant status in selected normal human cells," *International Journal of Nanomedicine*, vol. Volume 14, pp. 4991–5015, 2019.
- [36] Z. Miao, P. Liu, Y. Wang et al., "PEGylated tantalum nanoparticles: a metallic photoacoustic contrast agent for multiwavelength imaging of tumors," *Small*, vol. 15, no. 41, article 1903596, 2019.
- [37] H. Zhu, X. Ji, H. Guan et al., "Tantalum nanoparticles reinforced polyetheretherketone shows enhanced bone formation," *Materials Science and Engineering: C*, vol. 101, pp. 232–242, 2019.
- [38] P. Wang, P. Qiao, H. Xing, R. Zhang, E. Lingling, and H. Liu, "Cytotoxicity, oxidative stress, and autophagy effects of tantalum nanoparticles on MC3T3-E1 mouse osteoblasts," *Journal of Nanoscience and Nanotechnology*, vol. 20, no. 3, pp. 1417–1424, 2020.

- [39] C. Kang, L. Wei, B. Song et al., "Involvement of autophagy in tantalum nanoparticle-induced osteoblast proliferation," *International Journal of Nanomedicine*, vol. Volume 12, pp. 4323–4333, 2017.
- [40] M. Geiser, "Update on macrophage clearance of inhaled micro- and nanoparticles," *Journal of Aerosol Medicine and Pulmonary Drug Delivery*, vol. 23, no. 4, pp. 207–217, 2010.
- [41] A. M. Scherbart, J. Langer, A. Bushmelev et al., "Contrasting macrophage activation by fine and ultrafine titanium dioxide particles is associated with different uptake mechanisms," *Particle and fibre toxicology*, vol. 8, no. 1, p. 31, 2011.
- [42] Q. Chen, N. Wang, M. Zhu et al., "TiO₂ nanoparticles cause mitochondrial dysfunction, activate inflammatory responses, and attenuate phagocytosis in macrophages: a proteomic and metabolomic insight," *Redox Biology*, vol. 15, pp. 266–276, 2018.
- [43] Q. Huang, X. Li, T. A. Elkhooly et al., "The osteogenic, inflammatory and osteo-immunomodulatory performances of biomedical Ti-Ta metal-metal composite with Ca- and Si-containing bioceramic coatings," *Colloids and Surfaces B: Biointerfaces*, vol. 169, pp. 49–59, 2018.
- [44] C. Yang, J. Li, C. Zhu et al., "Advanced antibacterial activity of biocompatible tantalum nanofilm via enhanced local innate immunity," *Acta Biomaterialia*, vol. 89, pp. 403–418, 2019.
- [45] L. Burton, D. Paget, N. B. Binder et al., "Orthopedic wear debris mediated inflammatory osteolysis is mediated in part by NALP3 inflammasome activation," *Journal of Orthopaedic Research*, vol. 31, no. 1, pp. 73–80, 2013.
- [46] E. Jämsen, J. Pajarinen, V.-P. Kouri et al., "Tumor necrosis factor primes and metal particles activate the NLRP3 inflammasome in human primary macrophages," *Acta Biomaterialia*, vol. 108, pp. 347–357, 2020.
- [47] G. W. Manzano, B. P. Fort, G. R. Dubyak, and E. M. Greenfield, "Wear particle-induced priming of the NLRP3 inflammasome depends on adherent pathogen-associated molecular patterns and their cognate Toll-like receptors: an in vitro study," *Clinical orthopaedics and related research*, vol. 476, no. 12, pp. 2442–2453, 2018.
- [48] E. M. Greenfield, M. A. Beidelschies, J. M. Tatro, V. M. Goldberg, and A. G. Hise, "Bacterial pathogen-associated molecular patterns stimulate biological activity of orthopaedic wear particles by activating cognate Toll-like receptors," *Journal of Biological Chemistry*, vol. 285, no. 42, pp. 32378–32384, 2010.
- [49] J. S. Bezbradica, R. C. Coll, and K. Schroder, "Sterile signals generate weaker and delayed macrophage NLRP3 inflammasome responses relative to microbial signals," *Cellular & Molecular Immunology*, vol. 14, no. 1, pp. 118–126, 2017.
- [50] P. Khanna, C. Ong, B. H. Bay, and G. H. Baeg, "Nanotoxicity: an interplay of oxidative stress, inflammation and cell death," *Nanomaterials*, vol. 5, no. 3, pp. 1163–1180, 2015.
- [51] L. Wang, X. Hu, X. Ma et al., "Promotion of osteointegration under diabetic conditions by tantalum coating-based surface modification on 3-dimensional printed porous titanium implants," *Colloids and Surfaces B: Biointerfaces*, vol. 148, pp. 440–452, 2016.
- [52] C.-Q. Luo, L. Xing, P.-F. Cui et al., "Curcumin-coordinated nanoparticles with improved stability for reactive oxygen species-responsive drug delivery in lung cancer therapy," *International Journal of Nanomedicine*, vol. Volume 12, pp. 855–869, 2017.
- [53] K.-I. Lee, C.-C. Su, K.-M. Fang, C.-C. Wu, C.-T. Wu, and Y.-W. Chen, "Ultrafine silicon dioxide nanoparticles cause lung epithelial cells apoptosis via oxidative stress-activated PI3K/Akt-mediated mitochondria-and endoplasmic reticulum stress-dependent signaling pathways," *Scientific Reports*, vol. 10, no. 1, pp. 1–13, 2020.
- [54] T. Morishige, Y. Yoshioka, A. Tanabe et al., "Titanium dioxide induces different levels of IL-1 β production dependent on its particle characteristics through caspase-1 activation mediated by reactive oxygen species and cathepsin B," *Biochemical and Biophysical Research Communications*, vol. 392, no. 2, pp. 160–165, 2010.
- [55] T. Adachi, K. Takahara, J. Taneo, Y. Uchiyama, and K. Inaba, "Particle Size of Latex Beads Dictates IL-1 β Production Mechanism," *PLoS one*, vol. 8, no. 7, p. e68499, 2013.
- [56] H. Yao, Y. Zhang, L. Liu et al., "Inhibition of lanthanide nanocrystal-induced inflammasome activation in macrophages by a surface coating peptide through abrogation of ROS production and TRPM2-mediated Ca²⁺ influx," *Biomaterials*, vol. 108, pp. 143–156, 2016.
- [57] O. Lunov, T. Syrovets, C. Loos et al., "Amino-functionalized polystyrene nanoparticles activate the NLRP3 inflammasome in human macrophages," *ACS Nano*, vol. 5, no. 12, pp. 9648–9657, 2011.
- [58] X. Pan, X. Wu, D. Yan, C. Peng, C. Rao, and H. Yan, "Acrylamide-induced oxidative stress and inflammatory response are alleviated by N-acetylcysteine in PC12 cells: involvement of the crosstalk between Nrf2 and NF- κ B pathways regulated by MAPKs," *Toxicology Letters*, vol. 288, pp. 55–64, 2018.
- [59] S. S. Karuppagounder, L. Alin, Y. Chen et al., "N-Acetylcysteine targets 5 lipoxygenase-derived, toxic lipids and can synergize with prostaglandin E₂ to inhibit ferroptosis and improve outcomes following hemorrhagic stroke in mice," *Ann Neurol*, vol. 84, no. 6, pp. 854–872, 2018.
- [60] S. Kim, J. Jang, H. Kim, H. Choi, K. Lee, and I.-H. Choi, "The effects of silica nanoparticles in macrophage cells," *Immune network*, vol. 12, no. 6, pp. 296–300, 2012.

Research Article

Tetrandrine Inhibits Titanium Particle-Induced Inflammatory Osteolysis through the Nuclear Factor- κ B Pathway

Zige Liu ^{1,2}, Yan Li ³, Fengying Guo ³, Chen Zhang ¹, Guorui Song ¹, Jiahao Yang ²,
and Desheng Chen ¹

¹Department of Orthopedic Surgery, General Hospital of Ningxia Medical University, Yinchuan 750004, China

²School of Clinical Medicine, Shimane University, Shimane 693-8501, Japan

³School of Basic Medical Sciences, Ningxia Medical University, Yinchuan 750004, China

Correspondence should be addressed to Desheng Chen; chendesheng@nxmu.edu.cn

Received 26 May 2020; Revised 3 November 2020; Accepted 16 November 2020; Published 29 November 2020

Academic Editor: Marietta Herrmann

Copyright © 2020 Zige Liu et al. This is an open access article distributed under the Creative Commons Attribution License, which permits unrestricted use, distribution, and reproduction in any medium, provided the original work is properly cited.

Peri-implant osteolysis (PIO) and the subsequent aseptic loosening are the main reasons for artificial joint implant failure. Existing methods for treating aseptic loosening are far from satisfactory, necessitating advanced drug exploration. This study is aimed at investigating the effect and underlying mechanism of tetrandrine (Tet) on inflammatory osteolysis. We established a Ti particle-induced inflammatory osteolysis mouse model and administered Tet or an equal volume of phosphate-buffered saline (PBS). Two weeks later, specimens were collected. Histological staining showed that Tet administration inhibited Ti-stimulated osteolysis. Tartrate-resistant acid phosphate (TRAP) staining and transmission electron microscopy (TEM) demonstrated that osteoclast formation was remarkably inhibited in the groups treated with Tet in a dose-dependent manner. In addition, relevant inflammatory cytokines (tumor necrosis factor (TNF)- α , interleukin (IL)-1 β , and IL-6) were also significantly reduced in the calvaria of the Tet-treated groups. Exposure of receptor activator for nuclear factor- κ B ligand- (RANKL-) induced bone marrow-derived macrophages (BMMs) and RAW264.7 cells to Tet significantly reduced osteoclast formation, F-actin ring formation, bone resorption, and the expression of relevant genes (matrix metalloproteinase 9 (MMP-9), TRAP, and nuclear factor of activated T-cells, cytoplasmic 1 (NFATc1)) during osteoclastogenesis *in vitro*. Mechanistic studies using Western blotting demonstrated that Tet inhibited the nuclear factor (NF)- κ B signaling pathway by decreasing the phosphorylation of inhibitor of NF- κ B α (I κ B α) and p65, which play important roles in osteoclast formation. Collectively, our data indicate that Tet suppressed Ti-induced inflammatory osteolysis and osteoclast formation in mice, suggesting that Tet has the potential to be developed to treat and prevent wear particle-induced inflammatory osteolysis.

1. Introduction

Artificial joint replacement is recognized as an effective method for treating various end-stage joint diseases [1]. However, peri-implant osteolysis (PIO) is the major reason for prosthesis failure and remains unresolved. Abundant epidemiological evidence demonstrates that osteolysis and aseptic loosening around the prosthesis are predominantly attributable to the inflammation caused by the wear particles generated by repeated movement between prosthetic components [2–4]. Neutrophils are the first cells involved in the

sterile inflammatory process, and they lead to the chronic activation of other phagocytes, creating a local cellular environment of cyclical acute inflammatory events.

Wozniak et al. [5] showed that the elevated levels of nitric oxide (NO) and other inflammatory factors produced by neutrophils may be important in the loosening of the joint prosthesis. Macrophages activated by wear particles also secrete various proinflammatory cytokines such as tumor necrosis factor (TNF)- α , interleukin (IL)-1 β , and IL-6 [3, 6]. Recently, the concept of “osteimmunology” has been recognized by many researchers [7]. The changes

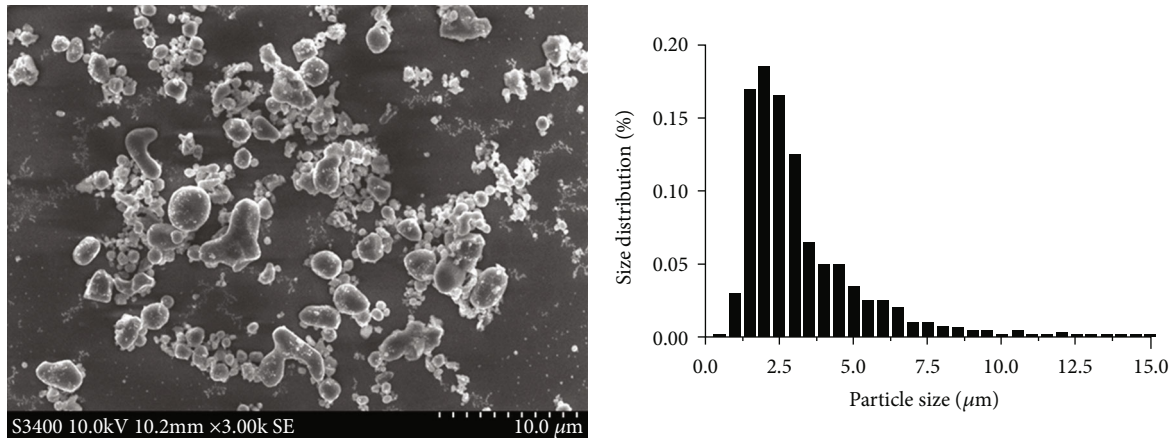


FIGURE 1: Scanning electron microscopy appearance of the Ti particles (magnification, 3000x).

associated with this phenomenon induce the excessive activation of osteoclasts, which promote bone resorption and inhibit bone formation, ultimately leading to osteolysis and aseptic loosening around the prosthesis. Osteoclast maturation is regulated directly or indirectly by multiple cytokines and signaling pathways in the body, including the NF- κ B pathway, which is documented as the most significant [8].

Therefore, the activation of the NF- κ B signaling pathway is an important event in wear particle-induced osteolysis. Osteoclasts are multinucleated bone resorption cells derived from hematopoietic stem cells. Nuclear factor of activated T-cells, cytoplasmic 1 (NFATc1) is the main transcription factor necessary for osteoclast differentiation, and its expression and activation are regulated by the NF- κ B pathway [9]. Thus, decreasing the generation of osteoclasts by inhibiting NF- κ B signaling appears to be a feasible strategy for the treatment of PIO.

In addition to extensive research on aseptic loosening, drug-mediated prevention has been found to be promising in the treatment of PIO. Tet is a bisbenzylisoquinoline alkaloid extracted from the root of *Stephania tetrandra* S. Moore. Tet has a wide range of pharmacological effects and has been shown to be effective against silicosis, cancer, inflammation, and hypertension in clinical trials [10]. As an anti-inflammatory drug, Tet inhibits the activation of NF- κ B by inhibiting the degradation of I κ B α , thereby inhibiting the production of proinflammatory cytokines [11]. Tet is also a calcium channel blocker that can act on both L-type and T-type Ca²⁺ channels and has cardiovascular effects [12].

Several studies have proven that calcium channel blockers such as felodipine, cilnidipine, and benidipine can improve osteoporosis in ovariectomized mice by inhibiting osteoclasts [13–15]. A previous study by Takahashi et al. [16] showed that Tet alleviated bone loss in sciatic-neurectomized mice; however, this is a model of disused osteolysis. Jia et al. [17] reported that Tet plays an essential role in bone metabolism. Overall, these previous findings suggest that Tet may be an effective treatment agent for PIO caused by wear particles. However, the effectiveness of Tet against PIO has not yet been reported. Thus, in the pres-

ent study, we aimed to explore the effect of Tet on wear particle-induced inflammatory osteolysis and the underlying molecular mechanisms.

2. Materials and Methods

2.1. Preparation of Ti Particles. Pure commercial Ti particles were obtained from Alfa Aesar Company (Ward Hill, MA, USA). A scanning electron microscope (Hitachi FESEM S-4800, Hitachi, Kyoto, Japan) was used to measure particle size, and more than 90% of particles were <10 μ m, which is the most common clinical size range (Figure 1). As previously described [18], Ti particles were washed three times with 70% ethanol solution for 48 h to remove the bound endotoxin. The particles were reconstituted in sterile phosphate-buffered saline (PBS) and diluted to 10 mg/mL. The absence of endotoxin was tested using a commercial Limulus assay kit (Chromogenic End-point TAL with a Diazo coupling kit, Xiamen Houshiji, Fujian, China). Particles with endotoxin levels <0.1 EU/mL were considered uncontaminated.

2.2. Ti Particle-Induced Mice Air Pouch Osteolysis Model. All animal-related experiments were conducted in accordance with the guidelines for the Care and Use of Laboratory Animals and were approved by the Animal Care Committee of NingXia Medical University (no: 2015–019). Sixty female-specific pathogen-free (SPF) BALB/c mice, 8–10 weeks old, weighing 22 \pm 3 g, and in good health were selected. The animals were housed at five mice per cage in the SPF animal room of the Experimental Animal Center of Ningxia Medical University at room temperature (22 \pm 2°C) and 60% relative humidity, under a 12 h light/dark cycle, and provided regular ad libitum access to food and water. The experiment was conducted after allowing acclimatization for 1 week.

No significant changes in the body weights of the mice were observed after modeling. Tet was obtained from Sigma-Aldrich (St. Louis, MO, USA). An air pouch osteolysis mouse model was established as previously described by Chen et al. [18, 19]. Briefly, 20 mice were selected and euthanized after anesthesia, and their skulls were immediately used

as donor skulls for air pouch bone grafting in the other mice. The skull bone slice of one mouse can be used for air pouch bone grafting in two live mice. The remaining 40 mice were subjected to air pouch formation. On day 1, the mice were anesthetized (pentobarbital 50 mg/kg), and their backs were shaved, disinfected, and draped aseptically. Subsequently, 2 mL of air was injected to form an air pouch; 0.5 mL sterile air was subsequently injected into this pouch on days 2–6.

The air pouches were formed on day 7; next, 40 mice were randomly assigned to four groups of 10 animals each. In the first (sham) group, 0.5 mL PBS solution was injected into the air pouch, and 0.1 mL normal saline was injected intraperitoneally. In the second (vehicle) group, 0.5 mL Ti particle suspension (5 mg Ti) was injected into the air pouch, and 0.1 mL normal saline was injected intraperitoneally. In both the third and fourth groups, 0.5 mL Ti particle suspension (5 mg Ti) was injected into the air pouch, followed by 15 and 30 mg/kg Tet intraperitoneally (low- and high-Tet group, respectively). The dose of Tet used in this experiment was based on the manufacturer's instructions and was proven safe in a related study [20]. The injections were performed daily for 2 weeks after the bone and Ti implantation procedures; finally, all the mice were euthanized, and the pouch membranes with the intact bone implants were harvested for histological analysis.

2.3. Histological Analysis. To decalcify and fix the collected skull and membrane tissue, specimens were placed in a 12.5% ethylenediaminetetraacetic acid (EDTA) decalcification solution for 2 weeks. After dehydration and xylene-clearing treatment to render the tissue transparent, the specimens were paraffin-embedded, marked in groups, and stored at room temperature. Continuous 5 μ m tissue sections were sliced, transferred onto glass slides, baked, and then subjected to hematoxylin and eosin (H&E) and tartrate-resistant acid phosphate (TRAP) staining. TRAP staining was performed using a TRAP kit (Sigma-Aldrich, St. Louis, MO, USA) as described previously [21].

Images of the stained sections were examined using an Olympus DP70 microscope (Olympus Optical Co., Tokyo, Japan), and representative images were captured. The method established by Wooley et al. [22] was used to determine the thickness of the air pouch membrane and the eroded surface area. TRAP-positive cells were determined as the number of purple particles near the absorbed bone. The number and percentage of osteoclasts per bone surface (OcS/BS, %) were calculated according to the method proposed by Sawyer et al. [23].

The thickness of the pouch membrane and the number of TRAP-positive cells were evaluated using ImageJ software (National Institutes of Health (NIH), Bethesda, MD, USA). We collected the tissue on a copper mesh coated with a formvar film. Sections were mounted on glass slides, stained with methylene blue, and examined under a microscope. Ultrathin sections were prepared and collected on a copper mesh, followed by staining with 5% uranyl acetate in water for 4 min and lead citrate for 2 min. The sections were then observed under a transmission electron microscope (TEM, Hitachi H-7650, Hitachi, Kyoto, Japan).

For the immunohistochemical staining of TNF- α , IL-1 β , and IL-6, paraffin-embedded sections were treated with 3% hydrogen peroxide added dropwise to inactivate endogenous peroxidases and then heated in a microwave to perform antigen retrieval. A 5% goat serum was used to block the antigen for 10 min; subsequently, the sections were stained with rabbit anti-mouse primary antibodies (1:500; all purchased from Abcam, Cambridge, MA, USA) at 4°C for 8 h. After washing with PBS, the sections were incubated with goat anti-rabbit IgG (Proteintech Group, Chicago, IL, USA) for 30 min, and then, 3,3'-diaminobenzidine (DAB) dye solution was added dropwise to develop the color. The slides were counterstained with hematoxylin, dehydrated, made transparent, and mounted.

As negative (secondary antibody-only) controls, specimens were treated with PBS instead of the primary antibody to rule out nonspecific binding of the secondary antibody. All slides were independently examined by two experimenters using the Olympus DP70 microscope following the double-blind method, and the results were evaluated. Cells with brown particles in the cytoplasm were considered positive. At 40x magnification, five random fields of view on each slide were analyzed, and the image analysis software, ImageJ, was used to evaluate the positive expression rates of TNF- α , IL-1 β , and IL-6 in each group.

2.4. Cell Culture and Osteoclast Differentiation. Mouse macrophages were isolated as previously described by Hu et al. [3] with a slight modification. Briefly, the mice were euthanized, and the bilateral femur and tibia were harvested and rinsed with PBS. After rinsing with the prepared medium and centrifugation, the cells were collected and incubated in Dulbecco's modified Eagle's medium (DMEM, Gibco, Thermo Fisher Scientific, Inc., Waltham, MA, USA) containing 10% fetal bovine serum (Gibco, Thermo Fisher Scientific, Inc.), 100 IU/mL penicillin, 100 μ g/mL streptomycin (Beijing Solarbio Science and Technology Co., Ltd., Beijing, China), and 50 ng/mL macrophage colony-stimulating factor (M-CSF, R&D Systems, Minneapolis, MN, USA) for 12 h. Unadhered cells were harvested and cultured in six-well plates in a 37°C/5% CO₂ incubator.

After overnight incubation, the adherent cells were considered BMMs. These cells were then transplanted into 96-well plates at a density of 8×10^3 cells/well and pretreated with or without Tet (0.0, 0.1, 0.5, and 1.0 μ M) for 4 h. To induce osteoclast differentiation, 50 ng/mL M-CSF and 100 ng/mL RANKL (R&D Systems, Minneapolis, MN, USA) were added to the medium, and the cells were cultured for an additional 5 days with a change of medium every 3 days. To determine the stage (early or late) at which Tet affects osteoclast formation, 1.0 μ M Tet was added to the induction medium on days 0, 1, 2, or 3, and TRAP staining was performed on day 5. The cell culture medium was changed every 3 days in this experiment. TRAP-positive multinucleated cells (three or more nuclei) were counted under the Olympus DP70 microscope.

2.5. Cell Viability Assay. RAW264.7 macrophages were obtained from the Type Culture Collection of the Chinese

Academy of Sciences (Shanghai, China). To ascertain that the Tet dose used in this experiment had no toxicity on BMMs and RAW264.7 cells, a cell viability assay was performed using cell counting kit-8 (CCK-8, Jiangsu KeyGen Biotech Co., Ltd., Nanjing, China). BMMs (5×10^3 cells/well) and RAW264.7 cells (3×10^3 cells/well) were seeded in a 96-well plate, incubated with M-CSF (50 ng/mL) and RANKL (100 ng/mL), and then treated with the indicated doses of Tet (0, 0.1, 0.3, 0.5, 0.7, 1.0, 5.0, and 10.0 μ M) for 72 h. Then, 10 μ L of a CCK-8 assay solution was added to each well, and the cells were incubated for an additional 2 h. The absorbance was measured at 450 nm using a E2500 microplate reader (Thermo Fisher Scientific, Inc.).

2.6. F-Actin Ring Staining Assay. BMMs (8×10^3 cells/well) were cultured in a 96-well plate as described in the previous section, fixed with 4% paraformaldehyde, and permeabilized with 0.1% (*v/v*) Triton X-100. After extensive rinsing with PBS, the cells were incubated with Alexa-Fluor 647 phalloidin (Invitrogen, San Diego, CA, USA) for 1 h. Subsequently, the BMMs were rinsed three times with PBS, the nuclei were counterstained with 4',6-diamidino-2-phenylindole (DAPI), and the stained cells were examined under a confocal microscope (Carl Zeiss, Oberkochen, Germany).

2.7. Resorption Pit Formation Assay. BMMs (2.4×10^4 cells/well) were plated in hydroxyapatite-coated six-well plates (Corning Inc., NY, USA). The cells were allowed to adhere to the wells for a few hours to overnight; they were then pretreated with various Tet concentrations in basal medium for 4 h. To induce osteoclast differentiation, RANKL (100 ng/mL) and M-CSF (50 ng/mL) were added to the medium, and the cells were cultured for an additional 5 days with a change of medium every 3 days. Sonication was used to remove the cells attached to the bottom of the wells. Resorption was observed under the DP70 microscope, and the resorption pit area was measured using ImageJ software.

2.8. Enzyme-Linked Immunosorbent Assay (ELISA). RAW264.7 cells (1×10^4 cells/well) were plated in six-well plates and divided into the following five groups that were treated as indicated: sham, cultured in DMEM; vehicle, 0.1 mg/mL Ti particles; and low-, medium-, and high-dose Tet, each treated with 0.1 mg/mL Ti particle suspension, followed by 0.1, 0.5, and 1.0 μ M Tet, respectively; subsequently, all the groups were cultured for 5 days with a change of medium every day. The culture supernatant was collected on days 1–5 and stored at -80°C . ELISA was performed using specific kits for TNF- α and MMP-9 (all purchased from eBioscience, San Diego, CA, USA) according to the manufacturer's instructions. Optical density was measured at 450 nm using a microplate reader (Thermo Fisher Scientific, Inc.).

2.9. Gene Expression of TRAP, MMP-9, and NFATc1. The various groups of RAW264.7 cells were cultivated for 5 days and then lysed; total RNA was extracted using TRIzol reagent (Invitrogen). Complementary cDNA was synthesized from 1 μ g total RNA using a RevertAid First Strand cDNA synthesis kit (Thermo Fisher Scientific, Inc.). Reverse transcription-

polymerase chain reaction (RT-PCR) was performed using a LightCycler PCR system (Roche, Switzerland) with the SYBR Premix Ex Tag kit (TaKaRa, Japan) in 10 μ L RT-PCR reaction buffer. After denaturation at 95°C for 5 min, PCR was performed with 40 cycles of denaturation at 95°C for 10 s, annealing at 60°C for 15 s, and extension at 72°C for 10 s. All experiments were performed in triplicate, and β -actin was used to normalize the target gene levels. The primer sequences used were as follows: β -actin, forward 5'-AGGG TGTGATGGTGGGAATG-3' and reverse 5'-GCTGGG GTGTTGAAGGTCTC-3'; TRAP, forward 5'-AGGGTG TGATGGTGGGAATG-3' and reverse 5'-GCTGGGGTG TTGAAGGTCTC-3'; MMP-9, forward 5'-GCTGAAACC AGACCCAGAC-3' and reverse 5'-TGACCTGAACC ATAACGCACA-3'; and NFATc1, forward 5'-CCAATG AGCCAGGGGATTAG-3' and reverse 5'-GCAGGAGAG GAAAGGTCGTG-3'. The relative expression of the target cellular mRNA was calculated using the $2^{-\Delta\Delta\text{Ct}}$ method.

2.10. Western Blot Assay. Western blotting was performed to determine the possible mechanisms mediating the inhibitory effects of Tet on osteoclastogenesis. The expression levels of $\text{I}\kappa\text{B}\alpha$, p- $\text{I}\kappa\text{B}\alpha$, NF- κB p65, p-NF- κB p65, and β -actin were detected using the following steps: (1) RAW264.7 cells were seeded in 6-well plates at a density of 6×10^5 cells/well until fully grown; they were then pretreated with or without 1.0 μ M Tet for 4 h. Subsequently, 100 ng/mL RANKL was added to stimulate the cells for 0, 15, 30, or 60 min. (2) For the ELISA of the treatment group samples, RAW 264.7 cells were cultured for 5 days and collected; they were then treated with 50 μ L radioimmunoprecipitation assay (RIPA) lysis buffer (Nanjing KeyGen Biotech Co., Ltd., Nanjing, China), containing proteinase and phosphatase inhibitors.

Protein samples (30 μ g) were separated using 10% sodium dodecyl sulfate (SDS)-polyacrylamide gel electrophoresis and transferred to polyvinylidene fluoride (PVDF) membranes; the membranes were blocked by incubating in 5% skim milk in Tris-buffered saline (TBS)-Tween (TBS-T, 10 mM Tris-HCl, 50 mM sodium chloride (NaCl), 0.25% Tween 20) for 1 h. The membrane was incubated overnight at 4°C with primary antibodies ($\text{I}\kappa\text{B}\alpha$, p- $\text{I}\kappa\text{B}\alpha$, NF- κB p65, p-NF- κB p65, all 1 : 1000; and β -actin, 1 : 2000; Cell Signaling Technology). After three rinses with TBS-T, the membranes were incubated with horseradish peroxidase (HRP) anti-rabbit secondary antibody (1 : 5000; Proteintech) for 1 h. The signals were detected via exposure in a Bio-Rad imaging system. Gray levels corresponding to the indicated proteins were quantified and normalized relative to β -actin using ImageJ software.

2.11. Statistical Evaluation. Data processing and statistical analysis were performed using the statistical package for the social sciences (SPSS) 22.0 (IBM Corp., Armonk, NY, USA). Data are expressed as the mean \pm standard error. Measured data were analyzed using analysis of variance, and an independent sample *t*-test was used to compare the groups, followed by Student's *t*-test (comparing two groups) or the least significant difference post hoc test (comparing more

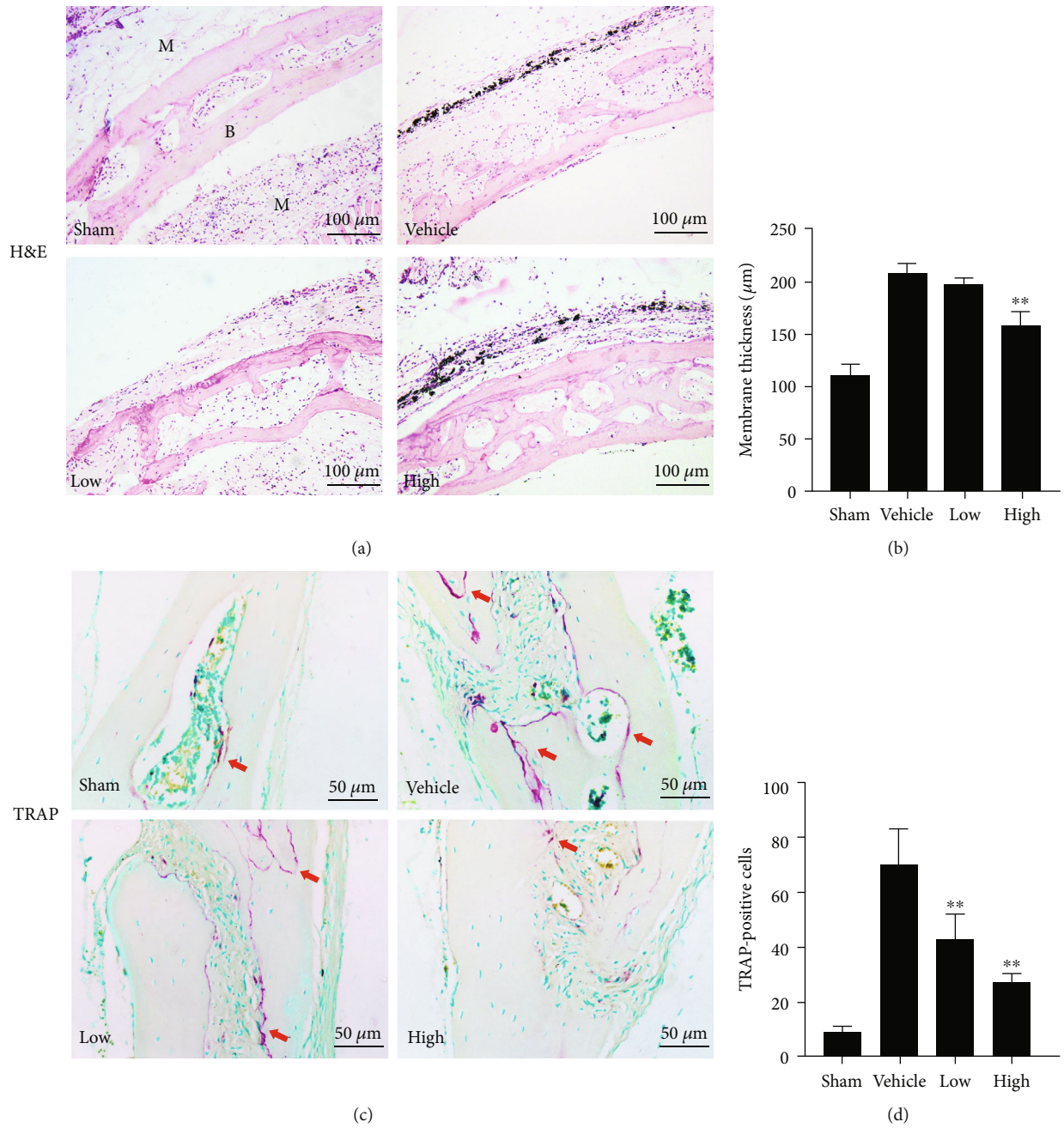


FIGURE 2: Continued.

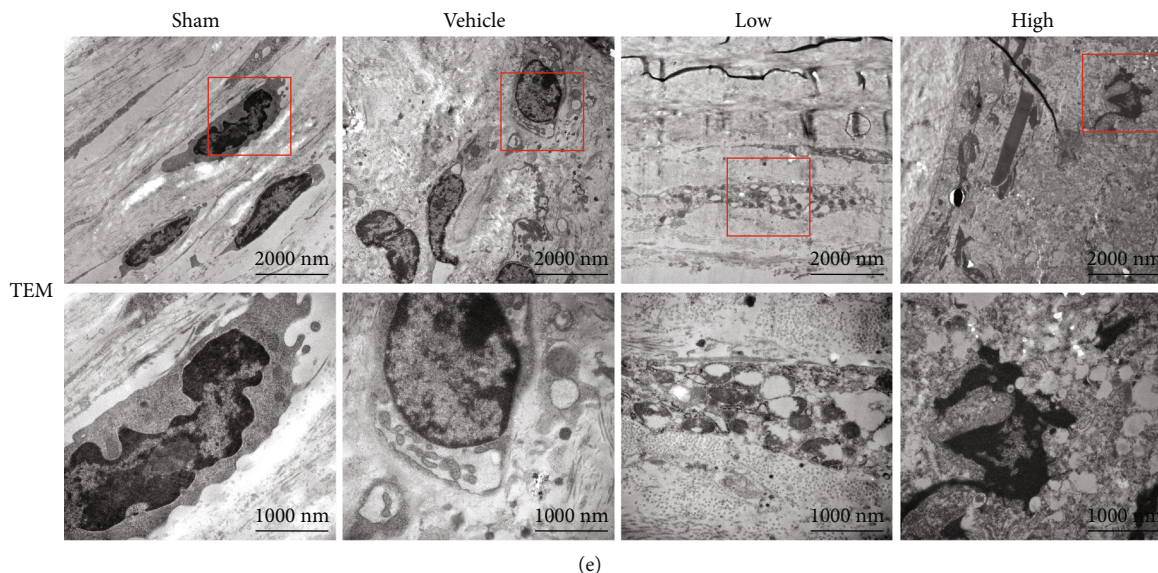


FIGURE 2: Tetrandrine (Tet) prevents Ti particle-induced chronic inflammation and osteolysis *in vivo*. (a) H&E-stained images of the tissue specimen sections in each group observed via light microscopy. (b) Membrane thickness were quantified. (c) TRAP-stained images of the tissue specimen sections in each group observed via light microscopy. (d) TRAP-positive cells were quantified. (e) Transmission electron microscopy (TEM) images of cells in the implanted bones and pouches around Ti particles. The air pouch membrane thickness (μm) and TRAP-positive cell numbers were quantified ($*p < 0.05$, $**p < 0.01$ compared with the vehicle group; $n = 5$ per group). M: membrane; B: bone; H&E: hematoxylin and eosin; TRAP: tartrate-resistant acid phosphatase. The red arrows indicate TRAP-positive cells.

than two groups). Differences were considered statistically significant at $*p < 0.05$ or $**p < 0.01$.

3. Results

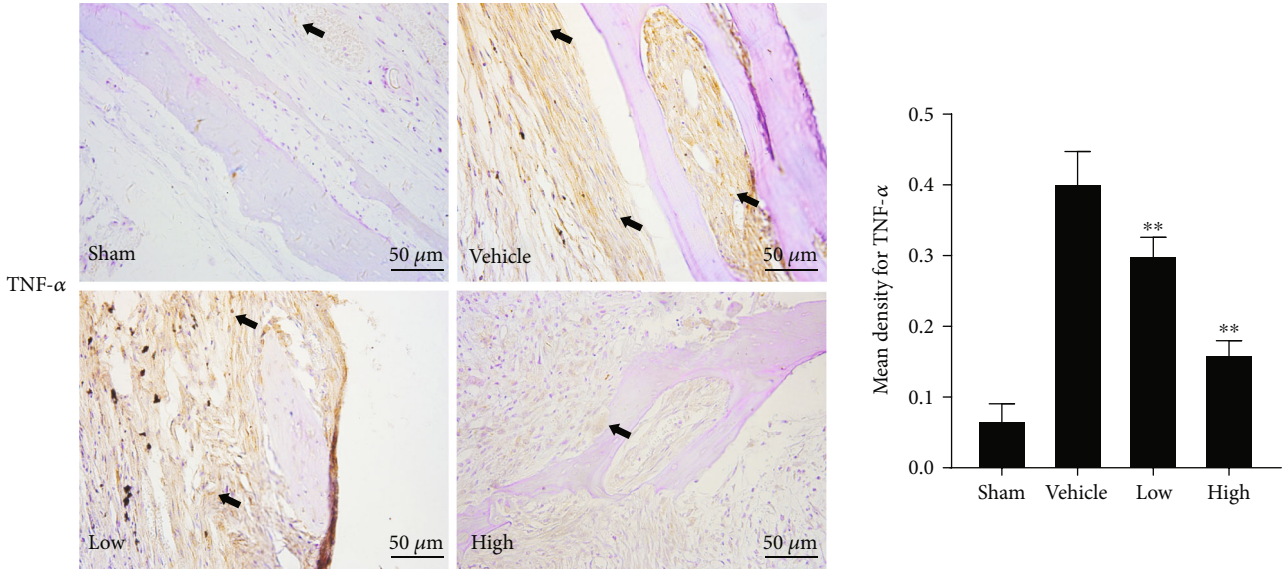
3.1. Tet Ameliorate Ti Particle-Induced Inflammatory Osteolysis In Vivo. To investigate the effect of Tet on Ti particle-induced inflammatory osteolysis, we created air pouches on the backs of BALB/c mice and embedded cranial bone allografts inside; this was followed by the injection of Ti particles. As shown in Figure 2(a), Ti stimulation obviously induced inflammatory reactions and bone erosion, whereas Tet administration significantly suppressed this inflammation and bone destruction in a dose-dependent manner. This was evidenced by the thinner air pouch membranes and fewer erosion pits in the bones of the Tet-treated groups than in those of the vehicle group (Figures 2(a) and 2(b)). In addition, TRAP staining showed a remarkably higher number of osteoclasts on the bone surface of the Ti-treated group than on that of the sham group. However, the number of osteoclasts was significantly decreased following Tet treatment (Figures 2(c) and 2(d)).

TEM was used to observe the ultrastructure of the tissues. As shown in Figure 2(e), the sham group osteoclasts exhibited a fine shape, clear nucleoli, fine chromatin particles, uniform distribution, clear cell boundaries, and few lysosomes, whereas the vehicle group showed multiple active osteoclasts, characterized by a large cell size, rich organelles, numerous rough endoplasmic reticulum and mitochondria in the cytoplasm, and an obvious increase in lysosomes. In contrast, the Tet-treated group showed fewer osteoclasts in the bone tissue than the vehicle group, and the osteoclasts exhibited fewer

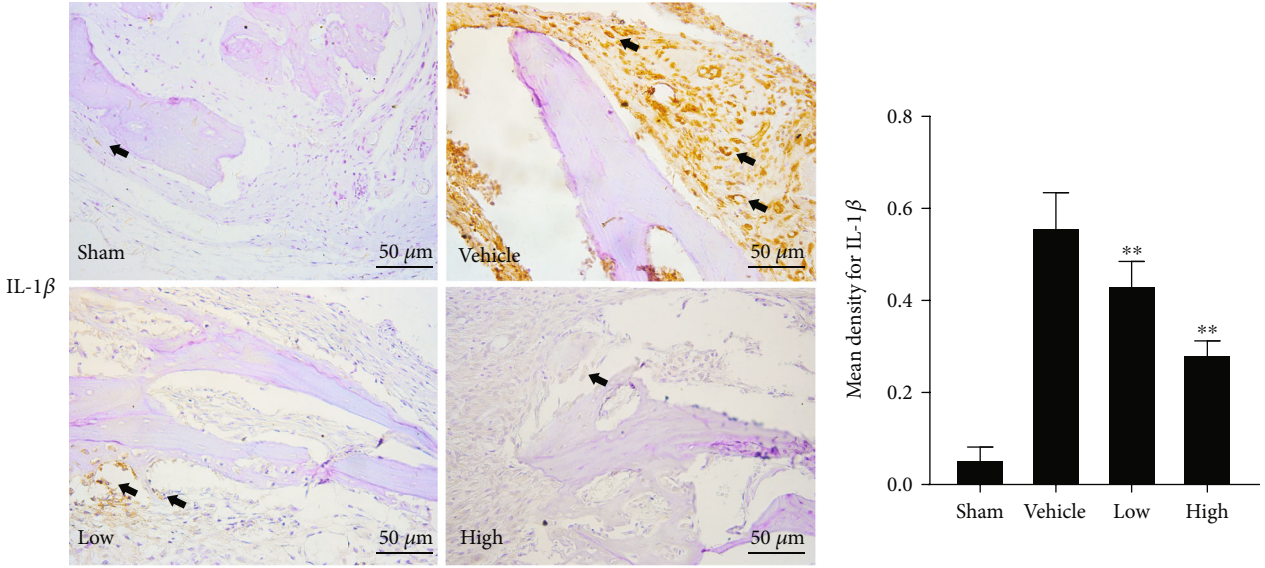
organelles, disorderly arrangement, swollen mitochondria, blurred mitochondrial cristae, damaged mitochondria, and serious cavitation. These results indicate that Tet effectively reduce the inflammatory bone erosion induced by Ti particles *in vivo*, which may be attributed to its inhibitory effect on osteoclast formation.

3.2. Tet Inhibits the Release of Inflammatory Cytokines Associated with Osteolysis In Vivo. Proinflammatory cytokines are believed to contribute to bone resorption through the promotion of osteoclast differentiation [24, 25]. Thus, we evaluated the expression of the following cytokines associated with osteoclastogenesis: TNF- α , IL-1 β , and IL-6. Immunohistochemical analysis revealed that Ti particles drastically increased the expression of TNF- α , IL-1 β , and IL-6 in the bone-graft samples (Figures 3(a)–3(c)). However, Tet treatment significantly and dose-dependently inhibited the expression of TNF- α , IL-1 β , and IL-6. These data demonstrate that Tet inhibits the secretion of proinflammatory cytokines induced by Ti particles *in vivo*.

3.3. Tet Inhibits RANKL-Induced Osteoclast Formation without Cytotoxicity In Vitro. To determine the effect of Tet on osteoclastogenesis, primary BMMs and the osteoclast precursor RAW264.7 cell line were cultured *in vitro*. We first performed a CCK-8 assay to evaluate the cytotoxicity of Tet and then confirmed the safe concentration for the *in vitro* experiments. The results showed that the viability of BMMs and RAW264.7 cells was not affected by Tet at concentrations $< 1.0 \mu\text{M}$ (Figure 4(b)). Then, RANKL-induced BMMs were treated with different concentrations of Tet (0, 0.1, 0.5, and $1.0 \mu\text{M}$) or an equal volume of vehicle for 5 days. We



(a)



(b)

FIGURE 3: Continued.

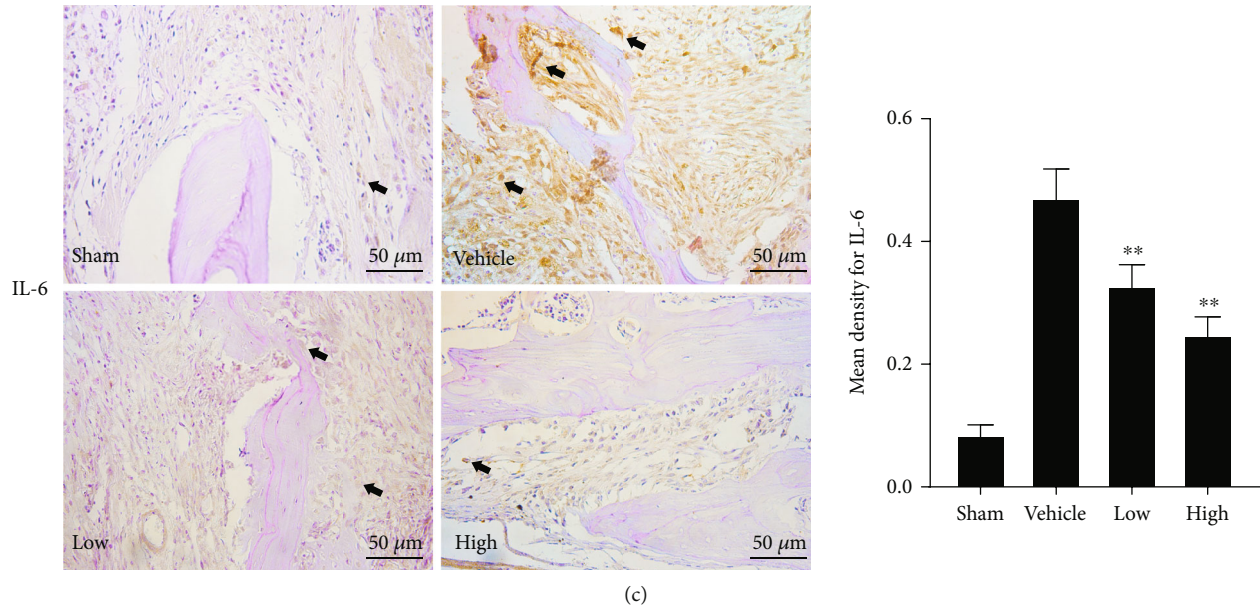


FIGURE 3: Tetrandrine (Tet) inhibits the expression of proinflammatory cytokines. (a) Immunohistochemical staining of tumor necrosis factor (TNF)- α . (b) Immunohistochemical staining of interleukin (IL)-1 β . (c) Immunohistochemical staining of IL-6. The mean density for TNF- α , IL-1 β , and IL-6 were quantified (* $p < 0.05$, ** $p < 0.01$ compared with the vehicle group; $n = 5$ per group). Black arrows indicate positive expression, respectively.

observed that Tet inhibited RANKL-stimulated osteoclast formation in a dose-dependent manner, as indicated by the significantly lower number of TRAP-positive osteoclasts in the Tet-treated groups than in the vehicle group (Figures 4(c) and 4(d)).

To further clarify the stage of the osteoclast formation process affected by Tet, RANKL-induced BMMs were treated with 1.0 μM Tet at different time points (days 0–2, 1–3, 2–4, or days 3–5), and vehicle-treated BMMs were used as the control. The results demonstrated that both the number and total area of Tet-treated osteoclasts were significantly smaller than those of the control in the early periods (days 0–2 and days 1–3). However, no obvious difference was observed with the Tet-treated cells in the later periods (days 2–4 or 3–5) (Figures 4(e) and 4(f)). These results suggest that Tet inhibited RANKL-induced osteoclast formation in the early stage *in vitro*.

3.4. Osteoclastic F-Actin Ring Formation and Bone Resorption Shows That Tet Inhibits Bone Resorption *In Vitro*. The actin cytoskeleton is a decisive structure for the maturation of functional osteoclasts [26]. In line with the results above, treatment with Tet remarkably reduced the size of the F-actin ring in RANKL-stimulated BMMs in a dose-dependent manner (Figure 5(a)). We further verified the effect of Tet on the bone resorption ability of osteoclasts by culturing BMMs in the wells of plates coated with hydroxyapatite. The sizes of the resorption pits were calculated to evaluate the resorption ability of the osteoclasts. As expected, the resorption area was significantly smaller in the groups exposed to Tet than in the control groups, and the effect was dependent on the Tet concentration (Figures 5(b) and 5(c)), indicating that Tet impaired osteoclast bone resorp-

tion. These findings demonstrate that Tet decreased osteoclast formation and subsequent bone resorption *in vitro*.

3.5. Tet Suppresses the Expression of NFATc1, TRAP, TNF- α , and MMP-9 in Osteoclasts. To explore the effect of Tet on the expression of osteoclastogenesis-related proteins, we collected the supernatants of Ti particle-stimulated RAW264.7 cells treated with different concentrations of Tet or the equivalent vehicle daily from days 1 to 5. Cells cultured without Ti particles and Tet were used as the sham group. An ELISA was performed to determine the time course of the secretion of TNF- α and MMP-9, which are involved in osteoclast formation [27]. The results showed that Tet dramatically inhibited TNF- α and MMP-9 secretion in the supernatants at all time points, in a dose-dependent manner (Figure 6(a)).

We further examined the expression of MMP-9, TRAP, and NFATc1, which play a critical role in osteoclast maturation and bone resorption [28, 29]. The real-time PCR showed that the expression of MMP-9, TRAP, and NFATc1 was markedly increased in RAW264.7 cells stimulated with Ti particles, whereas Tet treatment significantly reduced the expression of these genes (Figure 6(b)), which was consistent with the results showing decreased osteoclast formation and bone resorption ability. Thus, these results confirmed the inhibitory effect of Tet on osteoclast differentiation and bone resorption *in vitro*.

3.6. Tet Inhibits the RANKL-Induced Activation of the NF- κB Signaling Pathway. To further elucidate the mechanism underlying the Tet-induced inhibition of osteoclasts, Western blot analysis was conducted to determine its effect on the activation of NF- κB signaling, which is a key regulator of the differentiation and activity of osteoclasts [30]. We

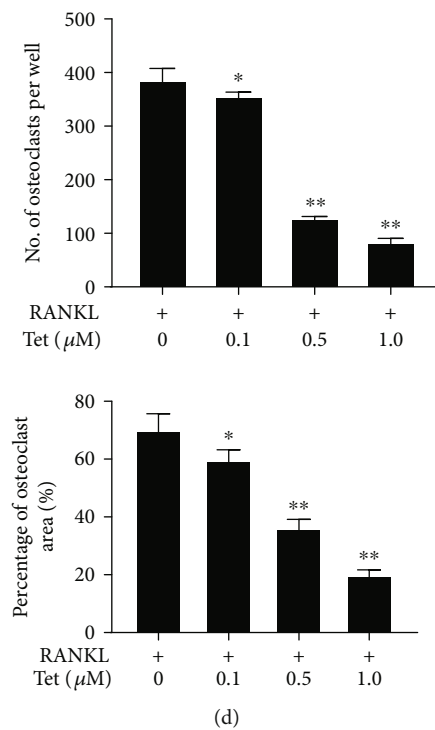
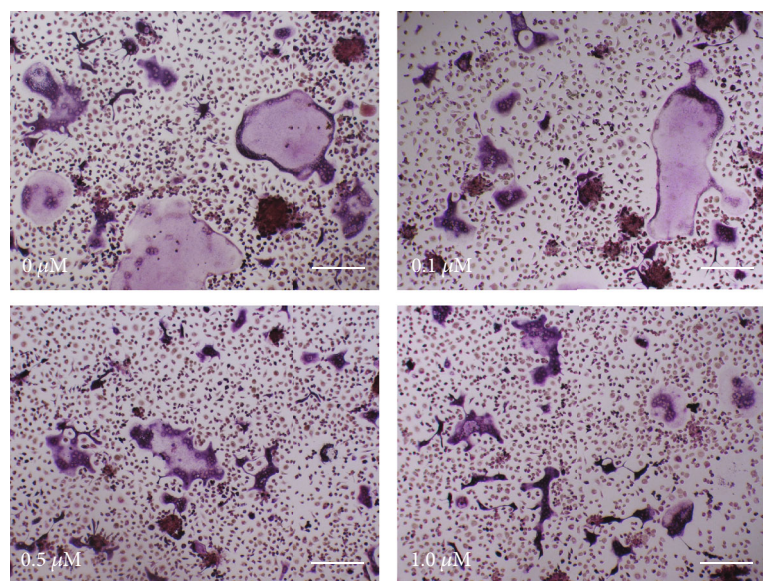
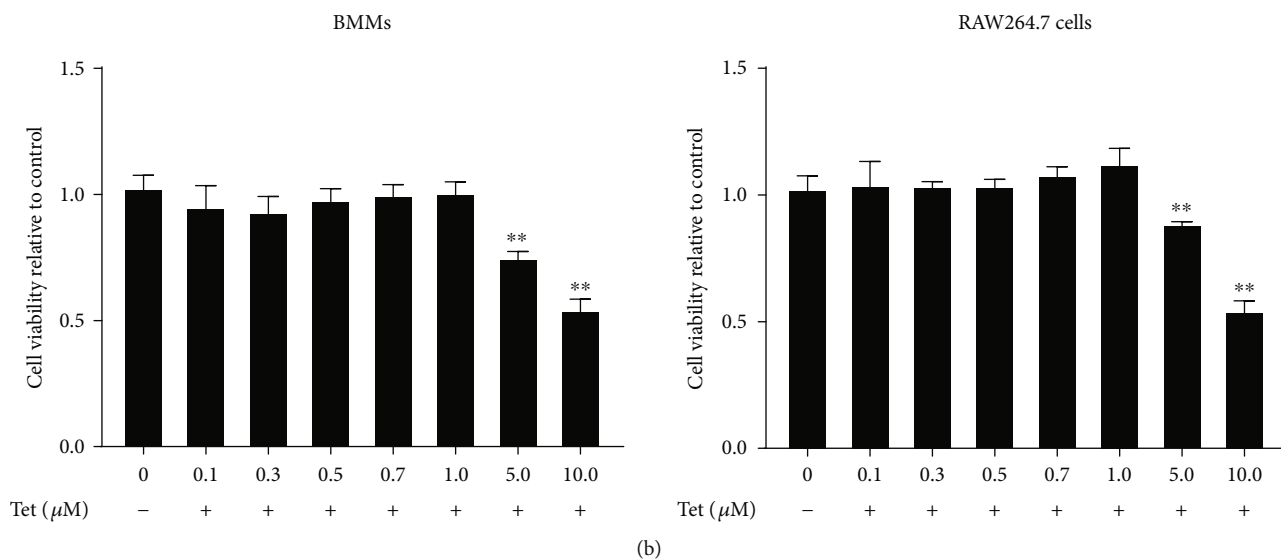
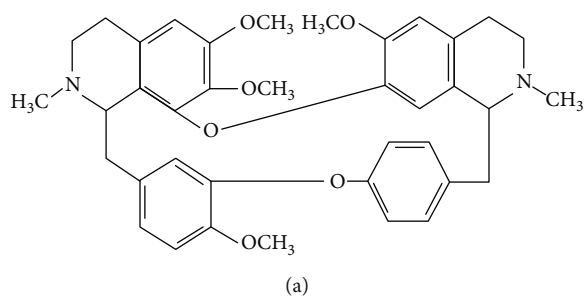


FIGURE 4: Continued.

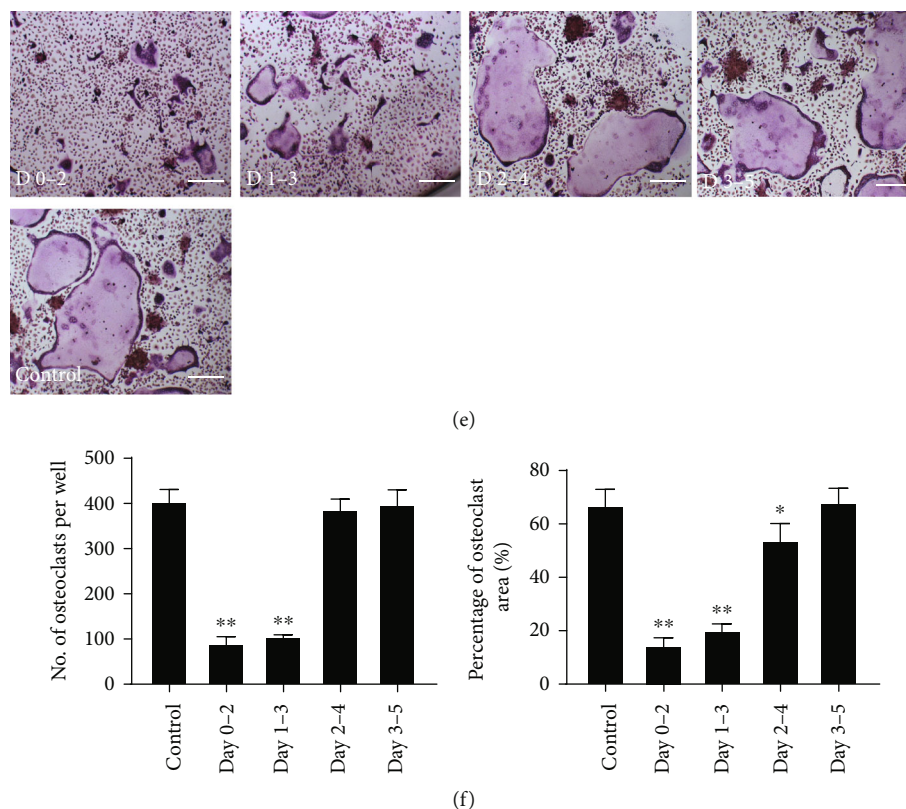


FIGURE 4: Tetrandrine (Tet) inhibits receptor activator for nuclear factor- κ B ligand- (RANKL-) induced osteoclast formation and is not cytotoxic. (a) Chemical structure of Tet. (b) Bone marrow-derived macrophages (BMMs) and RAW264.7 cell viabilities were detected using the cell counting kit-8 (CCK-8) assay, and the results were normalized to the control group (without Tet treatment). (c) BMMs were stimulated with the indicated concentrations of Tet in osteoclast differentiation medium and then fixed and subjected to TRAP staining on day 5 (scale bar = 100 μ m). (d) The number and area of osteoclasts. (e) BMMs were incubated in Dulbecco's modified Eagle's medium (DMEM) supplemented with M-CSF and RANKL, with Tet (1.0 μ M) administered on days 0-2, 1-3, 2-4, or 3-5, and TRAP staining was performed to analyze osteoclast formation (scale bar = 100 μ m). (f) The number and area of osteoclasts. All experiments were repeated three times (* p < 0.05, ** p < 0.01 compared with the control group; n = 5 per group). Data are the means of at least three independent experiments with similar results. TRAP: tartrate-resistant acid phosphatase; BMMs: bone marrow-derived macrophages; M-CSF: macrophage colony-stimulating factor.

examined the phosphorylation levels of the main NF- κ B subunits, I κ B α and p65, in RANKL-induced RAW264.7 cells treated with or without 1.0 μ M Tet at four time points (0, 15, 30, and 60 min). Unsurprisingly, RANKL stimulation obviously induced the phosphorylation of I κ B and p65; however, the expression levels of phosphorylated-I κ B α (p-I κ B α) and p-p65 were significantly decreased in the cells exposed to Tet (Figures 7(a)-7(c)), indicating that Tet suppressed the RANKL-induced activation of the NF- κ B signaling pathway. To further verify the effect of Tet on the NF- κ B pathway, the expression of related proteins was examined in RAW264.7 cells stimulated with Ti and different concentrations of Tet or the vehicle. As shown in Figures 4(d) and 4(e), the expression levels of p-I κ B and p-p65 were negatively correlated with the concentrations of Tet ranging from 0.1 to 1.0 μ M. Therefore, collectively, these and the previous results led us to conclude that Tet may hinder the differentiation and maturation of osteoclasts by inhibiting the NF- κ B signaling pathway.

4. Discussion

Artificial aseptic loosening is one of the main reasons for revision surgery after artificial joint replacement. Aseptic loosening is a process involving complex interplay between mechanical factors, such as poor matching, improper positioning, or aging of the prosthesis, and stress shielding [31]. Recent studies have shown that long-term friction causes the implanted prosthesis to produce tiny particles, which induce the release of inflammatory factors and the activation of osteoclasts, which play an essential role in the osteolysis around the prosthesis [32, 33].

Previously, micron-sized particles were considered the main particles that induce osteolysis, but the introduction of laser capture microdissection technology and TEM has led to the detection of various nanosized particles in loosened boundary membrane tissues, including metal, ceramic granular, and polymer polyethylene nanoparticles. Because nanoparticles are more easily engulfed by phagocytes than other

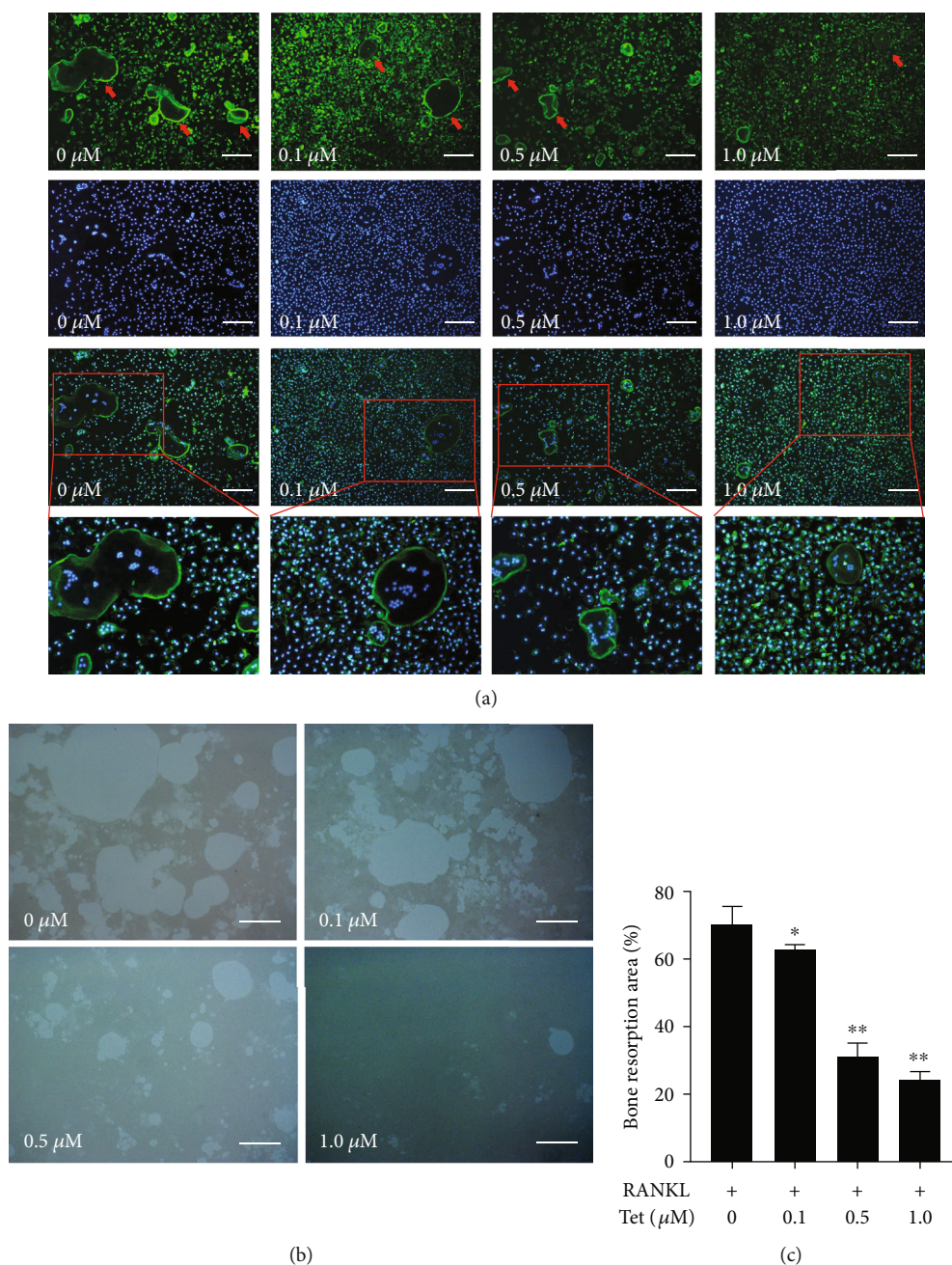


FIGURE 5: Tetrandrine (Tet) decreases osteoclast bone resorption and the formation of F-actin rings. (a) F-actin rings and nuclei were observed under a confocal microscope (scale bar = 100 μm). (b) Images of the bone resorption pits in each group (scale bar = 100 μm). (c) Quantification of bone resorption area (* $p < 0.05$, ** $p < 0.01$ compared with the control group; $n = 4$ per group). Data are the means of at least three independent experiments with similar results. The red arrows indicate the F-actin rings.

particles, they may play a considerably significant role in aseptic loosening. These particles activate NF- κB , mitogen-activated protein kinase (MAPK), and other signaling pathways, initiating the transcriptional expression of inflammatory factors such as TNF- α , IL-1 β , and IL-6 directly or indirectly. These factors induce the differentiation and maturation of osteoclasts and enhance their activity [34].

Presently, progress has been made in studies using bisphosphonate drugs and gene therapy to inhibit the adverse reactions of wear particles, but considerable modifications are still required before their clinical application. In this

study, we established an inflammatory osteolysis mouse model by transplanting cranium grafts into air pouches created in recipient mice, followed by Ti particle stimulation. Pathological changes similar to inflammatory osteolysis were observed, such as increased cellular infiltration and bone erosion. Tet treatment dramatically alleviated the inflammatory reaction and bone destruction, suggesting that it may be a potential agent for the prevention and treatment of osteolysis in artificial aseptic loosening. Although the air pouch osteolysis model is frequently used in wear debris-induced osteolysis studies, they have several limitations, which should not be

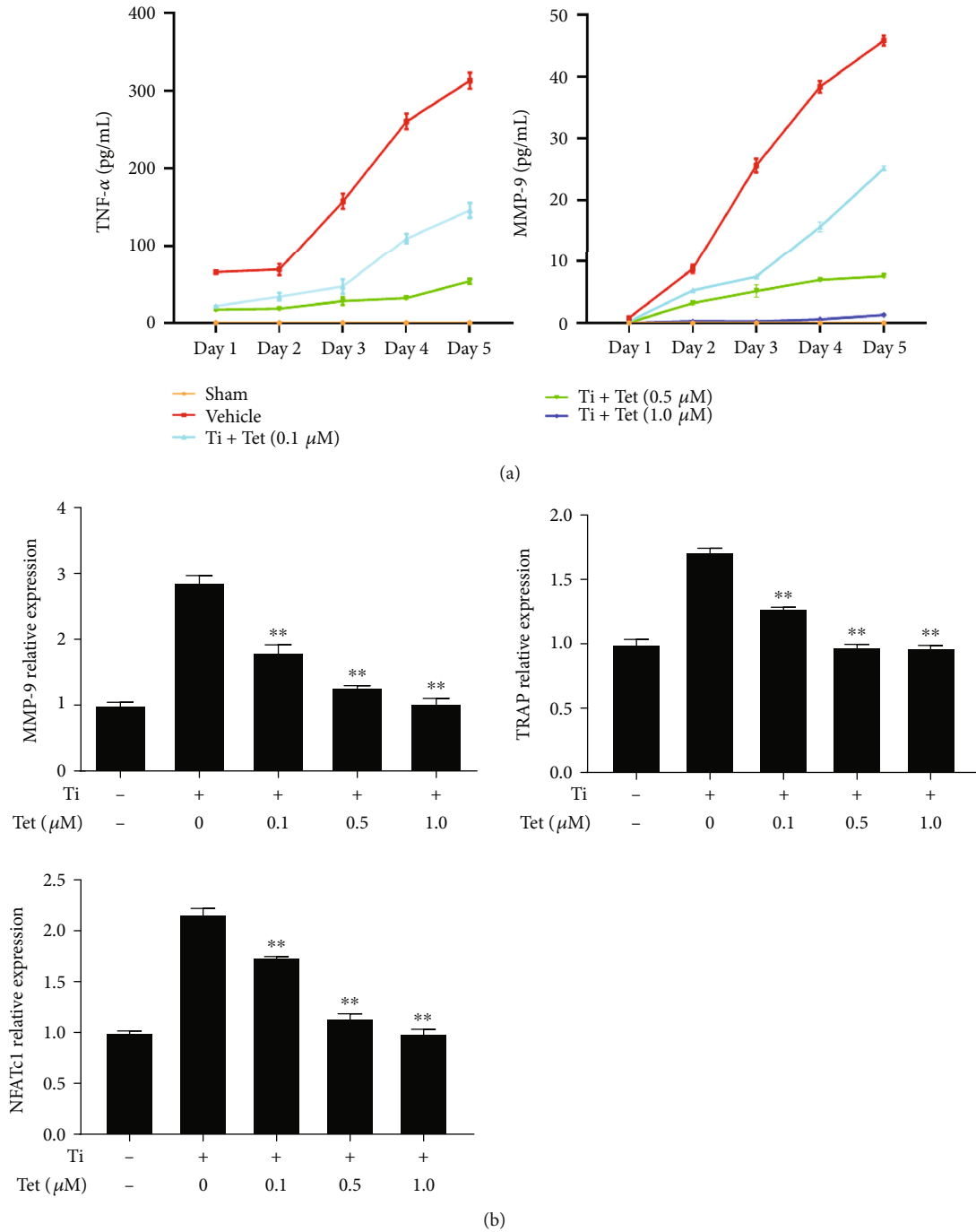


FIGURE 6: Tetrandrine (Tet) reduces the expression of osteoclast-related genes (including nuclear factor of activated T-cells, cytoplasmic 1 (NFATc1), tartrate-resistant acid phosphatase (TRAP), tumor necrosis factor (TNF)-α, and matrix metalloproteinase (MMP)-9). (a) TNF-α and MMP-9 secretion in the supernatant of the RAW264.7 cell culture medium in each group on days 1–5. (b) MMP-9, TRAP, and NFATc1 mRNA expression in each group on day 5 (**p* < 0.05, ***p* < 0.01 compared with the control group; *n* = 3 per group). Data are the means of at least three independent experiments with similar results.

ignored. These include the lack of blood supply to the bone graft and the use of bony surfaces, which are not typically involved in artificial aseptic loosening. It would be better to use a combination of different osteolysis models in the study, such as a calvarial osteolysis model where osteolysis is directly induced in the skull of animals, which we are considering for our future studies.

Recently, traditional herbs and extracts have been receiving increasing attention for the treatment of aseptic loosening of prostheses caused by osteolysis. Tet is a natural substance with a wide range of pharmacological effects, including antifibrosis, antitumor, and anti-inflammatory effects [10, 35–37]. Numerous studies have reported that Tet exerts anti-inflammatory effects through

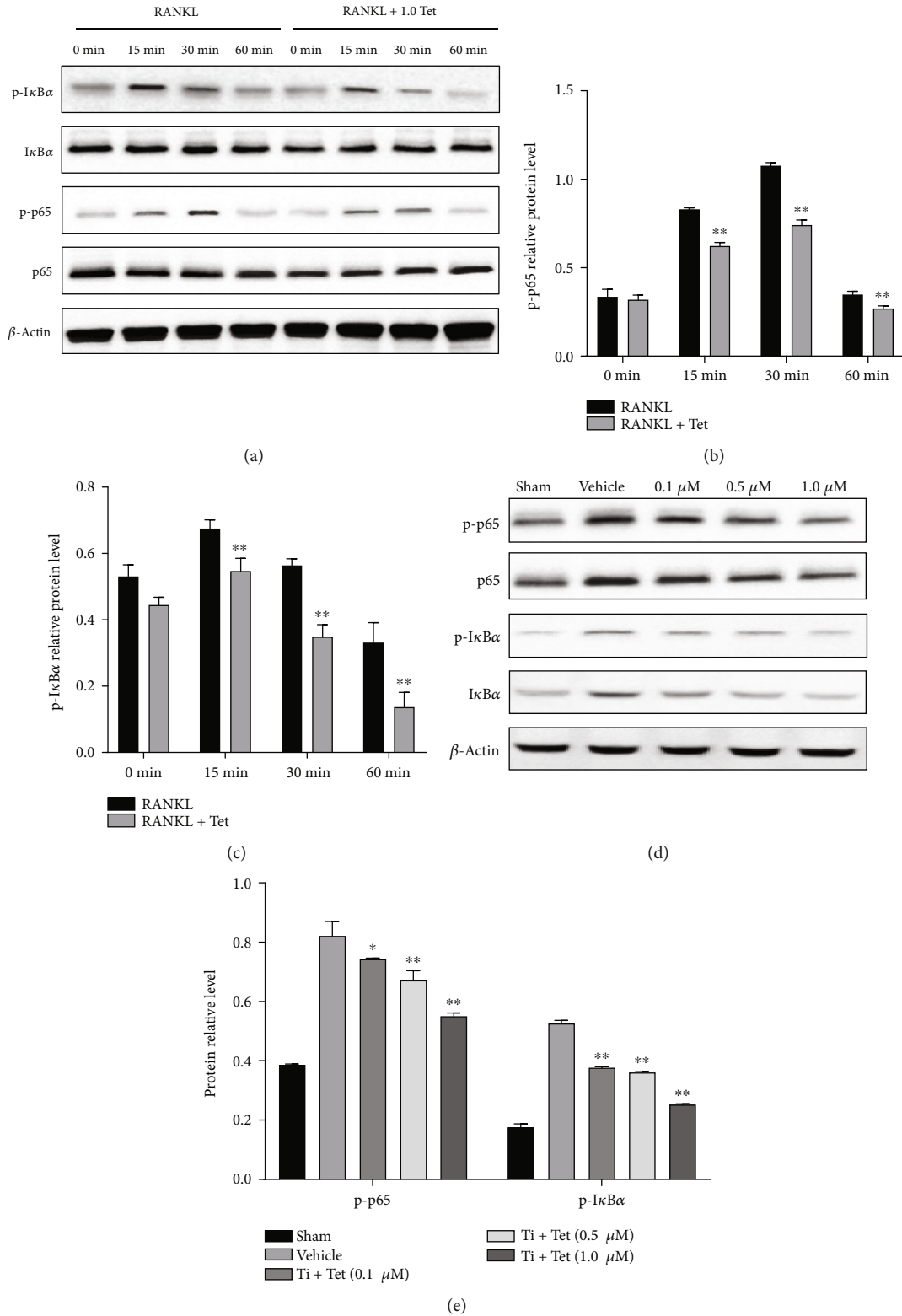


FIGURE 7: Tetrandrine (Tet) inhibits osteoclastogenesis through the nuclear factor (NF)-κB signaling pathway. (a) Protein expression of the NF-κB signaling pathway. (b, c) Gray band levels of the phosphorylated inhibitor of NF-κB α (p-IκBα) (b) and phosphorylated p-65 (p-p65) (c) were analyzed using Image J software. (d) After 5 days of treatment with various Tet concentrations, the cells were lysed for Western blotting, and the gray band levels of p-p65 and IκBα were analyzed using ImageJ software (**p* < 0.05, ***p* < 0.01 compared with the vehicle group; *n* = 3 per group). Data are the means of at least three independent experiments with similar results.

a variety of signaling pathways such as the NF- κ B, phosphoinositide 3-kinase (PI3K), and extracellular signal-regulated kinase (ERK), signal transducer and activator of transcription 3 (STAT3) signaling pathways [11, 38–40]. Guo et al. [41] found that aqueous extracts and alkaloids of *S. tetrandra* inhibited the release of NO, TNF- α , and IL-6, alleviating the LPS-induced inflammatory response in RAW264.7 cells.

NF- κ B is a multifunctional transcription factor that plays a critical role in both inflammation and osteoclast formation [42], suggesting that strategies targeting NF- κ B inhibition may be promising for the treatment of inflammatory osteolysis. In the present study, we found that Tet suppressed the activation of the NF- κ B pathway and relieved both inflammatory reactions and osteoclast formation in mice, indicating that it exerts therapeutic effects via dual functions of hindering inflammation and osteoclastogenesis.

Tet is also known to be a calcium channel blocker. Calcium (Ca^{2+}) signaling is important for multiple osteoclast functions, including gene transcription, differentiation, and bone resorption [43]. RANKL-induced Ca^{2+} oscillation mediates the activation of NFATc1, which is an essential transcription factor for osteoclast differentiation [44]. In this study, Tet administration significantly inhibited osteoclast formation and the mRNA expression of NFATc1 *in vitro*, suggesting that in addition to inhibiting the NF- κ B pathway, Tet may also hamper osteoclast formation by affecting Ca^{2+} signaling. However, we have not examined the role of Tet in Ca^{2+} signaling during osteoclast differentiation. We also cannot exclude the possible involvement of other mechanisms in the effect of Tet on osteoclastogenesis, which warrants further investigation.

We did not examine the toxicity of Tet in animals. Tet has been reported to induce transient toxicity in the kidneys, lungs, and liver of mice following intravenous injection of a single 150 mg/kg dose [45]. However, in this study, no obvious abnormal conditions were observed in mice intraperitoneally administered a single 30 mg/kg dose of Tet. In addition, a clinical study of the efficacy of Tet in patients with lung cancer reported no side effects [46]. Thus, Tet may be considered a safe candidate for clinical application in the treatment of inflammatory osteolysis, which warrants further examination.

5. Conclusions

The findings of this study demonstrated that Tet effectively reduced the inflammation and bone resorption induced by Ti particles *in vivo* and inhibited osteoclast differentiation and formation *in vitro* through the inhibition of NF- κ B signaling. Our study offers novel insights into the mechanism of the established anti-inflammatory and antibone resorption effects of Tet, providing an evidence-based rationale for its potential for use in the treatment of osteolysis developing around implants.

Data Availability

The data used to support the findings of this study are available from the corresponding author upon reasonable request: Desheng Chen: chendesheng@nxmu.edu.cn.

Conflicts of Interest

The authors declare that there is no conflict of interest regarding the publication of this paper.

Acknowledgments

We thank Jie Huang, MD; Yao Luo, MD; and Huiming Ma, PhD, for their helpful discussions; Jia Tian, MD; and Yang Liu, MS, for kindly assisting with the experiments; and Xiaoyu Li, PhD, for revising the draft. This work was supported by the National Science Foundation of China (grant nos. 81760405, 81760395, and 82060408).

References

- [1] A. Neuprez, A. H. Neuprez, J.-F. Kaux et al., “Total joint replacement improves pain, functional quality of life, and health utilities in patients with late-stage knee and hip osteoarthritis for up to 5 years,” *Clinical Rheumatology*, vol. 39, no. 3, pp. 861–871, 2020.
- [2] H. Koivu, I. Kohonen, K. Mattila, E. Loyttyniemi, and H. Tiisanen, “Medium to long-term results of 130 Ankle Evolutionary System total ankle replacements—inferior survival due to peri-implant osteolysis,” *Foot and Ankle Surgery*, vol. 23, no. 2, pp. 108–115, 2017.
- [3] X. Hu, Z. Ping, M. Gan et al., “Theaflavin-3, 3-digallate represses osteoclastogenesis and prevents wear debris-induced osteolysis via suppression of ERK pathway,” *Acta Biomaterialia*, vol. 48, pp. 479–488, 2017.
- [4] B. A. McArthur, R. Scully, F. Patrick Ross, M. P. G. Bostrom, and A. Falghren, “Mechanically induced periprosthetic osteolysis: a systematic review,” *HSS Journal*®, vol. 15, no. 3, pp. 286–296, 2019.
- [5] W. Wozniak, J. Markuszewski, M. Wierusz-Kozłowska, and H. Wysocki, “Neutrophils are active in total joint implant loosening,” *Acta Orthopaedica Scandinavica*, vol. 75, no. 5, pp. 549–553, 2009.
- [6] D. S. Amarasekara, H. Yun, S. Kim, N. Lee, H. Kim, and J. Rho, “Regulation of osteoclast differentiation by cytokine networks,” *Immune network*, vol. 18, no. 1, 2018.
- [7] M. Ponzetti and N. Rucci, “Updates on osteoimmunology: what’s new on the cross-talk between bone and immune system,” *Frontiers in Endocrinology*, vol. 10, p. 236, 2019.
- [8] S. An, F. Han, Y. Hu, Y. Liu, J. Li, and L. Wang, “Curcumin inhibits polyethylene-induced osteolysis via repressing NF- κ B signaling pathway activation,” *Cellular Physiology and Biochemistry*, vol. 50, no. 3, pp. 1100–1112, 2018.
- [9] Y. Zhang, S. Xu, K. Li et al., “mTORC1 inhibits NF- κ B/NFATc1 signaling and prevents osteoclast precursor differentiation, *in vitro* and *in mice*,” *Journal of Bone and Mineral Research*, vol. 32, no. 9, pp. 1829–1840, 2017.
- [10] N. Bhagya and K. R. Chandrashekar, “Tetrandrine – A molecule of wide bioactivity,” *Phytochemistry*, vol. 125, pp. 5–13, 2016.
- [11] L. N. Gao, Q. S. Feng, X. F. Zhang, Q. S. Wang, and Y. L. Cui, “Tetrandrine suppresses articular inflammatory response by inhibiting pro-inflammatory factors via NF- κ B inactivation,” *Journal of Orthopaedic Research*, vol. 34, no. 9, pp. 1557–1568, 2016.

- [12] S. Sandmann and T. Unger, "L- and T-type calcium channel blockade—the efficacy of the calcium channel antagonist mibefradil," *Journal of Clinical and Basic Cardiology*, vol. 2, no. 2, pp. 187–201, 1999.
- [13] S. Zhang, H. Li, H. Tang et al., "Felodipine blocks osteoclast differentiation and ameliorates estrogen-dependent bone loss in mice by modulating p38 signaling pathway," *Experimental Cell Research*, vol. 387, no. 2, p. 111800, 2020.
- [14] H. Shimizu, H. Nakagami, N. Yasumasa et al., "Cilnidipine, but not amlodipine, ameliorates osteoporosis in ovariectomized hypertensive rats through inhibition of the N-type calcium channel," *Hypertension Research*, vol. 35, no. 1, pp. 77–81, 2012.
- [15] H. Shimizu, H. Nakagami, N. Yasumasa et al., "Links between hypertension and osteoporosis: benidipine ameliorates osteoporosis in ovariectomized hypertensive rats through promotion of osteoblast proliferation and inhibition of osteoclast differentiation," *Current Cardiovascular Risk Reports*, vol. 6, no. 4, pp. 274–280, 2012.
- [16] T. Takahashi, Y. Tonami, M. Tachibana et al., "Tetrandrine prevents bone loss in sciatic-neurectomized mice and inhibits receptor activator of nuclear factor κ B ligand-induced osteoclast differentiation," *Biological and Pharmaceutical Bulletin*, vol. 35, no. 10, pp. 1765–1774, 2012.
- [17] Y. Jia, Y. Miao, M. Yue, M. Shu, Z. Wei, and Y. Dai, "Tetrandrine attenuates the bone erosion in collagen-induced arthritis rats by inhibiting osteoclastogenesis via spleen tyrosine kinase," *The FASEB Journal*, vol. 32, no. 6, pp. 3398–3410, 2018.
- [18] D. Chen, X. Zhang, Y. Guo et al., "MMP-9 inhibition suppresses wear debris-induced inflammatory osteolysis through downregulation of RANK/RANKL in a murine osteolysis model," *International Journal of Molecular Medicine*, vol. 30, no. 6, pp. 1417–1423, 2012.
- [19] D. Chen, Y. Li, F. Guo et al., "Protective effect of p38 MAPK inhibitor on wear debris-induced inflammatory osteolysis through downregulating RANK/RANKL in a mouse model," *Genetics and Molecular Research*, vol. 14, no. 1, pp. 40–52, 2015.
- [20] Z. Zhang, T. Liu, M. Yu, K. Li, and W. Li, "The plant alkaloid tetrandrine inhibits metastasis via autophagy-dependent Wnt/ β -catenin and metastatic tumor antigen 1 signaling in human liver cancer cells," *Journal of Experimental & Clinical Cancer Research*, vol. 37, no. 1, p. 7, 2018.
- [21] J. Huang, H. Yin, S.-S. Rao et al., "Harmine enhances type H vessel formation and prevents bone loss in ovariectomized mice," *Theranostics*, vol. 8, no. 9, pp. 2435–2446, 2018.
- [22] P. H. Wooley, R. Morren, J. Andary et al., "Inflammatory responses to orthopaedic biomaterials in the murine air pouch," *Biomaterials*, vol. 23, no. 2, pp. 517–526, 2002.
- [23] A. Sawyer, P. Lott, J. Titrud, and J. McDonald, "Quantification of tartrate resistant acid phosphatase distribution in mouse tibiae using image analysis," *Biotechnic & Histochemistry*, vol. 78, no. 5, pp. 271–278, 2009.
- [24] D. S. Amarasekara, J. Yu, and J. Rho, "Bone loss triggered by the cytokine network in inflammatory autoimmune diseases," *Journal of immunology research*, vol. 2015, Article ID 832127, 12 pages, 2015.
- [25] R. Baum and E. M. Gravallese, "Impact of inflammation on the osteoblast in rheumatic diseases," *Current Osteoporosis Reports*, vol. 12, no. 1, pp. 9–16, 2014.
- [26] A. Qin, T. S. Cheng, Z. Lin et al., "Prevention of wear particle-induced osteolysis by a novel V-ATPase inhibitor saliphenylhalamide through inhibition of osteoclast bone resorption," *PLoS ONE*, vol. 7, no. 4, 2012.
- [27] J. Y. Kim, S. H. Park, J. M. Baek et al., "Harpagoside inhibits RANKL-induced osteoclastogenesis via Syk-Btk-PLC γ 2-Ca2+ signaling pathway and prevents inflammation-mediated bone loss," *Journal of Natural Products*, vol. 78, no. 9, pp. 2167–2174, 2015.
- [28] J. H. Kim and N. Kim, "Regulation of NFATc1 in osteoclast differentiation," *Journal of bone metabolism*, vol. 21, no. 4, pp. 233–241, 2014.
- [29] F. Zhang, H. Tanaka, T. Kawato et al., "Interleukin-17A induces cathepsin K and MMP-9 expression in osteoclasts via celecoxib-blocked prostaglandin E2 in osteoblasts," *Biochimie*, vol. 93, no. 2, pp. 296–305, 2011.
- [30] D. V. Novack, "Role of NF- κ B in the skeleton," *Cell Research*, vol. 21, no. 1, pp. 169–182, 2011.
- [31] M. Bahraminasab, B. B. Sahari, K. L. Edwards, F. Farahmand, and M. Arumugam, "Aseptic loosening of femoral components – Materials engineering and design considerations," *Materials & Design*, vol. 44, pp. 155–163, 2013.
- [32] H. Shao, J. Shen, M. Wang et al., "Icariin protects against titanium particle-induced osteolysis and inflammatory response in a mouse calvarial model," *Biomaterials*, vol. 60, pp. 92–99, 2015.
- [33] S. Zhu, X. Hu, Y. Tao et al., "Strontium inhibits titanium particle-induced osteoclast activation and chronic inflammation via suppression of NF- κ B pathway," *Scientific Reports*, vol. 6, no. 1, 2016.
- [34] C. Yang, W. Liu, H. Shan et al., "Naringin inhibits titanium particles-induced up-regulation of TNF- α and IL-6 via the p38 MAPK pathway in fibroblasts from hip periprosthetic membrane," *Connective Tissue Research*, pp. 1–10, 2020.
- [35] Y. Jiang, M. Liu, H. Liu, and S. Liu, "A critical review: traditional uses, phytochemistry, pharmacology and toxicology of *Stephania tetrandra* S. Moore (Fen Fang Ji)," *Phytochemistry Reviews*, vol. 19, no. 2, pp. 449–489, 2020.
- [36] J. Zhang, Y. Wang, S. Zhang, J. Li, and H. Fang, "Effects of tetrandrine combined with acetylcysteine on exercise tolerance, pulmonary function and serum TNF- β 1 and MMP-7 in silicosis patients," *Experimental and Therapeutic Medicine*, vol. 19, no. 3, pp. 2195–2201, 2020.
- [37] N. Bhagya and K. R. Chandrashekar, "Tetrandrine and cancer – An overview on the molecular approach," *Biomedicine & Pharmacotherapy*, vol. 97, pp. 624–632, 2018.
- [38] C. J. Wu, Y. H. Wang, C. J. Lin, H. H. Chen, and Y. J. Chen, "Tetrandrine down-regulates ERK/NF- κ B signaling and inhibits activation of mesangial cells," *Toxicology In Vitro*, vol. 25, no. 8, pp. 1834–1840, 2011.
- [39] J. Xu, D. Liu, Q. Yin, and L. Guo, "Tetrandrine suppresses β -glucan-induced macrophage activation via inhibiting NF- κ B, ERK and STAT3 signaling pathways," *Molecular Medicine Reports*, vol. 13, no. 6, pp. 5177–5184, 2016.
- [40] G. Bao, C. Li, L. Qi, N. Wang, and B. He, "Tetrandrine protects against oxygen-glucose-serum deprivation/reoxygenation-induced injury via PI3K/AKT/NF- κ B signaling pathway in rat spinal cord astrocytes," *Biomedicine & Pharmacotherapy*, vol. 84, pp. 925–930, 2016.
- [41] C. Guo, M. Wang, J. Li et al., "Effect of inflammatory cytokines in the LPS-induced RAW264. 7 cells by the decoction and its

- split components from *Stephania tetrandra* S. Moore,” *Acta Chinese Medicine and Pharmacology*, vol. 43, pp. 33–36, 2015.
- [42] G. Mbalaviele, D. V. Novack, G. Schett, and S. L. Teitelbaum, “Inflammatory osteolysis: a conspiracy against bone,” *The Journal of Clinical Investigation*, vol. 127, no. 6, pp. 2030–2039, 2017.
- [43] S. Y. Hwang and J. W. Putney Jr., “Calcium signaling in osteoclasts,” *Biochimica et Biophysica Acta (BBA)-Molecular Cell Research*, vol. 1813, no. 5, pp. 979–983, 2011.
- [44] R. E. Dolmetsch, R. S. Lewis, C. C. Goodnow, and J. I. Healy, “Differential activation of transcription factors induced by Ca²⁺ response amplitude and duration,” *Nature*, vol. 386, no. 6627, pp. 855–858, 1997.
- [45] J. P. Shi, S. X. Li, Z. L. Ma, A. L. Gao, Y. J. Song, and H. Zhang, “Acute and sub-chronic toxicity of tetrandrine in intravenously exposed female BALB/c mice,” *Chinese Journal of Integrative Medicine*, vol. 22, no. 12, pp. 925–931, 2016.
- [46] W. Liu, J. Zhang, C. Ying et al., “Tetrandrine combined with gemcitabine and Cisplatin for patients with advanced non-small cell lung cancer improve efficacy,” *International journal of biomedical science: IJBS*, vol. 8, no. 1, p. 28, 2012.

Research Article

Negligible Effect of Estrogen Deficiency on Development of Skeletal Changes Induced by Type 1 Diabetes in Experimental Rat Models

Aleksandra Janas ¹, Ewa Kruczek,¹ Piotr Londzin ¹, Sławomir Borymski ²,
Zenon P. Czuba ³ and Joanna Folwarczna ¹

¹Department of Pharmacology, Faculty of Pharmaceutical Sciences in Sosnowiec, Medical University of Silesia, Katowice, Poland

²Institute of Biology, Biotechnology and Environmental Protection, Faculty of Natural Sciences,
University of Silesia in Katowice, Poland

³Department of Microbiology and Immunology, Faculty of Medical Sciences in Zabrze, Medical University of Silesia,
Katowice, Poland

Correspondence should be addressed to Joanna Folwarczna; jfolwarczna@sum.edu.pl

Received 14 May 2020; Revised 9 July 2020; Accepted 5 August 2020; Published 6 November 2020

Guest Editor: Michaela Tencerova

Copyright © 2020 Aleksandra Janas et al. This is an open access article distributed under the Creative Commons Attribution License, which permits unrestricted use, distribution, and reproduction in any medium, provided the original work is properly cited.

Although postmenopausal osteoporosis often occurs concurrently with diabetes, little is known about interactions between estrogen deficiency and hyperglycemia in the skeletal system. In the present study, the effects of estrogen deficiency on the development of biochemical, microstructural, and mechanical changes induced by streptozotocin-induced diabetes mellitus (DM) in the rat skeletal system were investigated. The experiments were carried out on nonovariectomized (NOVX) and ovariectomized (OVX) control and diabetic mature female Wistar rats. Serum levels of bone turnover markers (CTX-I and osteocalcin) and 23 cytokines, bone mass and mineralization, histomorphometric parameters, and mechanical properties of cancellous and compact bone were determined. The results were subjected to two-way ANOVA and principal component analysis (PCA). Estrogen deficiency induced osteoporotic changes, with increased bone resorption and formation, and worsening of microstructure (femoral metaphyseal BV/TV decreased by 13.0%) and mechanical properties of cancellous bone (the maximum load in the proximal tibial metaphysis decreased by 34.2%). DM in both the NOVX and OVX rats decreased bone mass, increased bone resorption and decreased bone formation, and worsened cancellous bone microarchitecture (for example, the femoral metaphyseal BV/TV decreased by 17.3% and 18.1%, respectively, in relation to the NOVX controls) and strength (the maximum load in the proximal tibial metaphysis decreased by 35.4% and 48.1%, respectively, in relation to the NOVX controls). Only in the diabetic rats, profound increases in some cytokine levels were noted. In conclusion, the changes induced by DM in female rats were only slightly intensified by estrogen deficiency. Despite similar effects on bone microstructure and strength, the influence of DM on the skeletal system was based on more profound systemic homeostasis changes than those induced by estrogen deficiency.

1. Introduction

Osteoporosis is a serious public health problem, leading, in developed countries, to fragility fractures in one of three women and in one of five men aged over 50 years [1]. Painful and disabling osteoporotic fractures not only worsen the quality of life but lead to premature death [2]. The main cause of

osteoporosis is estrogen deficiency in postmenopausal women; however, other factors contribute to the development of the disease, including, among others, immobilization, administration of glucocorticosteroids, or diabetes [3].

There are two main types of diabetes: type 1 diabetes (T1D), with β -cell destruction and insulin deficiency, and type 2 diabetes (T2D), with progressive defect of insulin

secretion on the background of insulin resistance [4]. Both types lead to numerous complications, including disorders of bone metabolism with increased fracture rate [5–7]. T1D, concerning about 5–10% of all diabetes cases, occurs in younger people, whereas T2D usually develops at a later age [4]. It is likely for T2D to occur concurrently with estrogen deficiency in postmenopausal women. However, increased life expectancy in T1D patients, resulting from the progress in the insulin therapy, increases the probability of its coexistence with postmenopausal osteoporosis.

It has been estimated that the trajectories of the epidemiology of diabetes and osteoporosis are similar, and the increase in the number of diabetic patients will contribute to the increase in the number of patients with osteoporosis induced by diabetes [8]. The clinical data on interactions between changes induced by estrogen deficiency and diabetes, concerning the skeletal system, are not abundant [9]. Also, little is known about interactions between estrogen deficiency and hyperglycemia in terms of effects on the skeletal system in experimental conditions *in vivo*.

Different experimental models are used in the preclinical bone pharmacology to investigate the effects of potential treatments on the development of osteoporotic changes. The well-established and almost fully adequate model of estrogen deficiency-induced postmenopausal osteoporosis is a model of bilaterally ovariectomized rats or mice [10]. The most widely used experimental model of T1D is diabetes induced by the administration of streptozotocin (STZ) in rats or mice (single *i.v.* or *i.p.* injection), which induces the destruction of pancreatic β -cells and severe hyperglycemia [11, 12]. As far as T2D is concerned, there are numerous different murine models used, none of them adequately mirroring the changes developing in the disease [13, 14].

The number of reports on the skeletal effects of diabetes in experimental models of estrogen deficiency is scarce. Up to very recently, there were early reports available, concerning mostly the effect on bone mineral density (BMD) and bone turnover markers [15–19]. However, in the last years, several reports have been published, shedding more light on the pathogenesis of changes developing under the influence of both pathologies in rodents [20–27].

The aim of the study was to evaluate the effects of estrogen deficiency on the development of biochemical, microstructural, and mechanical changes induced by T1D in the rat skeletal system. Taking into account the established role of some cytokines in the regulation of bone remodeling, we investigated the effects of estrogen deficiency and diabetes on the serum levels of a wide panel of cytokines, including both proinflammatory and anti-inflammatory ones.

2. Materials and Methods

2.1. Animals and Chemicals. Female Wistar rats were obtained from the Center of Experimental Medicine, Medical University of Silesia, Katowice, Poland. All procedures were approved by the Local Ethics Commission, Katowice, Poland (permission numbers: 9/2015 and 149/2015). The rats were maintained under monitored standard laboratory conditions according to the European Union guidelines (directive

2010/63/EU), in standard plastic cages (Tecniplast, Buguggiate, Italy), four–five rats per cage, under a 12 h light–12 h dark cycle (light on 7:00 a.m.). The experiment started after the acclimatization. The rats were 3 months old.

During the experiment, the following drugs were used: a drug used for the induction of T1D: streptozotocin (STZ; Cayman Chemical Company, Ann Arbor, MI, USA); drugs used in order to mark the calcification front: tetracycline hydrochloride (Sigma-Aldrich Co., St. Louis, MO, USA) and calcein (Sigma-Aldrich Co., St. Louis, MO, USA); drugs used for general anesthesia: ketamine (Bioketan; Vetoquinol Biowet Sp. z o.o., Gorzów Wielkopolski, Poland) and xylazine (Xylapan; Vetoquinol Biowet Sp. z o.o., Gorzów Wielkopolski, Poland). The rats were fed a standard laboratory diet (Labofeed B; Wytwórnia Pasz “Morawski”, Kcynia, Poland).

The experiments were performed on rats divided into the following groups ($n = 9 - 10$):

- (I) – Nonovariectomized control rats (NOVX)
- (II) – Ovariectomized control rats (OVX)
- (III) – Nonovariectomized rats with type 1 diabetes (DM-NOVX)
- (IV) – Ovariectomized rats with type 1 diabetes (DM-OVX)

The initial body mass of the rats before the start of the procedures was similar. The bilateral ovariectomy was performed under ketamine-xylazine (*i.p.*) anesthesia. T1D was induced by a single dose of STZ (60 mg/kg *i.p.*, dissolved in 0.1 M citrate buffer), administered three days after the bilateral ovariectomy was performed. A week after the ovariectomy, the first measurement of nonfasting blood glucose level took place in order to confirm the development of diabetes, using an Accu-Chek Performa Nano glucometer (Roche Diagnostics GmbH, Mannheim, Germany) and Accu-Chek Performa test strips (Roche Diabetes Care, Mannheim, Germany). The blood samples for the measurement were taken from the tail vessels of conscious rats by cutting the tail tip. Rats with the blood glucose level above 400 mg/100 mL were regarded as diabetic. Nonfasting blood glucose level was then measured once a week. The rats were weighed once a week, and, furthermore, on the day before the end of the experiment. Moreover, since all the rats served as controls in a bigger study, they were subcutaneously administered saline (1 mL/kg/day), starting one week after the ovariectomy. In order to label the calcification front, tetracycline hydrochloride at a dose of 20 mg/kg *i.p.* was administered seven days after the ovariectomy, and then calcein (10 mg/kg *i.p.*) was administered three weeks after the administration of tetracycline hydrochloride.

The experiment was terminated five weeks after the ovariectomy. The rats were fasted, anesthetized with the *i.p.* administration of the mixture of ketamine and xylazine, and sacrificed by cardiac exsanguination. After the vital functions ceased, the liver, thymus, uterus, adrenal glands, and bones (right and left tibias, right and left femurs, L4 vertebra)

were isolated. The soft organs and left bones and vertebrae, after cleaning from soft tissues, were weighed on an Ohaus analytical balance model Adventurer Pro type AV264CM (Ohaus Europe GmbH, Greifensee, Switzerland). The length and diameter in the midlength of the left tibias and left femurs were measured using a digital caliper (VOREL 15240, Toya, Wrocław, Poland). The left femurs, left tibias, and the proximal part of the right femurs, cut in the middle of the bone length, were wrapped in gauze soaked with saline and stored below -20°C [28]. Blood serum was frozen at -80°C until subjected to further measurements.

2.2. Bone Mechanical Properties Studies. The mechanical properties of bones were evaluated with an Instron 3342 500N apparatus (Instron, Norwood, MA, USA). Bluehill 2 software (version 2.14; Instron, Norwood, MA, USA) was used for data analysis. Mechanical properties were assessed with the use of three-point bending tests in the left proximal tibial metaphysis and the left femoral diaphysis (test parameters: displacement rate of 0.01 mm/s, sampling rate of 100 Hz), as previously described [28–30].

To evaluate the strength of the proximal tibial metaphysis, the proximal epiphysis was removed, and the load was applied perpendicularly to the long axis of the bone 3 mm from its proximal edge [29, 30]. The following parameters were determined based on the load-displacement curves obtained for each bone: Young's modulus and the load, displacement, energy, and stress for the yield point (0.05% offset), maximum load point, and fracture point. In order to calculate the intrinsic (independent of bone size and shape) parameters: stress and Young's modulus, the tibial metaphysis was assumed to be a circular beam and its diameter measured with a digital caliper.

To determine the mechanical properties of the femoral diaphysis [28, 30], the load was applied perpendicularly to the diaphysis in the middle of the bone length, with the distance between the supporting points of 16 mm. The same parameters were determined as for the tibial metaphysis; the calculations were based on the assumption that the femoral diaphysis was an elliptical pipe. For calculations, the internal and external diameters of the right femoral diaphysis were measured in histological preparations of the transverse cross-section of the right femur in the midlength, with the use of the set consisting of a Carl Zeiss Axio Imager.A1 microscope (Carl Zeiss, Göttingen, Germany) connected with an Olympus DP71 camera (Olympus, Tokyo, Japan) and a computer with OsteoMeasure XP 1.3.0.1 software (OsteoMetrics Inc., Decatur, GA, USA), with a graphics tablet (model Cintiq 22HD; Wacom, Kazo, Japan).

The strength of the femoral neck was studied using a compression test [30]. The load was applied to the head of the femur along the long axis of the bone. The maximum load (inducing fracture) was measured.

2.3. Bone Composition and Mineralization Studies. After performing the mechanical tests, left tibias and femurs and L4 vertebrae were lyophilized for ten days in FreeZone 6 lyophilizer (temperature: -51°C , pressure: 0.03 mBa; Labconco, Kansas City, MO, USA) and then mineralized at 640°C for

48 hours in a muffle furnace L9/11/C6 (Nabertherm, Lilienthal, Germany). The lyophilized and mineralized bones were weighed on an analytical balance Adventurer Pro type AV264CM (Ohaus Europe GmbH, Greifensee, Switzerland) in order to determine the mass of bone mineral, water, and organic substances in bones. The contents of bone mineral, water, and organic substances were calculated as the ratios to the bone mass. The ashed bones were dissolved in 6 M HCl and then diluted in distilled water to spectrophotometrically determine the calcium and phosphorus contents in the bone mineral, with the use of Pointe Scientific (Canton, MI, USA) kits.

2.4. Bone Histomorphometric Studies. The measurements of the transverse cross-sections of the tibial and femoral diaphysis were performed on undecalcified, unstained slides, prepared as previously described [30, 31]. The measurements of the longitudinal cross-sections of the femoral metaphysis were carried out on decalcified preparations which were stained with hematoxylin and eosin [32]. The OsteoMeasure system (OsteoMetrics Inc., Decatur, GA, USA) was used for the histomorphometric measurements, and the data were presented according to the American Society for Bone and Mineral Research (ASBMR) standardized nomenclature [33].

In the cancellous bone of the distal femoral metaphysis, the following parameters were determined: bone volume to tissue volume ratio (BV/TV), trabecular thickness (Tb.Th), trabecular separation (Tb.Sp), and trabecular number (Tb.N).

In cortical bone of the tibial and femoral diaphysis, the transverse cross-sectional area of the whole diaphysis (Tt.Ar), transverse cross-sectional area of the cortical bone (Ct.Ar), transverse cross-sectional area of the marrow cavity (Ma.Ar), and the Ma.Ar/Tt.Ar ratio were measured.

The periosteal and endosteal transverse growth (mineral apposition rate; MAR) in the tibial and femoral diaphysis were measured. However, the evaluation of the effect of diabetes on those parameters was impossible, because tetracycline and calcein labels could be observed only in the preparations of the nonovariectomized and ovariectomized controls.

2.5. Biochemical Studies. Serum concentrations of bone turnover markers, osteocalcin (a marker of bone formation) and C-terminal telopeptide fragments of type I collagen released from bone during bone resorption (CTX-I), were studied by the ELISA methods (Rat-MID Osteocalcin EIA and RatLaps (CTX-I) EIA, respectively, Immunodiagnostic Systems Ltd., Boldon, Tyne and Wear, UK). A microplate reader Stat Fax 2100 (Awareness Technology, Inc., Palm City, FL, USA) was used for the measurements.

Serum concentrations of calcium, inorganic phosphorus, glucose, fructosamine, and biochemical parameters of lipid metabolism (total cholesterol, high-density lipoprotein (HDL) cholesterol, low-density lipoprotein (LDL) cholesterol, and triglycerides) were determined spectrophotometrically, using kits produced by Pointe Scientific (Canton, MI, USA). Moreover, the concentration of advanced oxidation

protein products (AOPP), a marker of oxidative protein damage, was measured spectrophotometrically based on the method of Witko-Sarsat et al. [34, 35]. The calibration curve was prepared using chloramine T (Sigma-Aldrich, St. Louis, MO, USA), and the absorbance was measured at the wavelength of 340 nm. The AOPP concentration was expressed in μmol of chloramine T equivalents/L. The spectrophotometric measurements were performed with the use of Tecan Infinite M200 PRO microplate reader and Magellan 7.2 software (Tecan Austria GmbH, Grödig, Austria).

The measurements of serum concentrations of 23 cytokines were performed with the use of multiplex technology of magnetic beads combined with antibodies (Bio-Plex Pro Rat Cytokine 23-Plex Immunoassay; Bio-Rad Laboratories Inc., Hercules, CA, USA), using Bio-Plex 200 system and Bio-Plex Manager software (Bio-Rad). The full panel of 23 rat cytokines for which the technique was available was investigated. The following cytokines were assayed: interleukin-1 α (IL-1 α), IL-1 β , IL-2, IL-4, IL-5, IL-6, IL-7, IL-10, IL-12p70, IL-13, IL-17A, IL-18, granulocyte colony-stimulating factor (G-CSF), granulocyte-macrophage colony-stimulating factor (GM-CSF), growth-regulated oncogene/keratinocyte chemoattractant (GRO/KC), interferon- γ (IFN- γ), macrophage colony-stimulating factor (M-CSF), macrophage inflammatory protein-1a (MIP-1a), macrophage inflammatory protein-3a (MIP-3a), regulated on activation, normal T cell expressed and secreted (RANTES), tumor necrosis factor α (TNF- α), vascular endothelial growth factor (VEGF), and monocyte chemoattractant protein-1 (MCP-1; monocyte chemotactic and activating factor—MCAF).

2.6. Statistical Analysis. Results are presented as the mean \pm standard error of the mean (SEM). Statistical analysis was carried out with the use of two-way analysis of variance (ANOVA), with the main effects of estrogen deficiency (OVX) and type 1 diabetes (DM). In case of the statistical significance of any of the main effects or their interaction, the ANOVA was followed by Fisher's Least Significant Difference (LSD) *post hoc* test (Statistica 13.1; Tibco Software Inc., Palo Alto, CA, USA). *p* values < 0.05 were considered significant.

Moreover, the principal component analysis (PCA) was performed on the following groups of parameters:

- (I) – Body mass gain and mass of internal organs: the uterus, thymus, adrenals, and liver
- (II) – Serum metabolic biochemical parameters: concentrations of nonfasting and fasting blood glucose, triglycerides, total cholesterol, LDL cholesterol, HDL cholesterol, and AOPP
- (III) – Serum bone turnover parameters: CTX-I, osteocalcin, inorganic phosphorus, and total calcium concentrations
- (IV) – Bone mass and macrometric parameters: tibial mass, length and diameter, femoral mass, length and diameter, and vertebral mass
- (V) – Bone composition and mineralization: the content of bone mineral, water, and organic substances in the tibia, femur, and vertebra (calculated as the ratios of their mass to the bone mass), content of calcium and phosphorus in the bone mineral in the tibia, femur, and vertebra
- (VI) – Histomorphometric parameters of compact bone: Ma.Ar, Ct.Ar, Tt.Ar, and Ma.Ar/Tt.Ar in the tibial and femoral diaphysis
- (VII) – Histomorphometric parameters of cancellous bone of the femoral metaphysis: BV/TV, BS/TV, BS/BV, Tb.Th, Tb.Sp, and Tb.N
- (VIII) – Mechanical properties of cancellous bone: Young's modulus, load, displacement, energy, and stress for yield point, maximum load point, and fracture point in the tibial metaphysis
- (IX) – Mechanical properties of compact bone: Young's modulus, load, displacement, energy, and stress for yield point, maximum load point, and fracture point in the femoral diaphysis
- (X) – Serum concentrations of 23 cytokines

The PCA was carried out using the PAST 3.26 software [36, 37]. Correlation matrices were employed for data standardization. The correlation values presented on the graphs are autoscaled based on the algorithm built into the software. Statistical significance of the PCA results was evaluated using two-way MANOVA (multivariate analysis of variance; Statistica 13.1). In case of the statistical significance of any of the main effects or their interaction, further analysis for individual axes (PC1, PC2) was performed, followed by Fisher's LSD *post hoc* test. Only significant *post hoc* differences between DM-OVX versus DM-NOVX are mentioned in the figure legends; all results—see Supplementary Material 1.

3. Results

3.1. General Parameters. At the end of the experiment, five weeks after the bilateral ovariectomy surgery, the mean body mass of the diabetic rats, both nonovariectomized and ovariectomized, significantly decreased in relation to appropriate control rats, whereas the mean body mass of the nondiabetic ovariectomized rats significantly increased (Table 1).

The liver mass increased, and the mass of the uterus, thymus, and adrenal glands decreased in the diabetic rats independent of the estrogen status, whereas the uterus mass decreased, and thymus mass increased in the nondiabetic ovariectomized rats.

Both the nonovariectomized and ovariectomized rats administered STZ developed diabetes, as indicated by profoundly increased glucose and fructosamine levels in relation to appropriate controls, moreover, significant disorders of lipid metabolism were noted (Table 2). Estrogen deficiency itself did not affect the parameters connected with glucose metabolism; however, it increased the cholesterol and LDL cholesterol levels. The estrogen-deficient diabetic rats had

TABLE 1: Effects of diabetes (DM) and/or estrogen deficiency on the body mass gain and the mass of selected internal organs in rats.

| Parameter/group | Nonovariectomized (NOVX) rats | | Ovariectomized (OVX) rats | | Two-way ANOVA | | |
|--|-------------------------------|------------------|---------------------------|----------------------------------|------------------|------------------|------------------|
| | Control | DM | Control | DM | OVX | DM | OVXx DM |
| Initial body mass (g) ^{&} | 226.9 ± 3.3 | 208.7 ± 3.7** | 220.9 ± 4.5 | 207.4 ± 3.7*** ^X | NS | <i>p</i> < 0.001 | NS |
| 4-week body mass gain (g) | 12.1 ± 1.7 | -17.4 ± 4.1*** | 42.1 ± 5.2*** | -22.8 ± 5.6*** ^{XXX} | <i>p</i> < 0.01 | <i>p</i> < 0.001 | <i>p</i> < 0.001 |
| Uterus mass (g) | 0.511 ± 0.054 | 0.171 ± 0.030*** | 0.096 ± 0.006*** | 0.095 ± 0.007*** | <i>p</i> < 0.001 | <i>p</i> < 0.001 | <i>p</i> < 0.001 |
| Thymus mass (g) | 0.297 ± 0.019 | 0.093 ± 0.014*** | 0.529 ± 0.030*** | 0.056 ± 0.011*** ^{XXX} | <i>p</i> < 0.001 | <i>p</i> < 0.001 | <i>p</i> < 0.001 |
| Liver mass (g) | 5.656 ± 0.114 | 8.099 ± 0.329*** | 6.197 ± 0.180 | 7.926 ± 0.299*** ^{XXX} | NS | <i>p</i> < 0.001 | NS |
| Adrenals mass (g) | 0.078 ± 0.004 | 0.071 ± 0.004 | 0.073 ± 0.004 | 0.059 ± 0.003*** ^{XX a} | <i>p</i> < 0.05 | <i>p</i> < 0.01 | NS |

Bilateral ovariectomy was performed 5 weeks before the end of the experiment. Diabetes was induced 3 days after the ovariectomy by a single administration of streptozotocin (60 mg/kg *i.p.*). Results are presented as means ± SEM (*n* = 9 – 10). Two-way ANOVA followed by Fisher's LSD test was used for evaluation of the significance of the results. [&]Body mass one week after the ovariectomy; ***p* < 0.01, ****p* < 0.001—significantly different from the NOVX control rats; ^X*p* < 0.05, ^{XX}*p* < 0.01, ^{XXX}*p* < 0.001—significantly different from the OVX control rats; ^a*p* < 0.05—significantly different from the DM-NOVX rats.

TABLE 2: Effects of diabetes (DM) and/or estrogen deficiency on the serum metabolic parameters and calcium and phosphorus concentrations.

| Parameter/group | Nonovariectomized (NOVX) rats | | Ovariectomized (OVX) rats | | Two-way ANOVA | | |
|----------------------------------|-------------------------------|------------------|---------------------------|----------------------------------|------------------|------------------|-----------------|
| | Control | DM | Control | DM | OVX | DM | OVXx DM |
| Glucose (mg/100 mL) | 82.8 ± 2.7 | 561.4 ± 12.2*** | 82.9 ± 1.5 | 575.9 ± 12.5*** ^{XXX} | NS | <i>p</i> < 0.001 | NS |
| Fructosamine (mM/L) | 0.483 ± 0.010 | 1.106 ± 0.051*** | 0.491 ± 0.014 | 0.887 ± 0.111*** ^{XX a} | NS | <i>p</i> < 0.001 | NS |
| Triglycerides (mg/100 mL) | 35.8 ± 3.8 | 68.8 ± 7.3** | 40.8 ± 2.2 | 89.1 ± 11.4*** ^{XXX} | NS | <i>p</i> < 0.001 | NS |
| Cholesterol (mg/100 mL) | 47.5 ± 4.9 | 53.3 ± 3.1 | 65.7 ± 2.4*** | 69.8 ± 2.4*** ^{aa} | <i>p</i> < 0.001 | NS | NS |
| LDL cholesterol (mg/100 mL) | 25.0 ± 3.8 | 31.4 ± 4.5 | 49.6 ± 6.1*** | 34.4 ± 3.9 ^X | <i>p</i> < 0.01 | NS | <i>p</i> < 0.05 |
| HDL cholesterol (mg/100 mL) | 28.4 ± 2.0 | 30.8 ± 1.3 | 24.2 ± 0.5 | 34.2 ± 3.3 ^{XX} | NS | <i>p</i> < 0.01 | NS |
| AOPP (μmol/L) ^{&} | 14.3 ± 1.4 | 17.2 ± 1.3 | 15.6 ± 1.5 | 23.2 ± 3.3*** ^X | NS | <i>p</i> < 0.05 | NS |
| Calcium (mg/100 mL) | 9.97 ± 0.23 | 11.51 ± 0.25*** | 9.82 ± 0.27 | 11.86 ± 0.32*** ^{XXX} | NS | <i>p</i> < 0.001 | NS |
| Inorganic phosphorus (mg/100 mL) | 8.51 ± 0.48 | 4.98 ± 0.58*** | 9.40 ± 0.51 | 6.38 ± 0.62*** ^{XXX} | <i>p</i> < 0.05 | <i>p</i> < 0.001 | NS |

Bilateral ovariectomy was performed 5 weeks before the end of the experiment. Diabetes was induced 3 days after the ovariectomy by a single administration of streptozotocin (60 mg/kg *i.p.*). Results are presented as means ± SEM (*n* = 9 – 10). [&]The concentration of AOPP is presented in chloramine T equivalents. Two-way ANOVA followed by Fisher's LSD test was used for evaluation of the significance of the results. ***p* < 0.01, ****p* < 0.001—significantly different from the NOVX control rats; ^X*p* < 0.05, ^{XX}*p* < 0.01, ^{XXX}*p* < 0.001—significantly different from the OVX control rats; ^a*p* < 0.05, ^{aa}*p* < 0.01—significantly different from the DM-NOVX rats.

significantly increased the level of AOPP in relation to the ovariectomized controls, indicating oxidative protein damage.

The PCA indicated strong differences concerning the body mass gain, internal organ mass, and serum biochemical metabolic parameters between the diabetic and nondiabetic rats, as well as the nonovariectomized and ovariectomized rats (Figures 1 and 2, respectively).

3.2. Serum Bone Turnover Markers. Diabetes induced significant increases in the concentration of the bone resorption marker CTX-I (by 503.9% in the nonovariectomized rats and by 325.9% in the ovariectomized rats in relation to the appropriate nondiabetic controls) and decreases in that of the bone formation marker osteocalcin (by 51.5% in the nonovariectomized rats and by 72.7% in the ovariectomized rats in relation to the appropriate nondiabetic controls)

(Figure 3). Estrogen deficiency induced a significant increase in the osteocalcin concentration only in the nondiabetic rats (by 78.7% in relation to the nonovariectomized controls); the CTX-I level was insignificantly increased (by 54.0% in relation to the nonovariectomized controls). Diabetes induced increases in the calcium concentrations and decreases in the inorganic phosphorus concentrations, regardless of the estrogen status (Table 2).

The PCA analysis indicated strong differences concerning the serum concentrations of bone turnover markers, calcium, and inorganic phosphorus between the diabetic and nondiabetic rats, as well as the nonovariectomized and ovariectomized rats (Figure 4).

3.3. Bone Mass, Macrometric Parameters, Composition, and Mineralization. Regardless the estrogen status, the diabetic rats had significantly decreased the bone mass, bone mineral

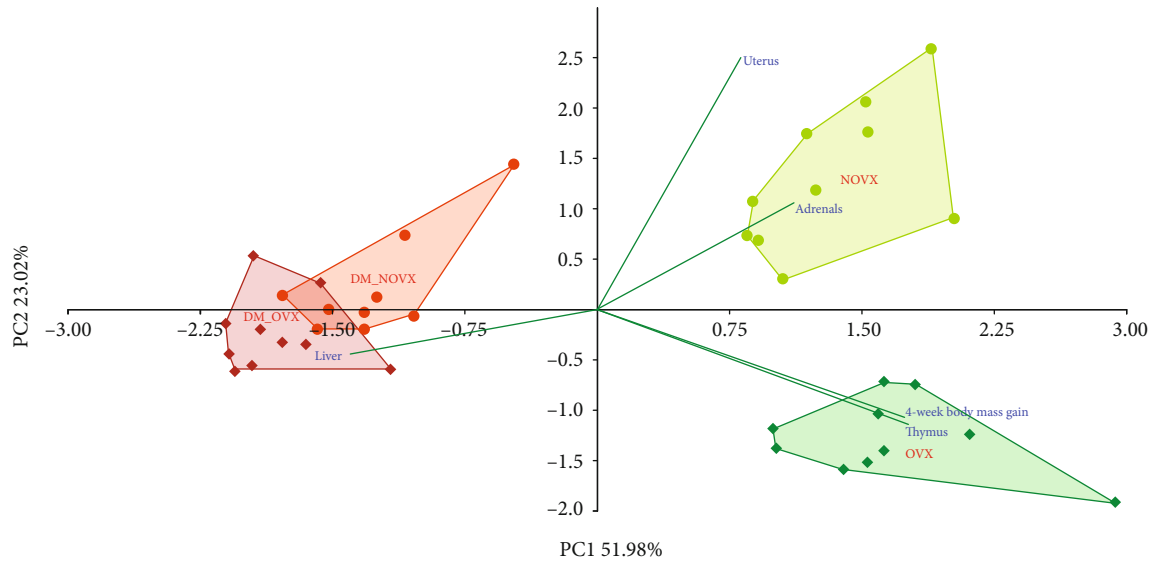


FIGURE 1: PCA biplot of the results concerning the body mass gain and the mass of internal organs (uterus, thymus, adrenal glands, and liver) in the diabetic and/or estrogen-deficient rats. Bilateral ovariectomy was performed 5 weeks before the end of the experiment. Diabetes was induced 3 days after the ovariectomy by a single administration of streptozotocin (60 mg/kg *i.p.*). Blue font and green lines indicate correlations of measured variables against experimental groups. Shades of red denote DM rats; shades of green denote nondiabetic rats. Darker shades and diamond symbols denote OVX rats; lighter shades and dot symbols denote NOVX rats. Group names are marked in red fonts inside the convex hulls comprised by individuals from the same group. The statistical significance between the groups along the PCs was analysed by two-way MANOVA. Significant results for PC1: DM— $p < 0.001$; OVXxDM interaction— $p < 0.01$; and for PC2: OVX— $p < 0.001$, OVXxDM interaction— $p < 0.001$. *Post hoc* LSD for PC1: DM-NOVX versus DM-OVX— $p < 0.01$. Detailed data—see Supplementary Material 1A.

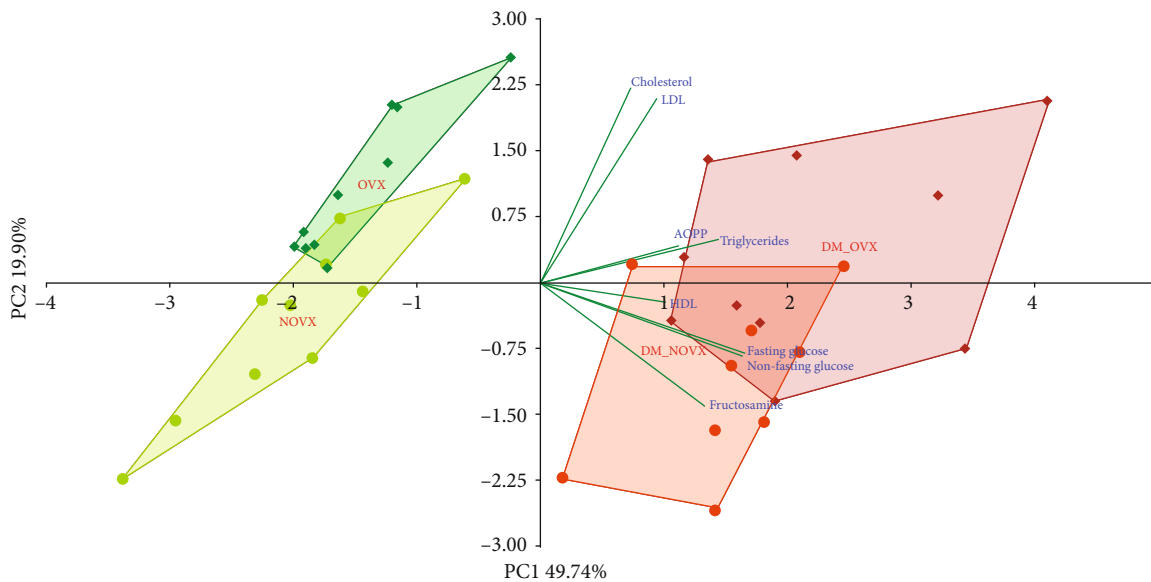


FIGURE 2: PCA biplot of the results concerning the concentrations of the serum biochemical metabolic parameters in the diabetic and/or estrogen-deficient rats. Bilateral ovariectomy was performed 5 weeks before the end of the experiment. Diabetes was induced 3 days after the ovariectomy by a single administration of streptozotocin (60 mg/kg *i.p.*). Blue font and green lines indicate correlations of measured variables against experimental groups. Shades of red denote DM rats; shades of green denote nondiabetic rats. Darker shades and diamond symbols denote OVX rats; lighter shades and dot symbols denote NOVX rats. Group names are marked in red fonts inside the convex hulls comprised by individuals from the same group. The statistical significance between the groups along the PCs was analysed by two-way MANOVA. Significant results for PC1: OVX— $p < 0.05$; DM— $p < 0.001$, and for PC2: OVX— $p < 0.001$; DM— $p < 0.05$. *Post hoc* LSD for PC2: DM-NOVX versus DM-OVX— $p < 0.01$. Detailed data—see Supplementary Material 1B.

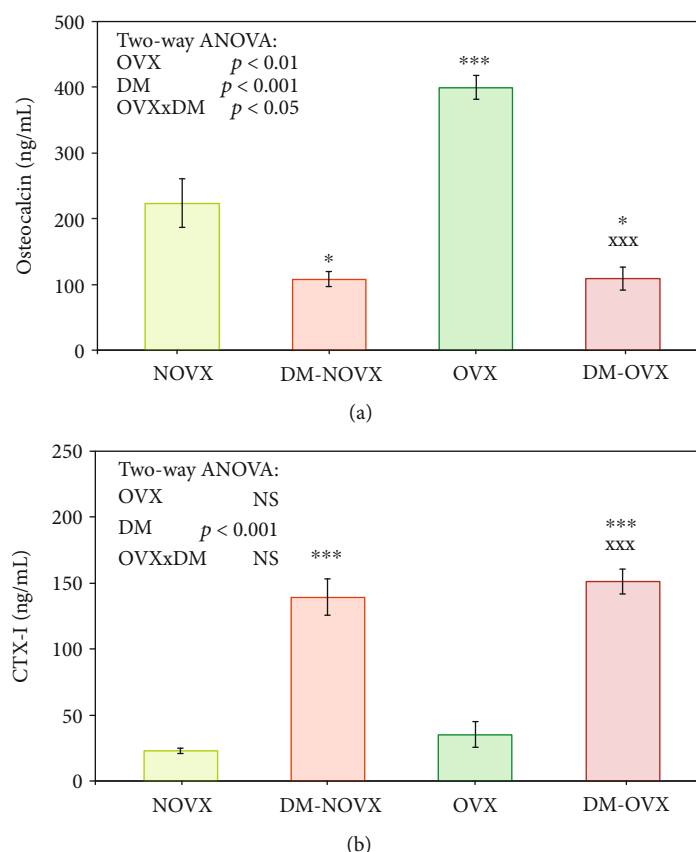


FIGURE 3: Effects of diabetes (DM) and/or estrogen deficiency on the serum bone turnover markers (osteocalcin and CTX-I) in rats. Bilateral ovariectomy was performed 5 weeks before the end of the experiment. Diabetes was induced 3 days after the ovariectomy by a single administration of streptozotocin (60 mg/kg *i.p.*). Results are presented as means \pm SEM ($n = 9 - 10$). NOVX: nonovariectomized control rats; DM-NOVX: rats with type 1 diabetes; OVX: ovariectomized control rats; DM-OVX: ovariectomized rats with type 1 diabetes. CTX-I: C-terminal telopeptide fragments of type I collagen. Two-way ANOVA followed by Fisher's LSD test was used for evaluation of the significance of the results. * $p < 0.05$, *** $p < 0.001$ —significantly different from the NOVX control rats; XXX $p < 0.001$ —significantly different from the OVX control rats.

mass, and bone mineral content (the bone mineral mass/bone mass ratio) both in the long bones and the vertebra, in relation to appropriate controls (Table 3, data for the tibia not shown). For example, the bone mineral content in the femur of the nonovariectomized diabetic rats decreased by 4.1% in comparison with the nonovariectomized controls, and that of the ovariectomized diabetic rats—by 3.2% in comparison with the ovariectomized controls. Also, the femoral length decreased. There was no effect of diabetes on the bone content of water and organic substances, as well as on the calcium content in the bone mineral. Estrogen deficiency did not significantly affect the abovementioned parameters, with the exception of decreasing the bone mineral content (by 2.6%) concomitantly with increasing the bone water content in the femur in relation to the nonovariectomized controls.

The PCA analysis indicated differences concerning the bone mass and macrometric parameters (Figure 5) and bone composition and mineralization (Figure 6) between the diabetic and nondiabetic rats.

3.4. Bone Histomorphometry. Diabetes induced deterioration of microarchitecture of the cancellous bone of the femoral

metaphysis, regardless of the estrogen status (Figure 7). In the nonovariectomized rats, diabetes decreased the bone volume to tissue volume ratio (BV/TV) and trabecular thickness (Tb.Th), whereas in the ovariectomized rats—Tb.Th was decreased and trabecular number (Tb.N) was increased due to diabetes. Estrogen deficiency, in the nondiabetic rats, induced significant decreases in BV/TV and Tb.N, as well as increases in trabecular separation (Tb.Sp). The changes in BV/TV induced by diabetes, estrogen deficiency, or both pathologies were of similar degree (decreases by 17.3%, 13.0%, and 18.1%, respectively, in relation to the nonovariectomized controls).

In cortical bone, diabetes decreased the transverse cross-sectional area of the cortical bone (Ct.Ar) and transverse cross-sectional area of the whole diaphysis (Tt.Ar), both in the tibial and femoral diaphysis, regardless the estrogen status (Table 4, data for the tibial diaphysis not shown). The Ct.Ar decreased, due to diabetes, by 5.8% in the nonovariectomized rats, and by 9.0% in the ovariectomized rats, in relation to the respective control rats. Estrogen deficiency did not affect the histomorphometric parameters of cortical bone.

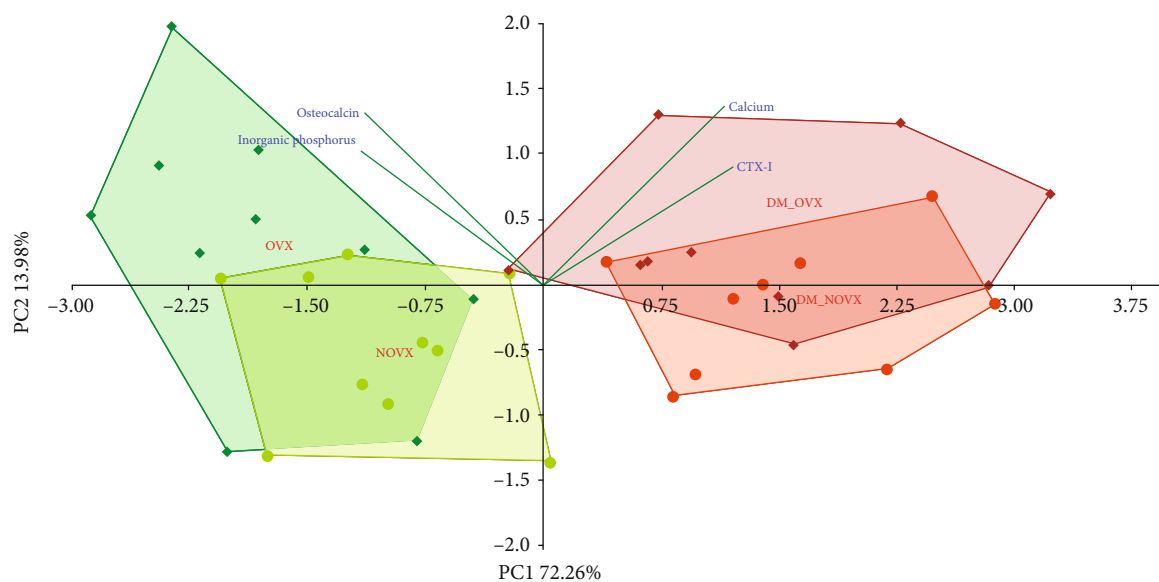


FIGURE 4: PCA biplot of the results concerning the concentrations of the serum bone turnover markers and concentrations of calcium and inorganic phosphorus in the diabetic and/or estrogen-deficient rats. Bilateral ovariectomy was performed 5 weeks before the end of the experiment. Diabetes was induced 3 days after the ovariectomy by a single administration of streptozotocin (60 mg/kg *i.p.*). Blue font and green lines indicate correlations of measured variables against experimental groups. Shades of red denote DM rats; shades of green denote nondiabetic rats. Darker shades and diamond symbols denote OVX rats; lighter shades and dot symbols denote NOVX rats. Group names are marked in red fonts inside the convex hulls comprised by individuals from the same group. The statistical significance between the groups along the PCs was analysed by two-way MANOVA. Significant results for PC1: DM— $p < 0.001$, and for PC2: OVX— $p < 0.01$. Detailed data—see Supplementary Material 1C.

The PCA analysis indicated differences concerning histomorphometric parameters of cancellous (Figure 8) and compact (Figure 9) between the diabetic and nondiabetic rats.

3.5. Bone Mechanical Properties. In the proximal tibial metaphysis, consisting mostly of cancellous bone, diabetes induced worsening of bone strength, regardless of the estrogen status (Figure 10, Table 5; data for the yield point not shown). In the ovariectomized control rats, most of the mechanical parameters were similar to those observed in the nonovariectomized diabetic rats. Moreover, in the ovariectomized control rats, Young's modulus was significantly decreased in relation to the nonovariectomized controls. The changes in the ovariectomized diabetic rats were in most cases less pronounced than in the nonovariectomized diabetic rats in relation to the appropriate nondiabetic controls, as indicated by significant interactions concerning the mechanical parameters of the tibial metaphysis noted in two-way ANOVA. For example, the decreases in the maximum load induced by diabetes, estrogen deficiency, or both pathologies were as follows: 35.4%, 34.2%, and 48.1%, respectively, in relation to the nonovariectomized control rats. However, the maximum load in the ovariectomized diabetic rats was decreased only by 21.1% in comparison with the ovariectomized controls.

In the femoral diaphysis, no effects of diabetes on the extrinsic mechanical parameters were observed; however, increases in the intrinsic parameters (Young's modulus in both the nonovariectomized and ovariectomized rats, stress

in the nonovariectomized rats) were observed (Table 5; data for the yield point not shown). The value of Young's modulus increased due to diabetes by 21.9% in the nonovariectomized rats and by 11.1% in the ovariectomized rats in comparison with appropriate controls. Estrogen deficiency alone did not affect the investigated parameters, whereas in the diabetic rats, it decreased the value of stress in relation to the nonovariectomized diabetic rats.

There was no effect of both diabetes and estrogen deficiency on the strength of the femoral neck (not shown).

The PCA analysis indicated differences concerning the mechanical properties of cancellous (Figure 11) and compact bone (Figure 12) between the diabetic and nondiabetic rats. Moreover, there were differences concerning the mechanical properties of cancellous bone between the nonovariectomized and ovariectomized rats.

3.6. Serum Cytokine Concentrations. STZ-induced diabetes led to the development of profound changes in the serum cytokine levels, both in the nonovariectomized and ovariectomized rats (significant main diabetes effects) (Table 6). The following cytokines were moderately (less than 5x) increased: IL-1 α , IL-4, IL-10, IL-13, IL-17A, G-CSF, IFN- γ , M-CSF, MIP-3a, RANTES, and TNF- α , and the following were strongly increased (more than 5x): IL-1 β , IL-7, GM-CSF, GRO/KC, MIP-1a, VEGF, and MCP-1 (MCAF). There were no significant changes in the cytokine levels induced by estrogen deficiency. The only significant interaction between the main effects (OVX and DM) concerned the RANTES concentration, which was increased only in the diabetic ovariectomized rats.

TABLE 3: Effects of diabetes (DM) and/or estrogen deficiency on the bone mass, macrometric parameters, composition, and mineralization in the femur and L4 vertebra.

| Parameter/group | Nonovariectomized (NOVX) rats | | Ovariectomized (OVX) rats | | Two-way ANOVA | | | |
|--|-------------------------------|---------------|---------------------------|----------------|-------------------------------|-----------------|------------------|-----------------|
| | Control | DM | Control | DM | OVX | DM | OVXx DM | |
| Bone mass (g) | Femur | 0.682 ± 0.014 | 0.629 ± 0.012** | 0.677 ± 0.014 | 0.618 ± 0.012***XX | NS | <i>p</i> < 0.001 | NS |
| | L4 vertebra | 0.214 ± 0.009 | 0.188 ± 0.008* | 0.214 ± 0.006 | 0.178 ± 0.005***XX | NS | <i>p</i> < 0.001 | NS |
| Femoral length (mm) | | 33.54 ± 0.18 | 32.83 ± 0.16* | 34.07 ± 0.22 | 32.80 ± 0.20***XX | NS | <i>p</i> < 0.001 | NS |
| Femoral diameter (mm) | | 3.36 ± 0.03 | 3.28 ± 0.03 | 3.37 ± 0.04 | 3.26 ± 0.04 | NS | <i>p</i> < 0.01 | NS |
| Bone mineral mass (g) | Femur | 0.331 ± 0.007 | 0.293 ± 0.007*** | 0.320 ± 0.006 | 0.283 ± 0.005***XX | NS | <i>p</i> < 0.001 | NS |
| | L4 vertebra | 0.086 ± 0.003 | 0.073 ± 0.003*** | 0.086 ± 0.002 | 0.068 ± 0.002***XX | NS | <i>p</i> < 0.001 | NS |
| Bone mineral content (g/g) | Femur | 0.485 ± 0.003 | 0.466 ± 0.006** | 0.473 ± 0.004* | 0.458 ± 0.003***XX | <i>p</i> < 0.05 | <i>p</i> < 0.001 | NS |
| | L4 vertebra | 0.407 ± 0.011 | 0.391 ± 0.008 | 0.403 ± 0.007 | 0.384 ± 0.005 | NS | <i>p</i> < 0.05 | NS |
| Bone water content (g/g) | Femur | 0.276 ± 0.004 | 0.294 ± 0.007 | 0.303 ± 0.013 | 0.301 ± 0.004 | <i>p</i> < 0.05 | NS | NS |
| | L4 vertebra | 0.345 ± 0.014 | 0.362 ± 0.010 | 0.347 ± 0.007 | 0.362 ± 0.009 | NS | NS | NS |
| Bone organic substances content (g/g) | Femur | 0.239 ± 0.002 | 0.240 ± 0.002 | 0.224 ± 0.012 | 0.241 ± 0.002 | NS | NS | NS |
| | L4 vertebra | 0.248 ± 0.004 | 0.248 ± 0.003 | 0.250 ± 0.002 | 0.254 ± 0.006 | NS | NS | NS |
| Calcium content (g/g of bone mineral) | Femur | 0.373 ± 0.007 | 0.364 ± 0.012 | 0.363 ± 0.007 | 0.377 ± 0.006 | NS | NS | NS |
| | L4 vertebra | 0.345 ± 0.018 | 0.347 ± 0.016 | 0.346 ± 0.015 | 0.339 ± 0.015 | NS | NS | NS |
| Phosphorus content (g/g of bone mineral) | Femur | 0.176 ± 0.003 | 0.173 ± 0.002 | 0.171 ± 0.002 | 0.180 ± 0.002 ^{XX a} | NS | NS | <i>p</i> < 0.01 |
| | L4 vertebra | 0.156 ± 0.004 | 0.155 ± 0.003 | 0.158 ± 0.004 | 0.153 ± 0.003 | NS | NS | NS |

Bilateral ovariectomy was performed 5 weeks before the end of the experiment. Diabetes was induced 3 days after the ovariectomy by a single administration of streptozotocin (60 mg/kg *i.p.*). Results are presented as means ± SEM (*n* = 9–10). Two-way ANOVA followed by Fisher's LSD test was used for evaluation of the significance of the results. **p* < 0.05, ***p* < 0.01, ****p* < 0.001—significantly different from the NOVX control rats; ^{XX}*p* < 0.01, ^{XXX}*p* < 0.001—significantly different from the OVX control rats; ^a*p* < 0.05—significantly different from the DM-NOVX rats.

The PCA analysis indicated strong differences concerning cytokine levels between the diabetic and nondiabetic rats, regardless of the estrogen status (Figure 13).

4. Discussion

Although postmenopausal osteoporosis often occurs concurrently with diabetes, little is known about interactions between estrogen deficiency and hyperglycemia in terms of effects on the skeletal system *in vivo*.

In the present study, bilateral ovariectomy induced estrogen deficiency, as confirmed by characteristic changes in estrogen-dependent organ mass (the uterus and thymus), significant increases in the body mass gain, and serum cholesterol levels. Also, osteoporotic microstructure and strength changes due to estrogen deficiency were demonstrated five weeks after the ovariectomy, as previously described [30, 38]. The microstructure changes concerned cancellous bone (decreases in BV/TV and Tb.N, increases in Tb.Sp) and led to worsening of the strength of the proximal tibial metaphysis, built mostly of cancellous bone. There were no significant changes in compact bone histomorphometric parameters

and mechanical properties (Ct.Ar, Tt.Ar, Ma.Ar in the tibial and femoral diaphysis, and strength of the femoral diaphysis, respectively). The bone resorption marker (CTX-I) concentration tended to increase, and the bone formation marker (osteocalcin) level significantly increased. The observed changes are consistent with well-established mechanisms of changes developing in the bone due to estrogen deficiency. Estrogen deficiency increases the rate of bone remodeling, and both bone resorption and formation accelerate. This is because estrogen decreases the number of remodeling cycles, inhibiting the birth rate of osteoclasts and osteoblasts from their progenitors, and has proapoptotic effects on osteoclasts and antiapoptotic effects on osteoblasts and osteocytes. The loss of bone mass and strength is the result of the shift of the balance toward bone resorption [39].

The nonovariectomized rats administered STZ developed diabetes, with hyperglycemia, polydipsia, polyuria, characteristic changes in the serum parameters, and decreased body mass. Very profound changes in the skeletal system were observed, consistent with other studies [18, 20–25]. Bone mass, mineralization, and mechanical properties of cancellous bone of the proximal tibial metaphysis profoundly

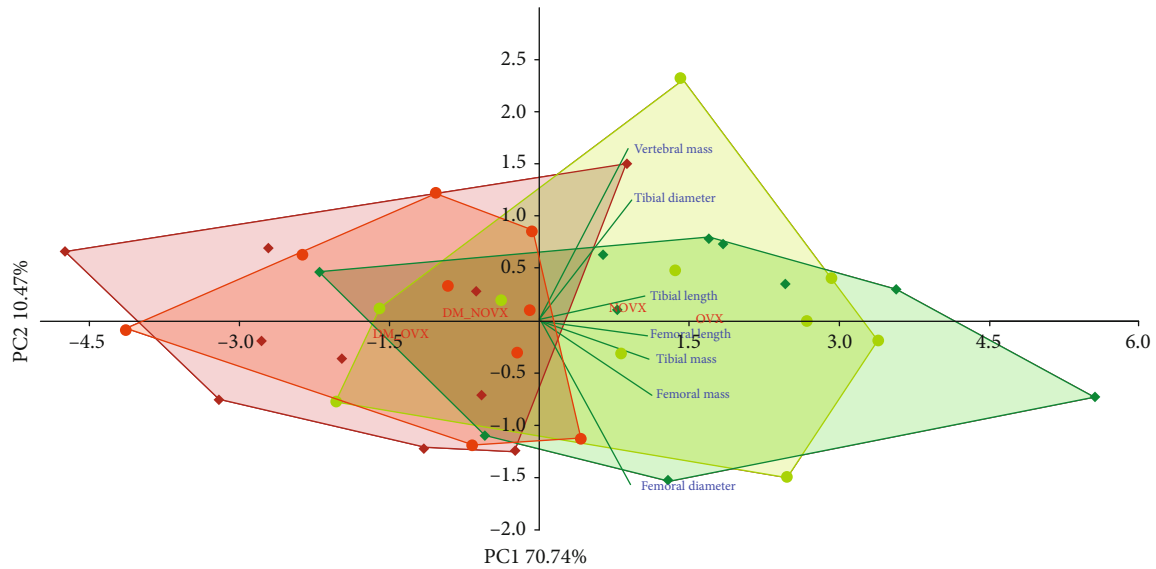


FIGURE 5: PCA biplot of the results concerning the bone mass and macrometric parameters in the diabetic and/or estrogen-deficient rats. Bilateral ovariectomy was performed 5 weeks before the end of the experiment. Diabetes was induced 3 days after the ovariectomy by a single administration of streptozotocin (60 mg/kg *i.p.*). Blue font and green lines indicate correlations of measured variables against experimental groups. Shades of red denote DM rats; shades of green denote nondiabetic rats. Darker shades and diamond symbols denote OVX rats; lighter shades and dot symbols denote NOVX rats. Group names are marked in red fonts inside the convex hulls comprised by individuals from the same group. The statistical significance between the groups along the PCs was analysed by two-way MANOVA. Significant results for PC1: DM— $p < 0.001$. Detailed data—see Supplementary Material 1D.

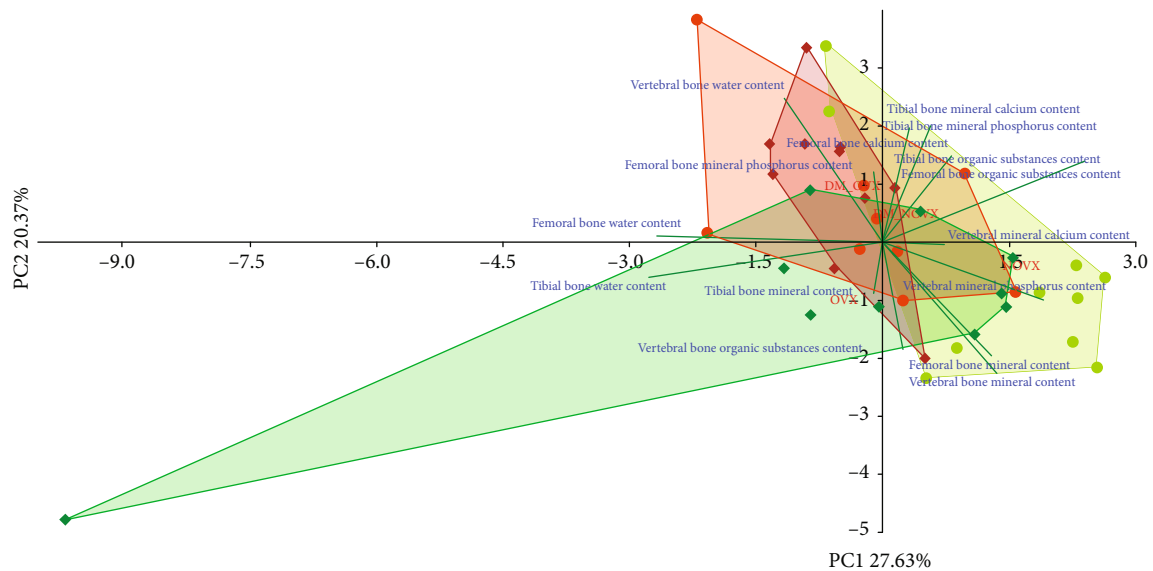


FIGURE 6: PCA biplot of the results concerning the bone composition and mineralization in the diabetic and/or estrogen-deficient rats. Bilateral ovariectomy was performed 5 weeks before the end of the experiment. Diabetes was induced 3 days after the ovariectomy by a single administration of streptozotocin (60 mg/kg *i.p.*). Blue font and green lines indicate correlations of measured variables against experimental groups. Shades of red denote DM rats; shades of green denote nondiabetic rats. Darker shades and diamond symbols denote OVX rats; lighter shades and dot symbols denote NOVX rats. Group names are marked in red fonts inside the convex hulls comprised by individuals from the same group. The statistical significance between the groups along the PCs was analysed by two-way MANOVA. Significant results for PC2: DM— $p < 0.01$. Detailed data—see Supplementary Material 1E.

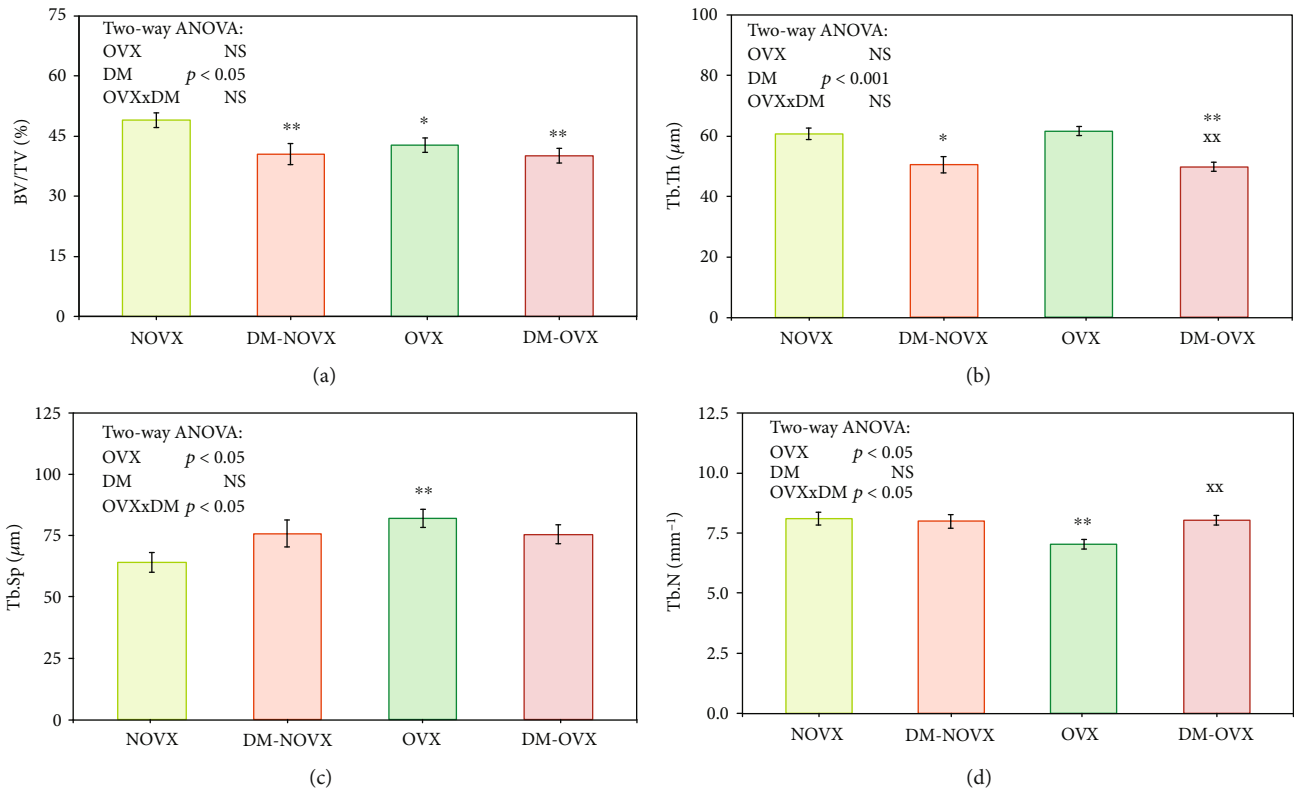


FIGURE 7: Effects of diabetes (DM) and/or estrogen deficiency on the histomorphometric parameters of cancellous bone of the distal femoral metaphysis in rats. Bilateral ovariectomy was performed 5 weeks before the end of the experiment. Diabetes was induced 3 days after the ovariectomy by a single administration of streptozotocin (60 mg/kg *i.p.*). Results are presented as means \pm SEM ($n = 9 - 10$). NOVX: nonovariectomized control rats; DM-NOVX: rats with type 1 diabetes; OVX: ovariectomized control rats; DM-OVX: ovariectomized rats with type 1 diabetes. BV/TV: bone volume to tissue volume ratio; Tb.Th: trabecular thickness; Tb.Sp: trabecular separation; Tb.N: trabecular number. Two-way ANOVA followed by Fisher's LSD test was used for evaluation of the significance of the results. * $p < 0.05$, ** $p < 0.01$ —significantly different from the NOVX control rats; ^{xx} $p < 0.01$ —significantly different from the OVX control rats.

TABLE 4: Effects of diabetes (DM) and/or estrogen deficiency on the histomorphometric parameters of compact bone of the femoral diaphysis in rats.

| Parameter/group | Nonovariectomized (NOVX) rats | | Ovariectomized (OVX) rats | | Two-way ANOVA | | |
|--------------------------|-------------------------------|-------------------------------|---------------------------|-----------------------------------|---------------|-------------|---------|
| | Control | DM | Control | DM | OVX | DM | OVXx DM |
| Tt.Ar (mm ²) | 8.21 \pm 0.11 | 7.81 \pm 0.16 | 8.39 \pm 0.18 | 7.79 \pm 0.13 ^{xx} | NS | $p < 0.01$ | NS |
| Ct.Ar (mm ²) | 5.42 \pm 0.06 | 5.10 \pm 0.08 ^{**} | 5.51 \pm 0.08 | 5.02 \pm 0.05 ^{***xxx} | NS | $p < 0.001$ | NS |
| Ma.Ar (mm ²) | 2.79 \pm 0.07 | 2.70 \pm 0.11 | 2.87 \pm 0.13 | 2.78 \pm 0.10 | NS | NS | NS |
| Ma.Ar/Tt.Ar | 0.340 \pm 0.005 | 0.346 \pm 0.008 | 0.341 \pm 0.009 | 0.355 \pm 0.007 | NS | NS | NS |

Bilateral ovariectomy was performed 5 weeks before the end of the experiment. Diabetes was induced 3 days after the ovariectomy by a single administration of streptozotocin (60 mg/kg *i.p.*). Results are presented as means \pm SEM ($n = 9 - 10$). Two-way ANOVA followed by Fisher's LSD test was used for evaluation of the significance of the results. ** $p < 0.01$, *** $p < 0.001$ —significantly different from the NOVX control rats; ^{xx} $p < 0.01$, ^{xxx} $p < 0.001$ —significantly different from the OVX control rats; Tt.Ar: transverse cross-section area of the whole diaphysis; Ct.Ar: transverse cross-section area of the cortical bone; Ma.Ar: transverse cross-section area of the marrow cavity; Ma.Ar/Tt.Ar: transverse cross-section area of the marrow cavity/diaphysis ratio.

worsened, whereas the strength of compact bone was not decreased. In fact, significant increases in the values of intrinsic mechanical parameters (stress, Young's modulus) in the femoral diaphysis were demonstrated in the diabetic rats, which however was rather the result of decreases in bone size than improvement of bone quality. Deterioration of cancellous bone microstructure was demonstrated (decreases in BV/TV and Tb.Th). Bone resorption was intensified, and

bone formation was decreased as demonstrated by the measurements of serum bone turnover marker concentrations (CTX-I and osteocalcin, respectively).

The pathomechanism of the development of the skeletal changes in diabetes is complex. There are differences between clinical skeletal manifestations of type 1 and type 2 diabetes. T1D leads to decreased BMD and increased fracture risk. In T2D, the decreases in BMD do not occur; however, the risk

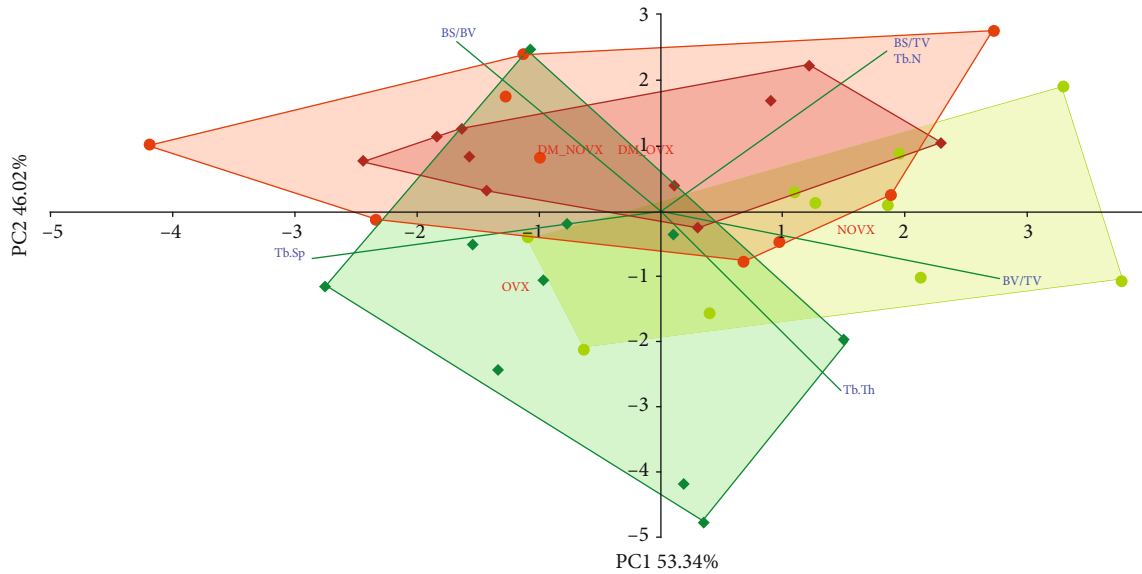


FIGURE 8: PCA biplot of the results concerning histomorphometric parameters of cancellous bone (the distal femoral metaphysis) in the diabetic and/or estrogen-deficient rats. Bilateral ovariectomy was performed 5 weeks before the end of the experiment. Diabetes was induced 3 days after the ovariectomy by a single administration of streptozotocin (60 mg/kg *i.p.*). Blue font and green lines indicate correlations of measured variables against experimental groups. Shades of red denote DM rats; shades of green denote nondiabetic rats. Darker shades and diamond symbols denote OVX rats; lighter shades and dot symbols denote NOVX rats. Group names are marked in red fonts inside the convex hulls comprised by individuals from the same group. The statistical significance between the groups along the PCs was analysed by two-way MANOVA. Significant results for PC2: DM— $p < 0.001$. Detailed data—see Supplementary Material 1F.

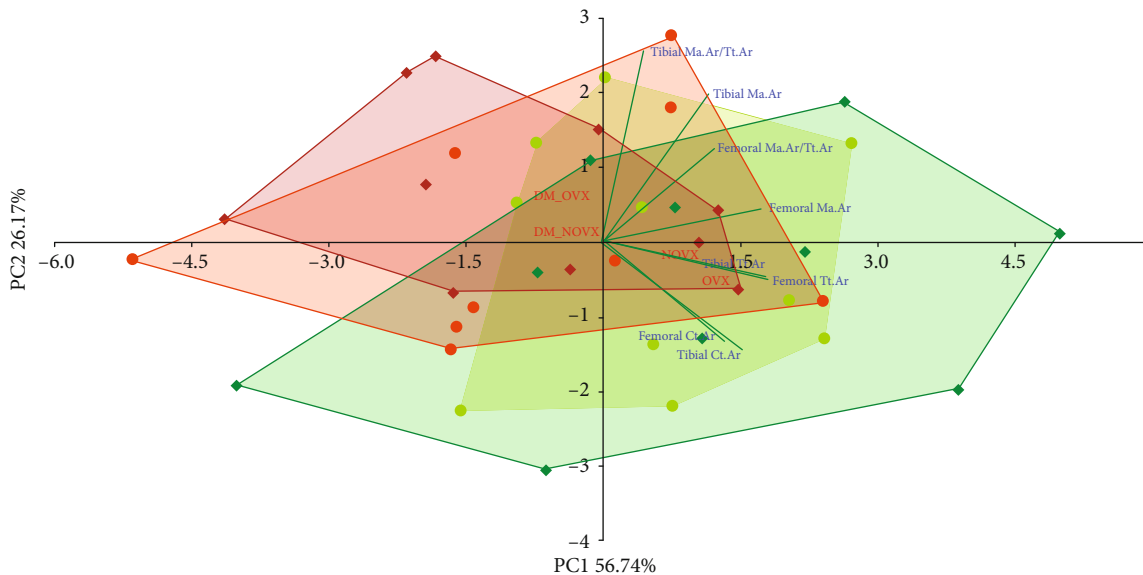


FIGURE 9: PCA biplot of the results concerning histomorphometric parameters of compact bone (the tibial and femoral diaphysis) in the diabetic and/or estrogen-deficient rats. Bilateral ovariectomy was performed 5 weeks before the end of the experiment. Diabetes was induced 3 days after the ovariectomy by a single administration of streptozotocin (60 mg/kg *i.p.*). Blue font and green lines indicate correlations of measured variables against experimental groups. Shades of red denote DM rats; shades of green denote nondiabetic rats. Darker shades and diamond symbols denote OVX rats; lighter shades and dot symbols denote NOVX rats. Group names are marked in red fonts inside the convex hulls comprised by individuals from the same group. The statistical significance between the groups along the PCs was analysed by two-way MANOVA. Significant results for PC1: DM— $p < 0.05$. Detailed data—see Supplementary Material 1G.

of fracture is also elevated [5, 6, 40]. In T1D, hyperglycemia and the inflammatory environment influence all types of bone cells, i.e., osteoblasts, osteocytes, and osteoclasts [41]. The mechanisms of the development of the bone changes,

demonstrated in experimental conditions, involved, among others: intensification of osteoclast activity, decreased function of osteoblasts induced by insulin deficiency, and increased expression of sclerostin by osteocytes, as well as

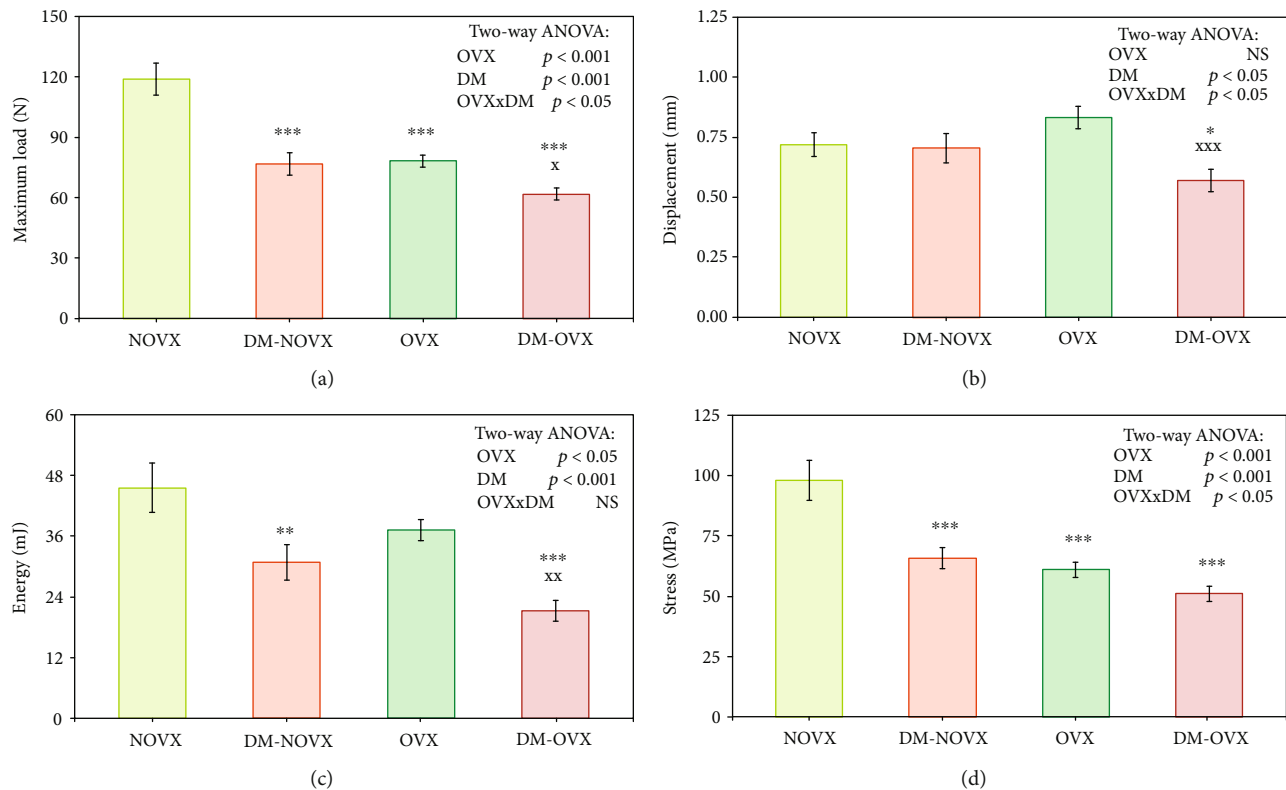


FIGURE 10: Effects of diabetes (DM) and/or estrogen deficiency on the mechanical properties of cancellous bone (the proximal tibial metaphysis – data for the maximum load point) in rats. Bilateral ovariectomy was performed 5 weeks before the end of the experiment. Diabetes was induced 3 days after the ovariectomy by a single administration of streptozotocin (60 mg/kg *i.p.*). Results are presented as means \pm SEM ($n = 9 - 10$). NOVX: nonovariectomized control rats; DM-NOVX: rats with type 1 diabetes; OVX: ovariectomized control rats; DM-OVX: ovariectomized rats with type 1 diabetes. Two-way ANOVA followed by Fisher's LSD test was used for evaluation of the significance of the results. * $p < 0.05$, ** $p < 0.01$, *** $p < 0.001$ —significantly different from the NOVX control rats; ^x $p < 0.05$, ^{xx} $p < 0.01$, ^{xxx} $p < 0.001$ —significantly different from the OVX control rats.

decreased bone quality caused by advanced glycation products [41, 42]. Moreover, diabetes increases oxidative stress [43, 44], which may intensify bone resorption and inhibit bone formation [39].

Summing up, the ovariectomy and STZ administration induced opposite actions on the body mass gain. Bone mass and macrometric parameters were not affected by estrogen deficiency, whereas diabetes induced significant decreases in the bone mass, length, and femoral diaphysis cross-section area. Nonetheless, the bone quality changes in the diabetic rats in the present study were very similar to those developing due to estrogen deficiency. In both experimental models, cancellous bone mechanical properties were worsened to almost the same extent, and there was no damaging effect on the strength of the compact bone of the femoral diaphysis. The differences concerning cancellous bone microstructure were slight: the decrease in BV/TV was caused by a decrease in Tb.N with an increase in Tb.Sp in the ovariectomized control rats, whereas in the diabetic rats, by a decrease in Tb.Th. The main difference between the models concerned the bone turnover markers. Although both endocrine changes induced increases in bone resorption, estrogen deficiency increased bone formation marker concentration, whereas diabetes decreased it. The decrease in bone formation may explain the decrease in Tb.Th in the diabetic rats.

The skeletal effects of diabetes in the estrogen-deficient rats were very similar to those induced in the rats with normal estrogen levels (nonovariectomized). No further decrease in BV/TV was demonstrated, and Tb.Th decreased and Tb.N increased in relation to the ovariectomized control rats. However, further deterioration in the mechanical properties of cancellous bone compared to the estrogen-deficient control rats was observed. Similarly to the effects in the non-ovariectomized rats, diabetes induced an increase in Young's modulus of the femoral diaphysis (compact bone) of the ovariectomized rats; however, no increases in the stress values were demonstrated. The bone resorption marker (CTX-I) further increased, and bone formation marker (osteocalcin) strongly decreased in relation to both the ovariectomized and nonovariectomized control rats. These observations are partially at variance with those of Liu et al. [25] who concluded, based on microstructural and gene expression studies, that STZ-induced diabetes, in estrogen-deficient rats, reversed high bone turnover osteoporosis into low bone turnover one (decreases in both formation and bone resorption indices), with stronger microstructure changes and bone loss. On the other hand, Wen et al. [20] reported increasing effects of concurrent diabetes and estrogen deficiency on the rat serum bone turnover markers and osteoblast and osteoclast number in bone tissue, similarly to

TABLE 5: Effects of diabetes (DM) and/or estrogen deficiency on the mechanical properties of cancellous (the proximal tibial metaphysis) and compact (the femoral diaphysis) bone in rats.

| Parameter/group | Nonovariectomized (NOVX) rats | | Ovariectomized (OVX) rats | | Two-way ANOVA | | |
|---|-------------------------------|----------------|---------------------------|-----------------------------|---------------|-------------|---------|
| | Control | DM | Control | DM | OVX | DM | OVXx DM |
| Young's modulus (MPa) | 4063 ± 430 | 3269 ± 390 | 2713 ± 248** | 3169 ± 182 | $p < 0.05$ | NS | NS |
| Fracture point load (N) | 89.5 ± 7.5 | 54.5 ± 5.0*** | 60.0 ± 2.8*** | 43.6 ± 2.2*** _X | $p < 0.001$ | $p < 0.001$ | NS |
| Tibia Displacement for fracture point load (mm) | 1.068 ± 0.054 | 1.004 ± 0.088 | 1.208 ± 0.074 | 0.953 ± 0.087 | NS | $p < 0.05$ | NS |
| Energy for fracture point load (mJ) | 80.8 ± 5.7 | 49.9 ± 7.0*** | 63.9 ± 5.0* | 40.7 ± 3.9*** _{XX} | $p < 0.05$ | $p < 0.001$ | NS |
| Stress for fracture point load (MPa) | 74.1 ± 7.8 | 47.3 ± 4.8*** | 47.4 ± 4.2*** | 35.6 ± 1.3*** | $p < 0.001$ | $p < 0.001$ | NS |
| Young's modulus (MPa) | 8929 ± 242 | 10886 ± 373*** | 8957 ± 418 | 9955 ± 333** _X | NS | $p < 0.001$ | NS |
| Maximum load (N) | 124.8 ± 4.3 | 125.8 ± 3.8 | 130.1 ± 3.7 | 119.3 ± 5.3 | NS | NS | NS |
| Displacement for maximum load (mm) | 0.502 ± 0.021 | 0.493 ± 0.019 | 0.516 ± 0.034 | 0.487 ± 0.016 | NS | NS | NS |
| Energy for maximum load (mJ) | 38.0 ± 2.8 | 38.2 ± 2.4 | 41.0 ± 3.7 | 35.7 ± 2.6 | NS | NS | NS |
| Femur Stress for maximum load (MPa) | 168.9 ± 4.2 | 189.7 ± 4.9** | 171.2 ± 4.3 | 174.6 ± 5.7 ^a | NS | $p < 0.05$ | NS |
| Fracture point load (N) | 123.3 ± 4.4 | 124.8 ± 3.6 | 129.4 ± 3.8 | 118.3 ± 5.2 | NS | NS | NS |
| Displacement for fracture point load (mm) | 0.517 ± 0.021 | 0.505 ± 0.021 | 0.524 ± 0.034 | 0.501 ± 0.019 | NS | NS | NS |
| Energy for fracture point load (mJ) | 39.8 ± 2.9 | 39.8 ± 2.6 | 42.0 ± 3.8 | 37.5 ± 3.2 | NS | NS | NS |
| Stress for fracture point load (MPa) | 166.8 ± 4.6 | 188.1 ± 4.6** | 170.3 ± 4.4 | 173.1 ± 5.7 ^a | NS | $p < 0.05$ | NS |

Bilateral ovariectomy was performed 5 weeks before the end of the experiment. Diabetes was induced 3 days after the ovariectomy by a single administration of streptozotocin (60 mg/kg *i.p.*). Results are presented as means ± SEM ($n = 9 - 10$). Two-way ANOVA followed by Fisher's LSD test was used for evaluation of the significance of the results. * $p < 0.05$, ** $p < 0.01$, *** $p < 0.001$ —significantly different from the NOVX control rats; ^X $p < 0.05$, ^{XX} $p < 0.01$ —significantly different from the OVX control rats; ^a $p < 0.05$ —significantly different from the DM-NOVX rats.

the effects induced by estrogen deficiency alone (whereas in diabetes alone, bone formation indices were decreased). The mouse studies indicated possible roles of renin-angiotensin and kallikrein-kinin systems [24] and increased expression of TNF- α [23] in the development of osteoporotic changes induced by diabetes and estrogen deficiency.

There are few studies that investigated bone mechanical properties in diabetic osteoporotic animals. As far as mechanical properties of cortical bone are concerned, de Mello-Sampayo et al. [22] reported on the favorable effect of hyperglycemia on the femoral strength, since the values of ultimate stress and Young's modulus increased in estrogen-deficient diabetic rats. We also observed increases in Young's modulus values for the femoral diaphysis of the diabetic rats, regardless of the estrogen status. Also, the maximum stress increased, but only in the nonovariectomized diabetic rats. The lack of such an effect in the estrogen-deficient rats does not support the hypothesis on the favorable effects of diabetes (hyperglycemia) on the mechanical properties of cortical bone. Moreover, it should be stressed that diabetes induced strong harmful effect on the mechanical properties of the cancellous bone of the tibial metaphysis, both in the nonovariectomized and ovariectomized rats. Similarly to our results for cancellous bone, no significant differences between the L4 vertebra strength of nonovariectomized and ovariectomized diabetic rats were observed by Lee et al.

[21] (the effects of estrogen deficiency alone were not investigated in that study).

The differences between the results concerning the effects of diabetes and estrogen deficiency on the skeletal system in different studies might have resulted from differences in the study designs. Stronger than in the present study aggravation of damaging effects of both pathologies over those induced by them separately were reported by other authors in mouse models [23, 24] or after longer periods of observation in rats [20, 21, 25]. However, the measurements were performed five weeks after the ovariectomy in the present study. Such a period in adult rats corresponds to about three years in humans [45]. The period of four-five weeks was long enough to demonstrate the effects of different treatments or estrogen deficiency on the skeletal system in rats in our previous studies [30, 38].

There are interactions between estrogen deficiency and energy metabolism. For example, it has been reported that long-term estrogen deficiency leads to the decline of whole-body glucose metabolism in ovariectomized rats [46]. However, based on the results of the present study, it seems that estrogen deficiency exerts very slight effects on the changes induced by diabetes in the rat skeletal system. This seems to agree with the lack of data on the effect of diabetes on postmenopausal osteoporosis in women. Consistently, it has been reported that, in patients, the presence of diabetes did not

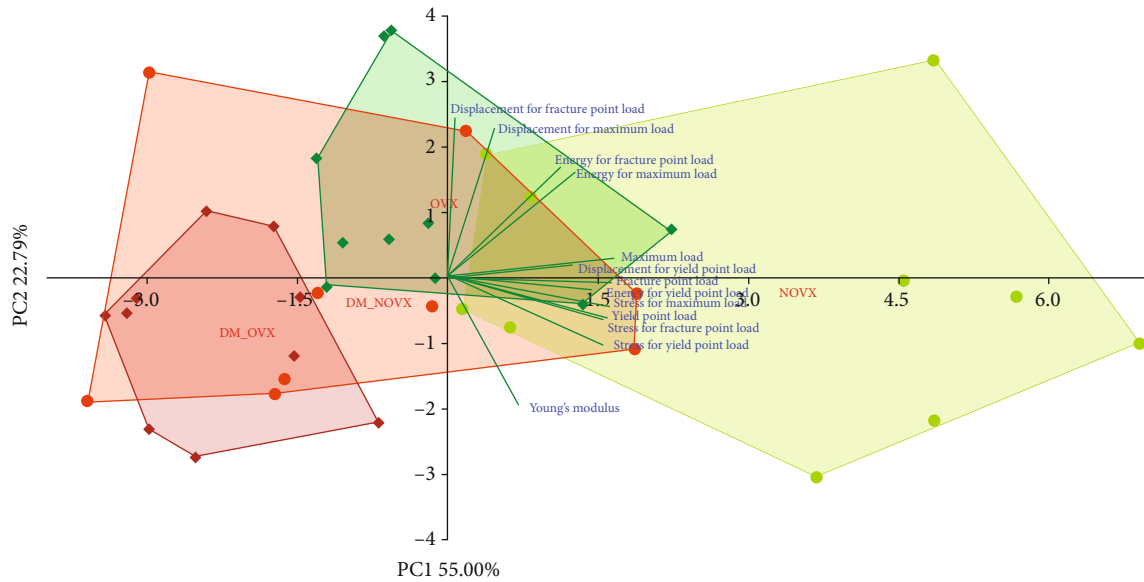


FIGURE 11: PCA biplot of the results concerning mechanical properties of cancellous bone (the proximal tibial metaphysis) in the diabetic and/or estrogen-deficient rats. Bilateral ovariectomy was performed 5 weeks before the end of the experiment. Diabetes was induced 3 days after the ovariectomy by a single administration of streptozotocin (60 mg/kg *i.p.*). Blue font and green lines indicate correlations of measured variables against experimental groups. Shades of red denote DM rats; shades of green denote nondiabetic rats. Darker shades and diamond symbols denote OVX rats; lighter shades and dot symbols denote NOVX rats. Group names are marked in red fonts inside the convex hulls comprised by individuals from the same group. The statistical significance between the groups along the PCs was analysed by two-way MANOVA. Significant results for PC1: OVX— $p < 0.001$; DM— $p < 0.001$. Detailed data—see Supplementary Material 1H.

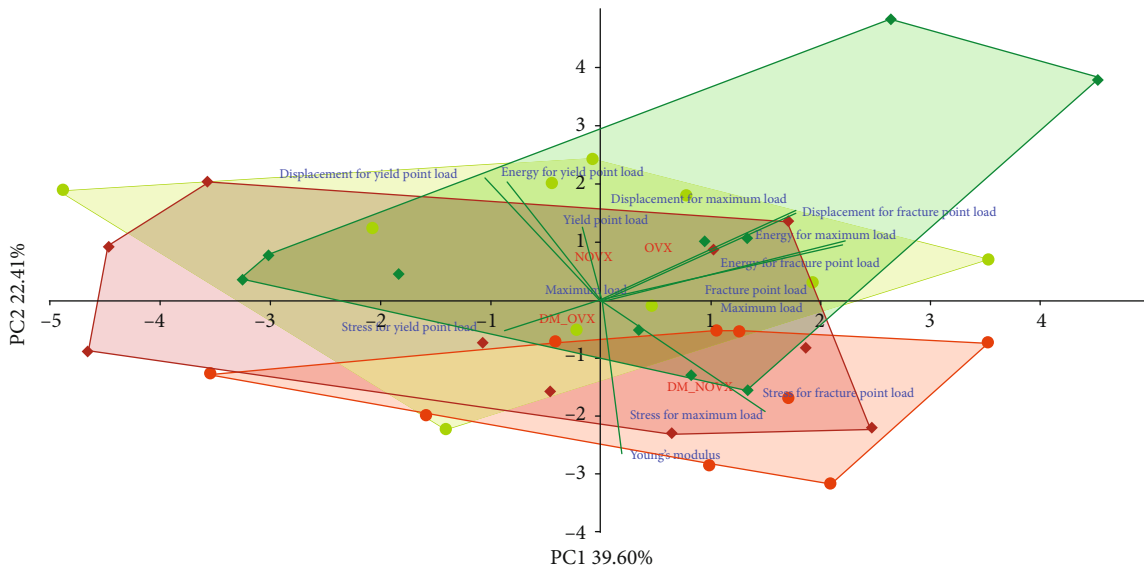


FIGURE 12: PCA biplot of the results concerning mechanical properties of compact bone (the femoral diaphysis) in the diabetic and/or estrogen-deficient rats. Bilateral ovariectomy was performed 5 weeks before the end of the experiment. Diabetes was induced 3 days after the ovariectomy by a single administration of streptozotocin (60 mg/kg *i.p.*). Blue font and green lines indicate correlations of measured variables against experimental groups. Shades of red denote DM rats; shades of green denote nondiabetic rats. Darker shades and diamond symbols denote OVX rats; lighter shades and dot symbols denote NOVX rats. Group names are marked in red fonts inside the convex hulls comprised by individuals from the same group. The statistical significance between the groups along the PCs was analysed by two-way MANOVA. Significant results for PC2: DM— $p < 0.01$. Detailed data—see Supplementary Material 1I.

TABLE 6: Effects of diabetes (DM) and/or estrogen deficiency on the serum concentrations of cytokines in rats.

| Parameter/group | Nonovariectomized (NOVX) rats | | Ovariectomized (OVX) rats | | Two-way ANOVA | | |
|-----------------------|-------------------------------|------------------------|---------------------------|--|---------------|-------------|------------|
| | Control | DM | Control | DM | OVX | DM | OVXx DM |
| IL-1 α (pg/mL) | 174.0 \pm 25.7 | 366.7 \pm 64.9** | 180.3 \pm 34.9 | 362.1 \pm 42.9** ^{XX} | NS | $p < 0.001$ | NS |
| IL-1 β (pg/mL) | 613.6 \pm 155.9 | 43675 \pm 23833 | 495.5 \pm 138.5 | 29915 \pm 22082 | NS | $p < 0.05$ | NS |
| IL-2 (pg/mL) | 585.7 \pm 260.4 | 2670 \pm 1394 | 419.3 \pm 141.9 | 743.9 \pm 377.8 | NS | NS | NS |
| IL-4 (pg/mL) | 105.9 \pm 19.9 | 233.7 \pm 37.8** | 106.6 \pm 22.9 | 152.3 \pm 19.9 ^a | NS | $p < 0.01$ | NS |
| IL-5 (pg/mL) | 565.7 \pm 39.6 | 649.2 \pm 42.1 | 543.4 \pm 49.2 | 610.9 \pm 78.6 | NS | NS | NS |
| IL-6 (pg/mL) | 470.5 \pm 214.2 | 750.6 \pm 185.5 | 379.1 \pm 86.4 | 635.2 \pm 158.5 | NS | NS | NS |
| IL-7 (pg/mL) | 506.5 \pm 108.7 | 5886 \pm 1750** | 426.7 \pm 91.8 | 5168 \pm 1873 ^X | NS | $p < 0.001$ | NS |
| IL-10 (pg/mL) | 84.8 \pm 15.0 | 193.2 \pm 33.5** | 80.8 \pm 18.0 | 170.8 \pm 29.3 ^X | NS | $p < 0.001$ | NS |
| IL-12p70 (pg/mL) | 250.4 \pm 62.7 | 307.5 \pm 57.7 | 274.3 \pm 92.3 | 324.2 \pm 75.2 | NS | NS | NS |
| IL-13 (pg/mL) | 139.2 \pm 25.5 | 424.1 \pm 140.4 | 128.2 \pm 35.1 | 209.2 \pm 63.7 | NS | $p < 0.05$ | NS |
| IL-17A (pg/mL) | 62.3 \pm 9.0 | 95.6 \pm 19.7 | 61.9 \pm 12.7 | 110.4 \pm 19.2 | NS | $p < 0.05$ | NS |
| IL-18 (pg/mL) | 3950 \pm 851 | 10802 \pm 5377 | 4341 \pm 208 | 4663 \pm 1651 | NS | NS | NS |
| G-CSF (pg/ml) | 2.16 \pm 0.77 | 5.98 \pm 2.07 | 1.56 \pm 0.72 | 5.45 \pm 1.65 | NS | $p < 0.05$ | NS |
| GM-CSF (pg/ml) | 874.2 \pm 224.5 | 26206 \pm 7878** | 793.5 \pm 216.4 | 22875 \pm 6940** ^{XX} | NS | $p < 0.001$ | NS |
| GRO/KC (pg/ml) | 627.1 \pm 65.4 | 12186 \pm 6622 | 659.9 \pm 178.6 | 6295 \pm 2398 | NS | $p < 0.05$ | NS |
| IFN- γ (pg/ml) | 308.6 \pm 50.8 | 618.8 \pm 146.8 | 293.8 \pm 76.3 | 459.3 \pm 87.4 | NS | $p < 0.05$ | NS |
| M-CSF (pg/ml) | 22.8 \pm 5.4 | 55.3 \pm 12.2** | 15.8 \pm 3.8 | 51.7 \pm 8.4 ^{XX} | NS | $p < 0.001$ | NS |
| MIP-1a (pg/ml) | 206.8 \pm 56.5 | 10541 \pm 2459*** | 157.7 \pm 35.3 | 10720 \pm 2032*** ^{XXX} | NS | $p < 0.001$ | NS |
| MIP-3a (pg/ml) | 28.6 \pm 4.1 | 106.5 \pm 13.9 | 26.3 \pm 4.9 | 206.4 \pm 67.2** ^{XX} | NS | $p < 0.01$ | NS |
| RANTES (pg/ml) | 2011 \pm 214 | 2192 \pm 223 | 2204 \pm 813 | 8095 \pm 1414*** ^{XXX} ^{aaa} | $p < 0.01$ | $p < 0.01$ | $p < 0.01$ |
| TNF- α (pg/ml) | 326.4 \pm 108.6 | 457.4 \pm 88.1 | 254.4 \pm 81.3 | 623.0 \pm 127.6 | NS | $p < 0.05$ | NS |
| VEGF (pg/ml) | 486.8 \pm 67.0 | 7360 \pm 2916** | 608.9 \pm 122.2 | 4020 \pm 991 | NS | $p < 0.01$ | NS |
| MCP-1 (MCAF) (pg/ml) | 3119 \pm 493 | 834106 \pm 241089*** | 4110 \pm 1334 | 598440 \pm 159609** ^{XX} | NS | $p < 0.001$ | NS |

Bilateral ovariectomy was performed 5 weeks before the end of the experiment. Diabetes was induced 3 days after the ovariectomy by a single administration of streptozotocin (60 mg/kg *i.p.*). Results are presented as means \pm SEM ($n = 7$). Two-way ANOVA followed by Fisher's LSD test was used for evaluation of the significance of the results. * $p < 0.05$, ** $p < 0.01$, *** $p < 0.001$ —significantly different from the NOVX control rats; ^X $p < 0.05$, ^{XX} $p < 0.01$, ^{XXX} $p < 0.001$ —significantly different from the OVX control rats; ^a $p < 0.05$, ^{aaa} $p < 0.001$ —significantly different from the DM-NOVX rats.

affect response to different antiosteoporotic drugs, regarding BMD increase and vertebral fracture risk reduction [47].

To evaluate the background of the skeletal changes observed in the present study, serum concentrations of a wide panel of cytokines was evaluated. Cytokines play major roles in numerous autoimmune diseases, hypersensitivity reactions, and pathologic conditions, like rheumatoid arthritis, dermatitis, asthma, and insulin-dependent diabetes [48]. Although cytokines mostly act locally, changes in their blood concentrations may exert general effects. It is likely that they are involved in the development of osteoporosis. Although no significant differences between the plasma levels of ten investigated cytokines in postmenopausal women with normal and low BMD were reported [49], some changes in cytokine profiles were demonstrated using advanced statistical methods [48].

The relationships between cytokines released by bone (osteoblasts, osteocytes, and osteoclasts) and immune cells are extremely complex and not fully recognized [50]. Apart from the best known RANKL/osteoprotegerin axis, the cytokines known to regulate the proliferation, differentiation, and

functions of osteoblastic and osteoclastic cells, include, among others, proosteoclastogenic cytokines, stimulating bone resorption (M-CSF, TNF- α , IL-1, IL-6, IL-8, and IL-17), and antiosteoclastogenic cytokines (transforming growth factor β (TGF- β), IFN- γ , IL-4, IL-10, and IL-12) [51, 52]. A shift in general immune balance towards an activated inflammatory immune status is considered a risk factor for osteoporosis [48]. Also, in diabetes, numerous changes in cytokine levels are observed [53, 54].

In the present study, no significant effect of estrogen deficiency on the examined cytokine levels was demonstrated. It has been suggested for many years that estrogen deficiency is connected with low-grade inflammation and increased levels of proinflammatory cytokines [55, 56]. However, our results are consistent with results concerning the evaluation of ten cytokines in postmenopausal women mentioned above [49]. They are also consistent with the study of Russell et al. [57], in which a lack of effect of estradiol administration on the serum levels of most of 24 cytokines was demonstrated in estrogen-deficient rats. It is possible that the estrogen deficiency-induced effects on serum cytokine levels need

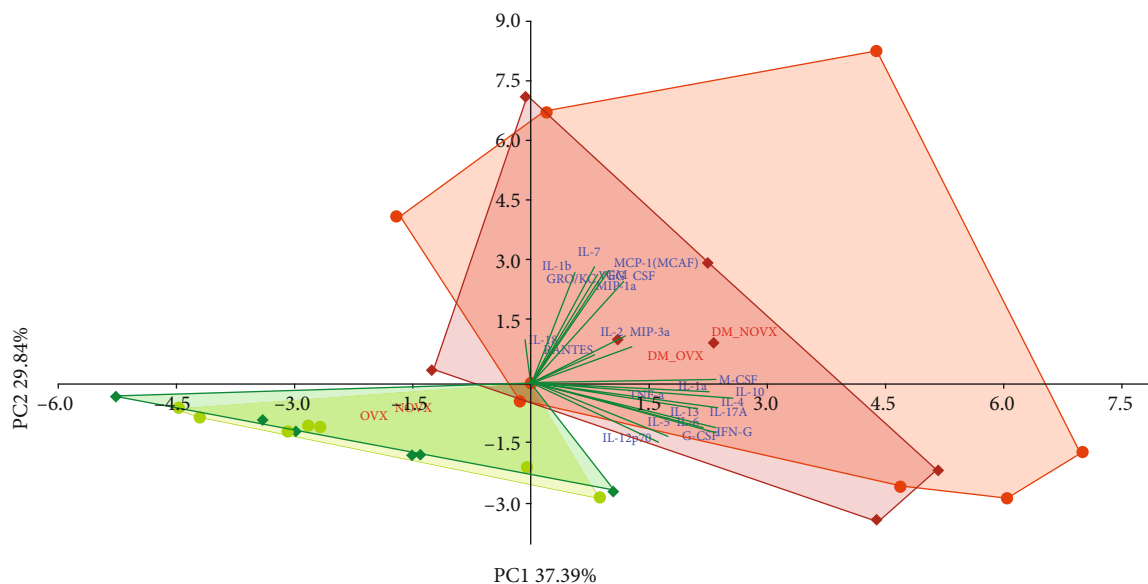


FIGURE 13: PCA biplot of the results concerning the serum concentrations of 23 cytokines in the diabetic and/or estrogen deficiency rats. Bilateral ovariectomy was performed 5 weeks before the end of the experiment. Diabetes was induced 3 days after the ovariectomy by a single administration of streptozotocin (60 mg/kg *i.p.*). Blue font and green lines indicate correlations of measured variables against experimental groups. Shades of red denote DM rats; shades of green denote nondiabetic rats. Darker shades and diamond symbols denote OVX rats; lighter shades and dot symbols denote NOVX rats. Group names are marked in red fonts inside the convex hulls comprised by individuals from the same group. The statistical significance between the groups along the PCs was analysed by two-way MANOVA. Significant results for PC1: DM— $p < 0.001$, and for PC2: DM— $p < 0.05$. Detailed data—see Supplementary Material 1J.

more time to develop, since significant changes in the IL-1 α , IL-6, and IFN- γ levels 3 months after ovariectomy were reported [58]. The diabetic rats, on the other hand, had increased levels of both proinflammatory and anti-inflammatory cytokines. The latter was probably the effect of compensatory mechanisms. It has been previously demonstrated that both estrogen deficiency and diabetes increased the bone expression of TNF- α mRNA in mice; the effect observed in diabetic mice was strongly intensified by estrogen deficiency [23]. Also in our study, the serum TNF- α concentration was the highest in the ovariectomized diabetic rats (however, the differences were insignificant).

An interesting observation of the present study is that the serum RANTES concentration was increased mainly in the ovariectomized diabetic rats. RANTES is a chemoattractant cytokine (chemokine). RANTES is, among others, secreted by osteoblasts and osteoclasts and promotes both osteoblast and osteoclast migration (with no effect on bone resorption), favoring bone formation [59]. An exceptional cytokine pattern with increased levels of RANTES and no significant effects on those of IL-6 and TNF- α was observed in fatty degenerative osteolysis/osteonecrosis in the jawbone [60]. Plasma RANTES has been proposed as a marker of the atherosclerotic process [61]. There is a report on the increased serum level of RANTES in osteoporotic patients [62]. It seems that the elevation of the serum RANTES concentration in the ovariectomized diabetic rats may be a compensatory reaction to strong inhibition of bone formation and an increase in bone resorption.

To better understand the interactions between diabetes- and estrogen deficiency-induced skeletal changes, the princi-

pal component analysis (PCA) was conducted on the obtained results. PCA is a multivariate technique where individual observations of variables in combined datasets are transformed into composite principal components (PCs) through data reduction. That allows for spatial differentiation of samples into clusters. The clusters separate in accordance with the differences observed in measured variables across the plane or multidimensional space built-up by two or more PCs [37, 63]. Since multiple variables take part in the PCA, their impact on the observed clustering and distance between clusters is not equal [37]. Unlike quantitative-only comparison of values for individual variables in datasets through analysis of variance (ANOVA), the PCA provides ranks which serve as an auxiliary qualitative information. The results of PCA clearly indicate significant effects of diabetes or estrogen deficiency on all the investigated groups of results. Also, differences concerning some general parameters (body mass and mass of internal organs, serum biochemical parameters) between the nonovariectomized and ovariectomized diabetic rats were observed. However, no interactions indicating differences in the skeletal or cytokine changes induced by diabetes depending on the estrogen status were demonstrated.

It must be noted that the effects of diabetes on numerous cytokine levels, regardless of the estrogen status, were very strong. Although the skeletal effects concerning the quality of bone (mechanical properties) induced by diabetes were similar to those induced by estrogen deficiency, the systemic diabetes effects, as indicated by profound changes in the cytokine levels, were much bigger.

Very strong effects of STZ-induced diabetes on cytokine levels indicate that the changes may be too profound to be

relevant to those observed in diabetic patients, since patients with T1D are treated with insulin. This seems to be the main limitation of the study. However, it has been reported that, in experimental conditions, the administration of insulin improves not only glycemia but also the bone status [64]. Another limitation of the study is that it was performed on young adult rats, whereas osteoporosis is predominantly a disease of the elderly. Also, it is possible that the use of an isoflavone-free (soy-free diet), instead of a standard laboratory diet, used in the present study, might provide more significant results concerning cytokine levels in estrogen-deficient rats [57]. Nevertheless, the results of the present study indicate that the model of STZ-induced diabetes, widely used in experimental pharmacology to investigate the effects of different potential antidiabetic treatments, may be too aggressive to mirror the clinical settings.

Although the effects of type 1 and type 2 diabetes on the skeletal system in humans are differential, we observed striking similarities in the effects on bone microstructure, mechanical properties, and serum bone turnover markers in rats with experimental T1D induced by STZ and T2D induced by high-fat diet and low-dose STZ [32, 65–67]. On the other hand, similar results, concerning decreased bone turnover, to those demonstrated for ovariectomized rats with T1D [25] were obtained in ovariectomized Goto-Kakizaki rats with T2D [26]. Thus, the observations from the present study may be relevant in relation to experimental T2D.

5. Conclusions

In conclusion, the unfavorable skeletal changes induced by diabetes in female rats were only slightly intensified by estrogen deficiency. Despite similar effects on bone microstructure and strength, the influence of STZ-induced T1D on the skeletal system was based on much more profound changes in systemic homeostasis than those induced by estrogen deficiency.

Abbreviations

| | |
|-----------------|--|
| ANOVA: | Analysis of variance |
| AOPP: | Advanced oxidation protein products |
| ASBMR: | American Society for Bone and Mineral Research |
| BMD: | Bone mineral density |
| BV/TV: | Bone volume to tissue volume ratio |
| Ct.Ar: | Transverse cross-sectional area of the cortical bone |
| CTX-I: | C-terminal telopeptide fragments of type I collagen |
| DM: | Diabetes mellitus |
| G-CSF: | Granulocyte colony-stimulating factor |
| GM-CSF: | Granulocyte-macrophage colony-stimulating factor |
| GRO/KC: | Growth-regulated oncogene/keratinocyte chemoattractant |
| HDL: | High-density lipoprotein |
| IFN- γ : | Interferon- γ |
| IL: | Interleukin |

| | |
|-----------------|---|
| LDL: | Low-density lipoprotein |
| LSD: | Least significant difference |
| Ma.Ar: | Transverse cross-sectional area of the marrow cavity |
| Ma.Ar/Tt.Ar: | Transverse cross-sectional area of the marrow cavity/total diaphysis area ratio |
| MANOVA: | Multivariate analysis of variance |
| MAR: | Mineral apposition rate |
| M-CSF: | Macrophage colony-stimulating factor |
| MCP-1 (MCAF): | Monocyte chemoattractant protein-1 (monocyte chemotactic and activating factor) |
| MIP-1a: | Macrophage inflammatory protein-1a |
| MIP-3a: | Macrophage inflammatory protein-3a |
| NOVX: | Nonovariectomized |
| NS: | Not significant |
| OVX: | Ovariectomized |
| PCA: | Principal component analysis |
| RANKL: | Receptor activator of nuclear factor κ B ligand |
| RANTES: | Regulated on activation, normal T cell expressed and secreted |
| SEM: | Standard error of the mean |
| STZ: | Streptozotocin |
| T1D: | Type 1 diabetes |
| T2D: | Type 2 diabetes |
| Tb.N: | Trabecular number |
| Tb.Sp: | Trabecular separation |
| Tb.Th: | Trabecular thickness |
| TGF- β : | Transforming growth factor β |
| TNF- α : | Tumor necrosis factor α |
| Tt.Ar: | Transverse cross-sectional area of the whole diaphysis |
| VEGF: | Vascular endothelial growth factor. |

Data Availability

The data used to support the findings of this study are available from the corresponding author upon request.

Ethical Approval

This study was approved by the Local Ethics Commission in Katowice, Poland (permission numbers: 9/2015 and 149/2015).

Conflicts of Interest

The authors declare that there is no conflict of interest regarding the publication of this paper.

Acknowledgments

The study was supported by grant No. KNW-1-123/K/8/O, Medical University of Silesia, Katowice, Poland.

Supplementary Materials

Supplementary Material 1 presents results for two-way MANOVA for the PCA biplots obtained for individual datasets concerning results presented in Figures 1 and 2,

Figures 4–6, Figures 8 and 9, and Figures 11–13. (Supplementary Materials)

References

- [1] L. Shepstone, E. Lenaghan, C. Cooper et al., “Screening in the community to reduce fractures in older women (SCOOP): a randomised controlled trial,” *Lancet*, vol. 391, no. 10122, pp. 741–747, 2018.
- [2] S. Khosla and E. Shane, “A crisis in the treatment of osteoporosis,” *Journal of Bone and Mineral Research*, vol. 31, no. 8, pp. 1485–1487, 2016.
- [3] U. Tarantino, G. Iolascon, L. Cianferotti et al., “Clinical guidelines for the prevention and treatment of osteoporosis: summary statements and recommendations from the Italian Society for Orthopaedics and Traumatology,” *Journal of Orthopaedics and Traumatology*, vol. 18, Supplement 1, pp. 3–36, 2017.
- [4] American Diabetes Association, “2. Classification and diagnosis of diabetes: standards of medical care in diabetes—2019,” *Diabetes Care*, vol. 42, Supplement 1, pp. S13–S28, 2019.
- [5] on behalf of the Bone and Diabetes Working Group of IOF, S. L. Ferrari, B. Abrahamsen et al., “Diagnosis and management of bone fragility in diabetes: an emerging challenge,” *Osteoporosis International*, vol. 29, no. 12, pp. 2585–2596, 2018.
- [6] J. Starup-Linde, M. Frost, P. Vestergaard, and B. Abrahamsen, “Epidemiology of fractures in diabetes,” *Calcified Tissue International*, vol. 100, no. 2, pp. 109–121, 2017.
- [7] J. Starup-Linde and P. Vestergaard, “Biochemical bone turnover markers in diabetes mellitus – a systematic review,” *Bone*, vol. 82, pp. 69–78, 2016.
- [8] S. Mohsin, M. M. Y. H. Baniyas, R. S. M. H. AlDarmaki, K. Tekes, H. Kalász, and E. A. Adeghate, “An update on therapies for the treatment of diabetes-induced osteoporosis,” *Expert Opinion on Biological Therapy*, vol. 19, no. 9, pp. 937–948, 2019.
- [9] S. Mishra and B. L. G. Nyomba, “Estrogen deficiency plus type 1 diabetes: a double-dip for bone loss,” *Endocrinology*, vol. 158, no. 7, pp. 2066–2067, 2017.
- [10] J. Zhao, Y. Jiang, C. F. Njeh, R. Bouillon, P. Geusens, and H. K. Genant, “Chapter 18: Animal studies,” *The Physical Measurement of Bone*, C. M. Langton and C. F. Njeh, Eds., pp. 571–600, Bristol and Philadelphia: Institute of Physics Publishing, 2003.
- [11] T. Szkudelski, “The mechanism of alloxan and streptozotocin action in B cells of the rat pancreas,” *Physiological Research*, vol. 50, no. 6, pp. 537–546, 2001.
- [12] S. Lenzen, “The mechanisms of alloxan- and streptozotocin-induced diabetes,” *Diabetologia*, vol. 51, no. 2, pp. 216–226, 2008.
- [13] M. Asrafuzzaman, Y. Cao, R. Afroz, D. Kamato, S. Gray, and P. J. Little, “Animal models for assessing the impact of natural products on the aetiology and metabolic pathophysiology of type 2 diabetes,” *Biomedicine & Pharmacotherapy*, vol. 89, pp. 1242–1251, 2017.
- [14] P. Masiello, “Animal models of type 2 diabetes with reduced pancreatic β -cell mass,” *The International Journal of Biochemistry & Cell Biology*, vol. 38, no. 5–6, pp. 873–893, 2006.
- [15] M. Fukuharu, J. Sato, I. Ohsawa et al., “Additive effects of estrogen deficiency and diabetes on bone mineral density in rats,” *Diabetes Research and Clinical Practice*, vol. 48, no. 1, pp. 1–8, 2000.
- [16] J. Verhaeghe, G. Oloumi, E. van Herck et al., “Effects of long-term diabetes and/or high-dose 17β -estradiol on bone formation, bone mineral density, and strength in ovariectomized rats,” *Bone*, vol. 20, no. 5, pp. 421–428, 1997.
- [17] V. Gopalakrishnan, J. Arunakaran, M. M. Aruldas, and N. Srinivasan, “Effects of streptozotocin-induced diabetes mellitus on some bone turnover markers in the vertebrae of ovari-intact and ovariectomized adult rats,” *Biochemistry and Cell Biology*, vol. 84, no. 5, pp. 728–736, 2006.
- [18] S. Herrero, O. M. Calvo, C. García-Moreno et al., “Low bone density with normal bone turnover in ovariectomized and streptozotocin-induced diabetic rats,” *Calcified Tissue International*, vol. 62, no. 3, pp. 260–265, 1998.
- [19] J. Verhaeghe, A. M. H. Suiker, T. A. Einhorn et al., “Brittle bones in spontaneously diabetic female rats cannot be predicted by bone mineral measurements: studies in diabetic and ovariectomized rats,” *Journal of Bone and Mineral Research*, vol. 9, no. 10, pp. 1657–1667, 1994.
- [20] B. Wen, L. Zhao, H. Zhao, and X. Wang, “Liraglutide exerts a bone-protective effect in ovariectomized rats with streptozotocin-induced diabetes by inhibiting osteoclastogenesis,” *Experimental and Therapeutic Medicine*, vol. 15, no. 6, pp. 5077–5083, 2018.
- [21] Y.-S. Lee, R. Gupta, J.-T. Kwon et al., “Effect of a bisphosphonate and selective estrogen receptor modulator on bone remodeling in streptozotocin-induced diabetes and ovariectomized rat model,” *The Spine Journal*, vol. 18, no. 10, pp. 1877–1887, 2018.
- [22] C. de Mello-Sampayo, A. A. Agripino, D. Stilwell et al., “Chronic hyperglycemia modulates rat osteoporotic cortical bone microarchitecture into less fragile structures,” *International Journal of Endocrinology*, vol. 2017, Article ID 4603247, 9 pages, 2017.
- [23] S. Raetz, H. Bierhalter, D. Schoenherr, N. Parameswaran, and L. R. McCabe, “Estrogen deficiency exacerbates type 1 diabetes-induced bone TNF- α expression and osteoporosis in female mice,” *Endocrinology*, vol. 158, no. 7, pp. 2086–2101, 2017.
- [24] Y. Zhang, L. Wang, J.-X. Liu, X. L. Wang, Q. Shi, and Y. J. Wang, “Involvement of skeletal renin-angiotensin system and kallikrein-kinin system in bone deteriorations of type 1 diabetic mice with estrogen deficiency,” *Journal of Diabetes and its Complications*, vol. 30, no. 8, pp. 1419–1425, 2016.
- [25] B. Liu, W. Feng, T. Hasegawa, N. Amizuka, and M. Li, “Type 1 diabetes mellitus induced low bone turnover in ovariectomized rats,” *Histology and Histopathology*, vol. 34, no. 1, pp. 57–67, 2019.
- [26] R. Aeimlapa, K. Wongdee, W. Tiyasatkulkovit, K. Kengkoom, N. Krishnamra, and N. Charoenphandhu, “Anomalous bone changes in ovariectomized type 2 diabetic rats: inappropriately low bone turnover with bone loss in an estrogen-deficient condition,” *American Journal of Physiology-Endocrinology and Metabolism*, vol. 317, no. 4, pp. E646–E657, 2019.
- [27] S. Mohsin, S. Kaimala, J. J. Sunny, E. Adeghate, and E. M. Brown, “Type 2 diabetes mellitus increases the risk to hip fracture in postmenopausal osteoporosis by deteriorating the trabecular bone microarchitecture and bone mass,” *Journal Diabetes Research*, vol. 2019, article 3876957, 10 pages, 2019.
- [28] C. H. Turner and D. B. Burr, “Basic biomechanical measurements of bone: a tutorial,” *Bone*, vol. 14, no. 4, pp. 595–608, 1993.

- [29] E. K. Stürmer, D. Seidlová-Wuttke, S. Sehmisch et al., “Standardized bending and breaking test for the normal and osteoporotic metaphyseal tibias of the rat: effect of estradiol, testosterone, and raloxifene,” *Journal of Bone and Mineral Research*, vol. 21, no. 1, pp. 89–96, 2006.
- [30] J. Folwarczna, M. Pytlik, M. Zych et al., “Favorable effect of moderate dose caffeine on the skeletal system in ovariectomized rats,” *Molecular Nutrition & Food Research*, vol. 57, no. 10, pp. 1772–1784, 2013.
- [31] J. Folwarczna, L. Śliwiński, U. Cegiela et al., “Raloxifene similarly affects the skeletal system of male and ovariectomized female rats,” *Pharmacological Reports*, vol. 59, no. 3, pp. 349–358, 2007.
- [32] P. Londzin, S. Siudak, U. Cegiela et al., “Phloridzin, an apple polyphenol, exerted unfavorable effects on bone and muscle in an experimental model of type 2 diabetes in rats,” *Nutrients*, vol. 10, no. 11, p. 1701, 2018.
- [33] D. W. Dempster, J. E. Compston, M. K. Drezner et al., “Standardized nomenclature, symbols, and units for bone histomorphometry: a 2012 update of the report of the ASBMR Histomorphometry Nomenclature Committee,” *Journal of Bone and Mineral Research*, vol. 28, no. 1, pp. 2–17, 2013.
- [34] V. Witko-Sarsat, M. Friedlander, C. Capeillère-Blandin et al., “Advanced oxidation protein products as a novel marker of oxidative stress in uremia,” *Kidney International*, vol. 49, no. 5, pp. 1304–1313, 1996.
- [35] M. Zych, W. Wojnar, S. Borymski, K. Szałabska, P. Bramora, and I. Kaczmarczyk-Sedlak, “Effect of rosmarinic acid and sinapic acid on oxidative stress parameters in the cardiac tissue and serum of type 2 diabetic female rats,” *Antioxidants*, vol. 8, no. 12, p. 579, 2019.
- [36] Ø. Hammer, D. A. T. Harper, and P. D. Ryan, “PAST: paleontological statistics software package for education and data analysis,” *Palaeontologia Electronica*, vol. 4, no. 1, p. 9, 2001.
- [37] M. Ringnér, “What is principal component analysis?,” *Nature Biotechnology*, vol. 26, no. 3, pp. 303–304, 2008.
- [38] J. Folwarczna, A. Janas, M. Pytlik, L. Śliwiński, M. Wiercigroch, and A. Brzeczek, “Modifications of histamine receptor signaling affect bone mechanical properties in rats,” *Pharmacological Reports*, vol. 66, no. 1, pp. 93–99, 2014.
- [39] S. C. Manolagas, “From estrogen-centric to aging and oxidative stress: a revised perspective of the pathogenesis of osteoporosis,” *Endocrine Reviews*, vol. 31, no. 3, pp. 266–300, 2010.
- [40] E. Kalaitzoglou, J. L. Fowlkes, I. Popescu, and K. M. Thraillkill, “Diabetes pharmacotherapy and effects on the musculoskeletal system,” *Diabetes/Metabolism Research and Reviews*, vol. 35, no. 2, Article ID e3100, 2019.
- [41] E. Kalaitzoglou, I. Popescu, R. C. Bunn, J. L. Fowlkes, and K. M. Thraillkill, “Effects of type 1 diabetes on osteoblasts, osteocytes, and osteoclasts,” *Current Osteoporosis Reports*, vol. 14, no. 6, pp. 310–319, 2016.
- [42] A. Palermo, L. D’Onofrio, R. Buzzetti, S. Manfrini, and N. Napoli, “Pathophysiology of bone fragility in patients with diabetes,” *Calcified Tissue International*, vol. 100, no. 2, pp. 122–132, 2017.
- [43] W. Yan and X. Li, “Impact of diabetes and its treatments on skeletal diseases,” *Frontiers in Medicine*, vol. 7, no. 1, pp. 81–90, 2013.
- [44] K. Maiese, “New insights for oxidative stress and diabetes mellitus,” *Oxidative Medicine and Cellular Longevity*, vol. 2015, Article ID 875961, 17 pages, 2015.
- [45] R. Quinn, “Comparing rat’s to human’s age: how old is my rat in people years?,” *Nutrition*, vol. 21, no. 6, pp. 775–777, 2005.
- [46] W. Min, P. Fang, G. Huang, M. Shi, and Z. Zhang, “The decline of whole-body glucose metabolism in ovariectomized rats,” *Experimental Gerontology*, vol. 113, pp. 106–112, 2018.
- [47] P. Anagnostis, S. A. Paschou, N. N. Gkekak et al., “Efficacy of anti-osteoporotic medications in patients with type 1 and 2 diabetes mellitus: a systematic review,” *Endocrine*, vol. 60, no. 3, pp. 373–383, 2018.
- [48] K. Dingle and F. Azizieh, “Multivariate comparison of cytokine profiles for normal- and low-bone-density subjects,” *Diagnostics*, vol. 9, no. 4, p. 134, 2019.
- [49] F. Y. Azizieh, D. Shehab, K. al Jarallah, O. Mojiminiyi, R. Gupta, and R. Raghupathy, “Circulatory pattern of cytokines, adipokines and bone markers in postmenopausal women with low BMD,” *Journal of Inflammation Research*, vol. 12, pp. 99–108, 2019.
- [50] C. Guder, S. Gravius, C. Burger, D. C. Wirtz, and F. A. Schildberg, “Osteoimmunology: a current update of the interplay between bone and the immune system,” *Frontiers in Immunology*, vol. 11, p. 58, 2020.
- [51] M. Tang, L. Tian, G. Luo, and X. Yu, “Interferon-gamma-mediated osteoimmunology,” *Frontiers in Immunology*, vol. 9, p. 1508, 2018.
- [52] D. S. Amarasekara, H. Yun, S. Kim, N. Lee, H. Kim, and J. Rho, “Regulation of osteoclast differentiation by cytokine networks,” *Immune Network*, vol. 18, no. 1, Article ID e8, 2018.
- [53] K. Alnek, K. Kisand, K. Heilman, A. Peet, K. Varik, and R. Uiibo, “Increased blood levels of growth factors, proinflammatory cytokines, and Th17 cytokines in patients with newly diagnosed type 1 diabetes,” *PLoS One*, vol. 10, no. 12, article e0142976, 2015.
- [54] J. Lu, J. Liu, L. Li, Y. Lan, and Y. Liang, “Cytokines in type 1 diabetes: mechanisms of action and immunotherapeutic targets,” *Clinical & Translational Immunology*, vol. 9, no. 3, Article ID e1122, 2020.
- [55] H. Carlsten, “Immune responses and bone loss: the estrogen connection,” *Immunological Reviews*, vol. 208, no. 1, pp. 194–206, 2005.
- [56] M. N. Weitzmann and R. Pacifici, “Estrogen deficiency and bone loss: an inflammatory tale,” *The Journal of Clinical Investigation*, vol. 116, no. 5, pp. 1186–1194, 2006.
- [57] A. L. Russell, J. M. Grimes, D. F. Cruthirds et al., “Dietary isoflavone-dependent and estradiol replacement effects on body weight in the ovariectomized (OVX) rat,” *Hormone and Metabolic Research*, vol. 49, no. 6, pp. 457–465, 2017.
- [58] J. M. Guerra, M. A. Hanes, C. Rasa et al., “Modulation of bone turnover by *Cissus quadrangularis* after ovariectomy in rats,” *Journal of Bone and Mineral Metabolism*, vol. 37, no. 5, pp. 780–795, 2019.
- [59] S. Yano, R. Mentaverri, D. Kanuparthi et al., “Functional expression of β -chemokine receptors in osteoblasts: role of regulated upon activation, normal T cell expressed and secreted (RANTES) in osteoblasts and regulation of its secretion by osteoblasts and osteoclasts,” *Endocrinology*, vol. 146, no. 5, pp. 2324–2335, 2005.
- [60] J. Lechner, T. Rudi, and V. von Baehr, “Osteoimmunology of tumor necrosis factor-alpha, IL-6, and RANTES/CCL5: a review of known and poorly understood inflammatory patterns in osteonecrosis,” *Clinical, Cosmetic and Investigational Dentistry*, vol. 10, pp. 251–262, 2018.

- [61] O. M. Koper-Lenkiewicz, J. Kamińska, A. Lisowska, A. Milewska, T. Hirnle, and V. Dymicka-Piekarska, "Factors associated with RANTES concentration in cardiovascular disease patients," *BioMed Research International*, vol. 2019, Article ID 3026453, 11 pages, 2019.
- [62] F. Fatehi, M. Mollahosseini, G. Hassanshahi et al., "CC chemokines CCL2, CCL3, CCL4 and CCL5 are elevated in osteoporosis patients," *Journal of Biomedical Research*, vol. 31, no. 5, pp. 468–470, 2017.
- [63] M. Mazziotta and A. Pareto, "Use and misuse of PCA for measuring well-being," *Social Indicators Research*, vol. 142, no. 2, pp. 451–476, 2019.
- [64] J. S. Nyman, E. Kalaitzoglou, R. Clay Bunn, S. Uppuganti, K. M. Thraikill, and J. L. Fowlkes, "Preserving and restoring bone with continuous insulin infusion therapy in a mouse model of type 1 diabetes," *Bone Reports*, vol. 7, pp. 1–8, 2017.
- [65] J. Folwarczna, A. Janas, U. Cegiela et al., "Caffeine at a moderate dose did not affect the skeletal system of rats with streptozotocin-induced diabetes," *Nutrients*, vol. 9, no. 11, p. 1196, 2017.
- [66] P. Sołtysiak, M. Pytlik, U. Cegiela, A. Janas, and J. Folwarczna, "Curcumin did not affect the skeletal system in male rats with streptozotocin-induced diabetes," in *44th European Calcified Tissue Society Congress*, vol. 100 of *Calcified Tissue International*, p. S110, Salzburg, 2017.
- [67] J. Folwarczna, M. Zych, A. Janas, W. Wojnar, P. Londzin, and I. Kaczmarczyk-Sedlak, "Effects of sinapic and rosmarinic acids on the skeletal system of rats with experimental type 2 diabetes," in *20th International Congress of the Polish Pharmacological Society*, pp. 132-133, Lublin, 2019, Abstract. book.

Research Article

Hypertryptasemia and Mast Cell-Related Disorders in Severe Osteoporotic Patients

Giulia Carosi,^{1,2} Gregorio Guabello,³ Matteo Longhi,³ Federica Grifoni,⁴ Elena Passeri,⁵ and Sabrina Corbetta ^{5,6}

¹Endocrinology Unit, IRCCS Fondazione Ca' Granda Ospedale Maggiore Policlinico, Milan, Italy

²Department of Experimental Medicine, Sapienza University of Rome, Rome, Italy

³Rheumatology Unit, IRCCS Istituto Ortopedico Galeazzi, Milan, Italy

⁴Hematology and Transplantation Unit, IRCCS Fondazione Ca' Granda Ospedale Maggiore Policlinico, Milan, Italy

⁵Endocrinology and Diabetology Service, IRCCS Istituto Ortopedico Galeazzi, Milan, Italy

⁶Department of Biomedical, Surgical and Dental Sciences, University of Milan, Milan, Italy

Correspondence should be addressed to Sabrina Corbetta; sabrina.corbetta@unimi.it

Received 21 July 2020; Revised 28 September 2020; Accepted 3 October 2020; Published 22 October 2020

Academic Editor: Alanna Green

Copyright © 2020 Giulia Carosi et al. This is an open access article distributed under the Creative Commons Attribution License, which permits unrestricted use, distribution, and reproduction in any medium, provided the original work is properly cited.

Purpose. Systemic mastocytosis (SM) is characterized by a clonal proliferation of neoplastic mast cells (MCs) in one or more extracutaneous organs including the bone marrow (BM). SM is often associated with osteoporosis (OP) and fractures. Hypertryptasemia usually occurs in SM. We investigated the prevalence of hypertryptasemia in a series of severe osteoporotic patients, the performance of the tryptase test in diagnosing SM in these patients, and their bone features. **Methods.** The medical records of 232 patients (168 females and 64 males) with a diagnosis of OP (50.4% with fractures) and a serum tryptase assessment were reviewed. BM assessment was performed in a subset of hypertryptasemic patients; clinical, biochemical, and radiographic data were collected. **Results.** Hypertryptasemia was detected in 33 patients. BM assessment ($n = 16$) was normal in 8 hypertryptasemic patients, while BM criteria for the diagnosis of SM were met in 3 patients, MC alterations were detected in 4 patients, and one patient presented a polycythemia vera. Serum tryptase levels were higher than 11.4 ng/ml in all patients with BM alterations. The best cut-off of tryptase level related to BM alterations was 17.9 ng/ml, with a sensibility and sensitivity of 75% (AUC = 0.797 and $P = 0.015$ by ROC analysis). All osteoporotic patients with hypertryptasemia experienced at least one vertebral fracture associated with a severe reduction of the lumbar bone mineral density. **Conclusions.** The prevalence of MC-related disorders in severe OP was 3.0%, accounting for the 7.4% of the secondary causes of OP. MC-related disorders may be involved in bone fragility and assessment of serum tryptase is useful to detect MC-related disorders.

1. Introduction

Osteoporosis (OP) is a systemic skeletal disorder characterized by decreased bone mass and impairment of bone quality, which is associated with increased risk of fragility fractures. Several diseases and drugs are known to contribute to OP development. International guidelines recommend screening for secondary cause of OP in order to assess the fracture probability [1–3]. Diagnostic workup for the secondary causes of OP requires extensive biochemical evaluation. In this context, the assessment of serum tryptase, a mastocyte cell-specific serine protease, could be considered in order to rule out sys-

temic mastocytosis, a rare hematological disorder generally associated with hypertryptasemia [4]. Mastocytosis comprises a heterogeneous group of disorders characterized by expansion and accumulation of neoplastic mast cells (MCs) in one or more organ systems. In patients with systemic mastocytosis (SM), neoplastic MCs form focal and/or diffuse infiltrates in various internal organs, including the bone marrow (BM), spleen, liver, and gastrointestinal tract [5]. Epidemiological data are sparse in the general population, reporting a prevalence of 0.5–1.0 per 10,000, which is probably underestimated [5, 6]. Two main variants of the disorder are described: cutaneous mastocytosis, generally observed in the childhood,

and systemic mastocytosis (SM), an adult disease. While the cutaneous mastocytosis spontaneously regresses in most cases, SM is a persistent disease, and it can evolve in more aggressive disorders, namely, aggressive SM or mast cell leukemia. In most adult patients, a gain-of-function somatic mutation in the *KIT* gene, encoding for the stem cell growth factor receptor, is detected, the D816V mutation being the most frequent. Symptoms and signs are related to MC proinflammatory and vasoactive mediators' release (e.g., flushing, urticaria, and anaphylaxis) and to MC infiltration (e.g., spleen enlargement) [7]. Diagnostic criteria have recently been updated on current WHO classification [5, 8, 9]; they include a biochemical finding, namely, serum tryptase levels higher than 20.0 ng/ml and histopathological, morphological, cytofluorimetric, and molecular criteria resulted from a bone marrow evaluation with bone marrow biopsy (BMB) and bone marrow aspirate (BMA). Three minor criteria (persistent tryptase levels > 20.0 ng/ml, CD25 with or without CD2 aberrant expressions, abnormal mast cells morphology, and detection of the D816V *KIT* mutation) or one minor associated with the major criteria (i.e., multifocal dense mast cell aggregates) have to be met.

Some studies described a high prevalence of bone fragility in patients affected with SM, up to 33% [10–13], suggesting SM as a cause of secondary OP. Besides, no consistent data on SM prevalence in osteoporotic patients are available. The present study is aimed at assessing the prevalence of hypertryptasemia and SM in a series of patients with unexplained OP and/or skeletal fragility, who were evaluated looking for secondary OP.

2. Subjects and Methods

The study was carried out at the IRCCS Istituto Ortopedico Galeazzi in Milan, where osteoporotic patients firstly referred to the Rheumatology and Endocrinology Units were enrolled. The diagnostic workup for SM was performed at the Hematology and Transplantation Unit, IRCCS Fondazione Ca' Granda Ospedale Maggiore Policlinico, Milan. We retrospectively analyzed the records of a series of referred patients from May 2014 to July 2018 presenting two main features: a diagnosis of OP and a serum tryptase assessment in their medical records. OP was assessed using bone mineral density (BMD) measurement at lumbar spine and femur by dual-energy X-ray absorptiometry (DXA) technique. In postmenopausal women and men aged 50 years and older, a diagnosis of OP was made in presence of a T – score < –2.5 at any site according to WHO criteria [14]. In premenopausal women and men less than 50 years, Z -scores were used, considering Z -score values of –2.0 or lower as reduced BMD for age. All patients with fragility fractures were considered as affected with severe OP, regardless of BMD values [1]. Data about secondary OP causes as well as comorbidities and concomitant treatments reported in patients' medical history were collected. All patients were screened for secondary causes of OP by an extensive biochemical workup, and data were collected. Data about BMD and bone fractures were also recorded in an electronic database.

Serum tryptase was routinely assessed in patients with prevalent vertebral fractures and/or severe bone demineralization at vertebral site (T – score < –3.0 by DXA) in line with previous reports (reviewed in [15]) describing high prevalence of vertebral bone impairment in patients with SM.

All procedures performed in studies involving human participants were in accordance with the ethical standards of the institutional committee and with the 1964 Helsinki declaration and its later amendments or comparable ethical standards. The study follows the STROBE guidelines for observational studies.

2.1. Biochemical Screening for Secondary OP Detection. Patients were assessed for the occurrence of hypercalciuria (24-hour urine collection calcium), hypophosphatemia (serum phosphate and 24-hour urine collection phosphate), thyroid dysfunction (serum TSH levels), male hypogonadism (calculated free testosterone, LH, and FSH), primary and secondary hyperparathyroidism (serum calcium and PTH), hypophosphatasia (serum total ALP), hypercortisolism (low-dose dexamethasone suppression test), multiple myeloma and monoclonal gammopathies (MGUS) (serum protein electrophoresis and urinary immunofixation test), hematologic disorders (hemocromocytometry), rheumatoid arthritis and connectivities (rheumatoid factor test, ANA, ENA, and ESR), chronic liver diseases (AST, ALT, and γ GT), and chronic kidney diseases (serum creatinine and estimated glomerular filtration rate).

2.2. Definition of Hypertryptasemia. Serum tryptase assessment was performed in different laboratories using the same assay method (ImmunoCAP Tryptase, Phadia Laboratory Systems, Thermo Fisher Scientific Inc., Uppsala, Sweden). The upper limit of the normal reference intervals varied among the laboratories ranging from 5.0 to 11.4 ng/ml [16].

Serum tryptase levels higher than 11.4 ng/ml and 20.0 ng/ml were considered suspicious and strongly suspicious for SM, respectively, according to the current most widely accepted ranges [4, 7].

2.3. Diagnosis of Systemic Mastocytosis (SM). Diagnosis of SM was carried out according to current WHO criteria based on bone marrow assessment and biochemical findings [4, 7, 17], including immunohistochemistry staining for tryptase, serum tryptase levels, analysis of CD2/CD25 expression on mast cells by flow or immunohistochemistry, and genotyping of *cKIT* (D816V) mutation. *cKIT* mutation was evaluated by reverse transcriptase polymerase chain reaction (RT-PCR) restriction fragment length polymorphism (RFLP) analysis or direct Sanger sequencing.

Based on the associated clinical features, SM was further classified as reported in the legend of Table 1 [17].

2.4. Statistical Analysis. Data are presented as mean \pm standard deviation (SD), and percentages where not otherwise stated. T -test was used to compare normally distributed continuous variables. Normality was tested by D'Agostino-Pearson test. Correlation analyses between continuous and categorical data were performed using Spearman's correlation. Receiver operator characteristic (ROC) analysis was

TABLE 1: Bone marrow assessment and clinical findings in osteoporotic patients with hypertryptasemia.

| Pts | Sex | Age years | Serum tryptase (ng/ml) | Diagnosis | Bone marrow histology | Major criterion* | Minor criteria* | | | | Comorbidities |
|-----|-----|-----------|------------------------|-----------------|--|------------------|-----------------|---|---|---|---|
| | | | | | | | 1 | 2 | 3 | 4 | |
| 1 | M | 62 | 24.0 | SM | Rare interstitial, perivascular, and paratrabeular MCs | - | - | + | + | + | Hypogonadism |
| 2 | M | 41 | 26.0 | SM | No MC infiltration, no MC granuloma | + | - | - | + | - | Active smoke, hypogonadism, alcoholism |
| 3 | F | 65 | 19.2 | SM | No MC infiltration, no MC granuloma | - | + | + | + | - | - |
| 4 | F | 57 | 23.0 | MCs alterations | No MC infiltration, no MC granuloma | - | + | - | - | - | - |
| 5 | M | 70 | 16.3 | MCs alterations | No MC infiltration, no MC granuloma | - | - | + | - | - | Hypogonadism, DM2, CKD, psoriatic arthropathy |
| 6 | M | 73 | 15.4 | MCs alterations | No MC infiltration, no MC granuloma | - | - | - | + | - | Adrenal incidentaloma, kidney stones, psoriasis |
| 7 | F | 41 | 48.4 | MCs alterations | Perivascular MC aggregates | - | - | - | + | + | IBD, pregnancy, lactation |
| 8 | M | 79 | 21.0 | PV | - | - | - | - | - | - | Previous prostate cancer, coronaropathy |
| 9 | M | 62 | 12.7 | Normal | - | - | - | - | - | - | Active smoke, MS |
| 10 | M | 73 | 11.5 | Normal | - | - | - | - | - | - | COPD |
| 11 | F | 67 | 13.2 | Normal | - | - | - | - | - | - | - |
| 12 | M | 52 | 16.0 | Normal | - | - | - | - | - | - | - |
| 13 | F | 50 | 11.4 | Normal | - | - | - | - | - | - | COPD, hypothyroidism |
| 14 | F | 42 | 16.9 | Normal | - | - | - | - | - | - | Previous anorexia nervosa |
| 15 | F | 65 | 26 | Normal | - | - | - | - | - | - | Iatrogenic thyrotoxicosis |
| 16 | M | 79 | 18 | Normal | - | - | - | - | - | - | Coronaropathy, MGUS |

BM: bone marrow; SM: systemic mastocytosis; MCs: mast cells; PV: polycythemia vera; DM2: type 2 diabetes mellitus; CKD: chronic kidney disease; IBD: inflammatory bowel disease; MS: metabolic syndrome; COPD: chronic obstructive pulmonary disease. *The diagnosis of SM can be made when the major criterion and at least 1 minor criterion are present or when ≥ 3 minor criteria are present [8, 9]. Major criterion: multifocal dense infiltrates of MCs (≥ 15 MCs in aggregates) in BM biopsies and/or in sections of other extracutaneous organ(s). Minor criteria: (1) $>25\%$ of all MCs are atypical cells (type I or type II) on BM smears or are spindle shaped in MC infiltrates detected on sections of visceral organs. (2) KIT point mutation at codon 816 in the BM or another extracutaneous organ. (3) MCs in BM or blood or another extracutaneous organ exhibit CD2 and/or CD25. (4) Baseline serum tryptase level > 20 ng/ml (in case of an unrelated myeloid neoplasm, item "d" is not valid as an SM criterion).

performed to assess threshold value of serum tryptase that detects patients with bone marrow alterations. The analyses were performed with Prism 6.0.

3. Results

3.1. Prevalence of Hypertryptasemia in Severe Osteoporotic Patients. The medical records of 232 outpatients (168 females and 64 males) evaluated for bone fragility from May 2014 to July 2018 to the third-level center IRCCS Istituto Ortopedico Galeazzi in Milan presenting a diagnosis of OP and a serum tryptase assessment were reviewed. The mean age at the first evaluation was 64.0 ± 11.0 and 63.0 ± 13.0 years for females and males, respectively. Osteoporotic fractures occurred in 117 out of 232 patients (50.4%). In the 232 evaluated patients, mean tryptase level (\pm SD) was 7.1 ± 6.0 ng/ml, with any significant difference between males (7.4 ± 5.8 ng/ml) and females (7.0 ± 6.1 ng/ml; $P = 0.735$). In the whole series, serum tryptase levels did not correlate with T -scores or Z -scores ($P = 0.33$ and 0.27 for lumbar spine T -scores and Z -scores, respectively; $P = 0.25$ and 0.27 for femoral neck T

-scores and Z -scores, respectively; $P = 0.59$ and 0.52 for total hip T -scores and Z -scores, respectively; analyzed by Spearman's correlation).

According to local laboratories' reference ranges, hypertryptasemia was detected in 33 patients, indicating a prevalence of 14.2%. None of the hypertryptasemic patients was affected with severe chronic kidney disease (defined as stage 3 or higher stage CKD) or with known hematological disorders determining tryptase elevation. Hypertryptasemic osteoporotic patients did not report symptoms related to the tryptase release; moreover, hepatomegaly, splenomegaly, and/or lymphadenopathy were not recorded on physical examination, and cytopenia was absent in all patients.

3.2. BM Findings in Osteoporotic Patients with Hypertryptasemia. BM data were available from 16 out of the 33 identified hypertryptasemic osteoporotic patients, and the remaining 17 refused the procedure (serum tryptase levels 19.2 ± 0.1 vs. 9.7 ± 7.2 ng/ml, respectively; $P = 0.003$). BM assessment was performed in 2 out of 17 patients with serum tryptase levels lower than or equal to 11.4 ng/ml, in 9

out of 9 patients with serum tryptase levels within the interval 11.5-20.0 ng/ml, and in 5 out of 7 patients with tryptase levels higher than 20.0 ng/ml (Figure 1).

BM assessment revealed normal bone marrow parameters in 8 out of 16 hypertryptasemic patients, while in the remaining 8 bone marrow alterations could be detected. Specifically, criteria for the diagnosis of SM [5, 8, 9] could be unequivocally defined in 3 patients. In additional 4 patients, MC alterations in BM, not fully matching WHO criteria for SM diagnosis, were detected (Table 1).

MC alterations were consistent with abnormal mast cell morphology in 1 patient and with CD25 aberrant expression in 3. Lastly, in 1 patient, BM findings diagnosed the previously unrecognized myeloproliferative disorder polycythemia vera harboring the *JAK2* gene mutation. Considering patients with both SM and MC alterations, the prevalence of mast cell disorders in severe osteoporotic patients was 3.0%.

All the 8 patients harboring MC-related BM abnormalities showed a serum tryptase level higher than 11.4 ng/ml, which were below the threshold of 20.0 ng/ml in 4 patients and higher than 20.0 ng/ml in the remaining 4 patients (Table 1, Figure 1).

The ROC analyses indicated 17.9 ng/ml as the best cut-off of tryptase level related to BM alterations, with a sensibility and sensitivity of 75% (AUC = 0.797, $P = 0.015$). Accordingly, considering the threshold of 20.0 ng/ml, which is generally considered as highly suggestive of SM, tryptase assessment showed a positive predictive value of 0.80, while the negative predictive value was 0.36 in detecting MC-related bone marrow alterations in the present series of osteoporotic patients.

3.3. Calcium and Bone Metabolism Parameters in Patients with SM and MC Alterations. None of the patients with diagnosis of MS and MC alterations showed abnormal calcium and bone metabolism parameters; in particular, they were normocalcemic and normophosphatemic, with serum PTH levels in the normal low range and serum 25OHD levels above 30 ng/ml in 5 out of 7; total alkaline phosphatase levels were in the normal high range (Table 2).

Any significant difference could be detected in the mineral metabolism parameters between patients with and without BM alterations: mean serum phosphate levels were 3.5 ± 0.4 vs. 3.3 ± 0.5 mg/dl, $P = 0.46$; total ALP 101.4 ± 17.0 vs. 63.8 ± 16.0 U/L, $P = 0.08$; 25OHD 31.0 ± 7.0 vs. 31.4 ± 6.7 ng/ml, $P = 0.94$; PTH 32.6 ± 11.0 vs. 36.5 ± 5.8 pg/ml, $P = 0.54$. Indeed, mean serum calcium level was slightly higher in patients with BM alterations with respect to patients without BM alterations (9.6 ± 0.3 vs. 9.2 ± 0.2 mg/dl, $P = 0.03$), though both were within the normal range.

3.4. Bone Features in Patients with SM and MC Alterations. Skeletal involvement, with osteolytic lesions occurring in the skull, ribs, humeral bones, and pelvis, was detected in only one patient (no. 1) with SM diagnosis (Table 3).

All the patients with SM or MC alterations experienced at least one vertebral fracture, while any fracture at alternative sites was reported (Table 3). About half of the vertebral fractures were symptomatic and clinically evident, while the

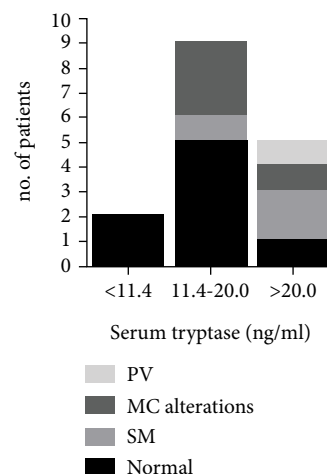


FIGURE 1: Bone marrow assessment results related to serum tryptase levels. MC: mastocyte cells; SM: systemic mastocytosis; PV: polycythemia vera.

remaining was diagnosed by X-ray vertebral morphometry. In the present series, vertebral fractures were characterized by biconcave deformation, similarly to what reported by Kanitez et al. [18] (Figures 2(a)–2(d)). Indeed, additional bone alterations were detected in patients with MS or MC alterations: one patient (no. 6) experienced bilateral aseptic femur head necrosis 4 years before the occurrence of the vertebral fracture and the diagnosis of MC alteration (Figure 2(e)).

Spinal impairment occurred in 87.5% of patients with BM alterations, while it could be detected only in 37.5% of patients with normal BM result ($P = 0.11$). Patients with SM or MC alterations showed a more severe reduction of the lumbar BMDs with respect to the femur BMDs, with the exception of patient no. 5; indeed, she was affected with severe lumbar calcifying enthesopathy (Table 2). Comparing densitometric values of patients with BM alterations with all normotryptasemic patients, we observed that spinal *T*-scores resulted lower in patients with BM alterations (mean lumbar spine *T*-score, -3.8 vs. -2.8; $P = 0.02$), while the other densitometric parameters were similar.

Patients treated with antiresorptive drugs did not experience any incident fracture, and two patients showed increasing BMDs (Table 3); indeed, the median clinical follow-up was limited [12 months (6-84 months)]. Though any correlation could be detected between bone mineralization, in terms of *T*-scores, and the serum tryptase levels, the number of vertebral fractures showed a trend towards a positive correlation with the serum tryptase levels in osteoporotic patients with hypertryptasemia suggestive for SM (serum tryptase levels > 11.4 ng/ml; $r = 0.239$ and $P = 0.054$). Besides, a significant positive correlation between the number of vertebral fractures and the tryptase levels could be detected in patients with SM/MC alterations ($r = 0.778$ and $P = 0.01$).

3.5. Prevalence of the SM and MC Alterations among the Secondary Causes of Osteoporosis. In 95 (41%) out of the 232 patients with serum tryptase assessment, secondary OP

TABLE 2: Mineral metabolic features in patients with SM and MC alterations.

| Pts | Diagnosis | History of allergy/anaphylaxis | Ca mg/dl | P mg/dl | PTH pg/ml | ALP U/L | 25OHD ng/ml |
|------|----------------|--------------------------------|-------------|------------|--------------|------------|----------------|
| n.v. | | | 8.4-10.4 | 2.8-5.0 | 10.0-65.0 | 40-120 | >30 |
| 1 | SM | Yes | 9.6 | 3.8 | 26.0 | 116 | 41 |
| 2 | SM | No | 9.7 | 3.7 | 30.0 | 86 | 32 |
| 3 | SM | No | 9.6 | 3.5 | 33.0 | 110 | 22 |
| 4 | MC alterations | No | 9.8 | 3.5 | 23.0 | 90 | 31 |
| 5 | MC alterations | No | 9.8 | 2.8 | 21.0 | 117 | 23 |
| 6 | MC alterations | No | 9.2 | 3.3 | 49.5 | 76 | 38 |
| 7 | MC alterations | No | 9.2 | 3.9 | 45.5 | 115 | 30 |

Pts: patients; n.v.: normal values; Ca: serum total calcium; P: serum phosphate; PTH: serum parathyroid hormone; ALP: serum total alkaline phosphatase activity; 25OHD: serum 25-hydroxyvitamin D; SM: systemic mastocytosis; MC alterations: mast cell alterations.

TABLE 3: Bone mineral densities and vertebral fractures in patients with SM and MC alterations.

| Patient | Diagnosis | LS T _s | LS Z _s | FN T _s | FN Z _s | TH T _s | TH Z _s | Vertebral fracture | Treatment | Treatment efficacy (follow-up) |
|---------|-------------------|----------------------|----------------------|----------------------|----------------------|----------------------|----------------------|---|--|--|
| 1 | SM | -4.30 | | -2.80 | | -1.80 | | T6, T8, T9, T11, T12, L1, L3 | Alendronate 70 mg/week | No incident fractures (12 months) |
| 2 | SM | | n.a. | | -1.50 | | -1.00 | T6, L4, L5 | Zoledronate 5 mg/12 months | No incident fractures (12 months) |
| 3 | SM | -4.20 | | -2.30 | | -2.40 | | T12 | Alendronate 70 mg/week | No incident fractures (24 months) |
| 4 | MC alterations | -3.40 | | -2.50 | | -2.30 | | T7, T8, T9, L2, L3, L4 | Teriparatide 20 mcg/day+denosumab 60 mg/25 weeks | No incident fractures and significant increases in BMDs (24 + 12 months) |
| 5 | MC alterations | 0.30* | | -1.60 | | -0.20 | | T11, T12 | Treatment refused | Not available |
| 6 | MC alterations | -4.30 | | -2.80 | | -2.60 | | L2 | Alendronate 70 mg/week | No incident fractures (12 months) |
| 7 | MC alterations | | -3.90 | | -1.50 | | -1.30 | T5, T6, T8, T10, T11, T12, L1, L2, L3, L5 | Alendronate 70 mg/week | Not available (6 months) |
| 8 | PV | -2.8 | | -2.4 | | -1.7 | | No fracture detected | Risedronate 35 mg/week | Significant increases in BMDs (84 months) |

*Severe lumbar enthesopathies; SM: systemic mastocytosis; MC: mastocytosis; PV: polycythemia vera; LS T_s: lumbar spine T-score; LS Z_s: lumbar spine Z-score; FN T_s: femoral neck T-score; FN Z_s: femoral neck Z-score; TH T_s: total hip T-score; TH Z_s: total hip Z-score; n.a.: not assessed due to previous arthrodesis.

was diagnosed. In 51 (22%), the cause of OP was evident only after the extensive biochemical and hormonal diagnostic workup for secondary OP (Figure 3). SM accounts for about 3.1% of the cases with secondary OP, while considering also the MC alterations, the prevalence raised to 7.4%.

4. Discussion

A growing number of diseases contribute to bone demineralization and/or to increasing the bone fracture risk. Osteoporosis and fragility fractures are often clinical features of systemic diseases, whose diagnosis is mandatory in the management of osteoporosis. Disorders of the bone marrow cells affect skeletal bone metabolism. Bone manifestations are one of the most frequent symptoms of SM, particularly in adults. Osteoporosis in SM has been attributed either to neoplastic infiltration or to the local release of mediators (histamine, heparin, tryptase, lipid mediators, and cytokines) [15]; bone

fragility may be also related to osteolytic lesions. Patients may experience a wide spectrum of bone symptoms from poorly localized bone pain, diffuse osteopenia, or osteoporosis with fragility fractures, to diffuse osteosclerosis, or both focal osteolytic and osteosclerotic bone lesions [10, 12, 18]. The prevalence of osteoporosis in adult patients with SM is uncertain, though it has been estimated to occur in up to one-third of patients with indolent SM [15]. Nonetheless, osteoporosis may be the symptom of presentation of bone marrow SM [15, 19]. Hypertryptasemia represents the circulating biochemical marker suggestive for the diagnosis of SM, though cases of SM with normal tryptase levels have been reported [15]. It often reflects the mast cell burden, and tryptasemia persistently higher than 20.0 ng/ml is one of the minor criteria for the diagnosis of SM [8, 9].

By retrospectively investigating the prevalence of hypertryptasemia in severe osteoporotic patients, defined by the occurrence of fragility fractures and/or lumbar spine T –

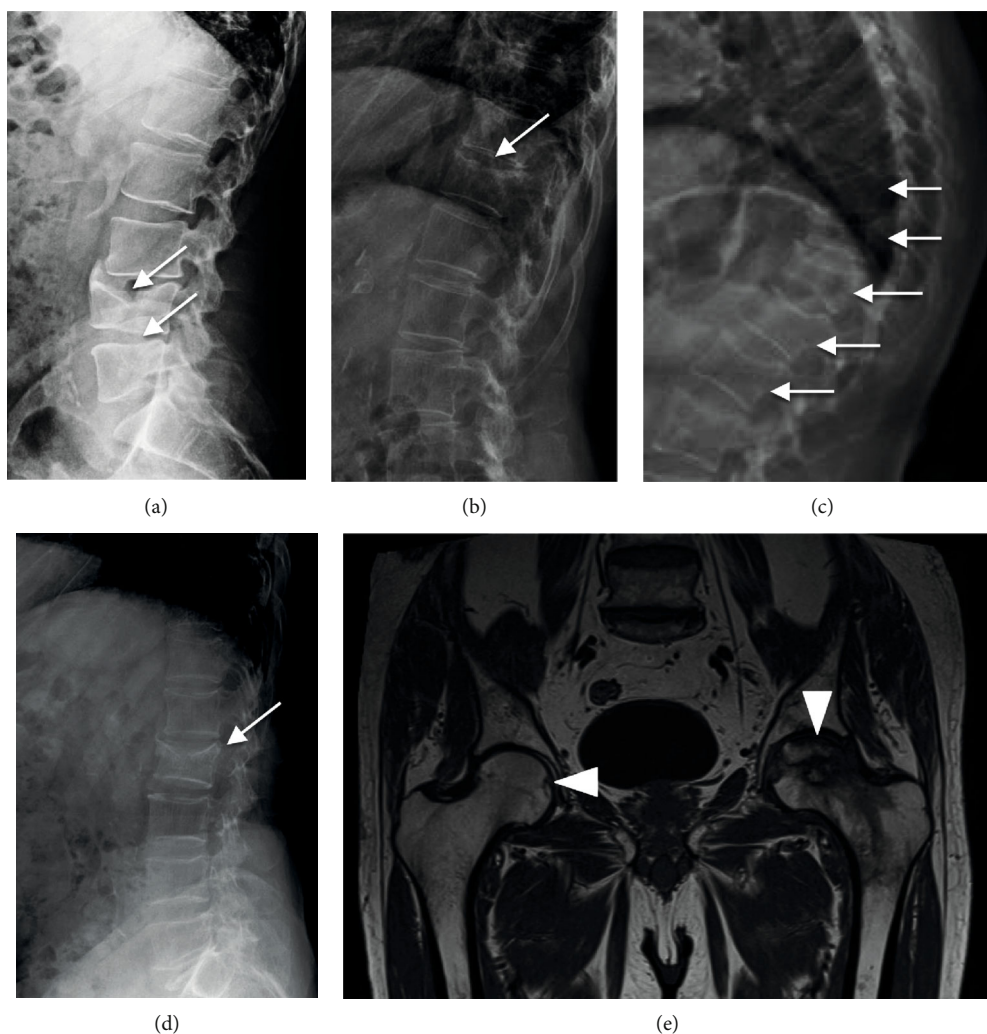


FIGURE 2: Radiological skeletal findings in patients with SM and MC alterations: (a) L4-L5 vertebral biconcave deformities (white arrows) in patient no. 2 with SM diagnosis; (b) T11 vertebral deformity (white arrow) in patient no. 3 with SM; (c) multiple vertebral biconcave deformities (L2-T10) (white arrows) in patient no. 7 with MC alterations; (d) L2 vertebral biconcave deformity (white arrow); (e) NMR image of the bilateral necrosis of femur heads in patient no. 6 with MC alterations; initial necrotic lesion of the right femoral head (white arrowhead on the left) and extensive necrosis of the left femoral head (white arrowhead on the right). SM: systemic mastocytosis; MC: mast cells; NMR: nuclear magnetic resonance.

score < -3.0 , in the setting of the extensive biochemical workup for the screening of secondary causes of osteoporosis, we report that hypertryptasemia occurred in about 14% of the patients, suggesting that including serum tryptase assay in the screening of osteoporotic patients for secondary causes will induce clinicians to familiarize with and to move on with further analysis.

Bone marrow is almost always involved in SM; therefore, BM histopathological evaluation is crucial to establish the diagnosis of SM, to assess tissue burden of MCs, and to rule out the presence of other hematological disorders. In the present series of hypertryptasemic osteoporotic patients, BM assessment diagnosed SM in about 19% of patients and identified MC alterations in further 25% of patients. Therefore, considering the whole series of osteoporotic patients with serum tryptase assessment, the prevalence of SM was 1.3%, and, including the MC alterations, it increased to 3.0%. These frequencies are similar to those previously reported in a series

of iliac crest bone biopsies from osteoporotic patients (1.3%) [20] and in a series of diagnostic biopsies in fractured vertebrae (3.1%) [21].

Considering the threshold of 20.0 ng/ml, the diagnostic serum tryptase levels for SM [4, 7, 17], tryptase test showed high sensitivity but low specificity in osteoporotic patients, as 40% of patients with serum tryptase levels ranging 11.4-20.0 ng/ml showed MC alterations in BM, suggesting that in this set of patients, MC alterations and/or SM should be considered also when tryptase is included in the range 11.4-20.0 ng/ml. Accordingly, ROC analysis in the present series of hypertryptasemic osteoporotic patients identified 17.9 ng/ml as the best cut-off associated with MC alterations.

Moreover, hypertryptasemia may be associated with other hematologic diseases such as polycythemia vera also in osteoporotic patients. Increased tryptase levels may be consequent to a number of concomitant conditions: chronic urticaria, acute anaphylactic reactions, renal insufficiency,

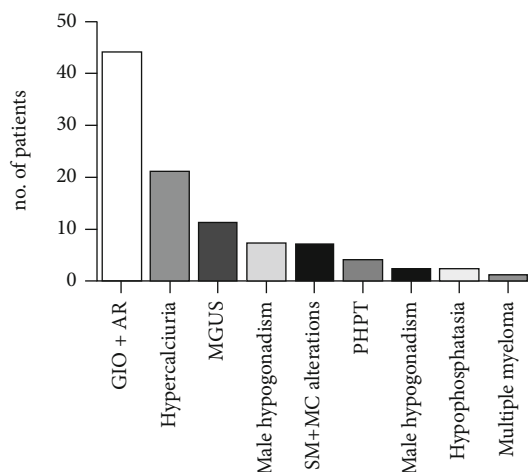


FIGURE 3: Causes of secondary osteoporosis in the analyzed patients' series. *GIO*: glucocorticoid-induced osteoporosis; *AR*: rheumatoid arthritis and connectivities; *hypercalciuria*: idiopathic hypercalciuria; *MGUS*: monoclonal gammopathy of undetermined significance; *PHPT*: primary hyperparathyroidism; *SM*: systemic mastocytosis; *MC*: mast cells.

other hematological diseases, onchocercosis, and ischemic myocardial disease or in the presence of heterophile antibodies [22]. None of these conditions could be detected in the hypertryptasemic osteoporotic patients with bone marrow normal findings. Recently, a hereditary autosomal dominant form of hypertryptasemia, caused by increased germline copies of the *TPSAB1* gene encoding alpha-tryptase, has been recognized [22–25]. However, genetic analysis could not be performed in the present series of hypertryptasemic patients.

Considering the bone fragility, previous studies reported a typical spine involvement, regarding both fractures and BMD values [13, 15]. We actually observed a high prevalence of vertebral fractures in SM patients, mostly multiple, in agreement with previous studies [26–28], and the spine represented the unique site of fracture. The differences between spine and femoral BMDs are noticeable, with a consistent impairment in spine BMD values. Indeed, a previous study reported lower femur *T*-score, besides older age at diagnosis and elevated bone turnover markers, as risk factors for osteoporosis and fragility fractures in SM patients [26]. Moreover, vertebral fractures were characterized by biconcave deformities as reported in previous studies [12, 15, 29], but we found additional bone alterations in patients with SM and MC alterations, such as osteolytic lesions and bilateral necrosis of the femur heads.

At variance with previous reports, in the present study, we also consider the finding of MC alterations in BM, which do not match the major criteria for SM diagnosis. These patients, according to some authors, may have a “prediagnostic SM,” whose natural history needs to be defined [4].

Though the number of patients reported in the present series is limited, the prevalent vertebral BMD impairment, the occurrence of multiple vertebral fractures, and the biconcave deformities are similar to those observed in patients with diagnosis of SM. Noteworthy, the number of vertebral fractures positively correlated with the serum tryptase levels in

osteoporotic patients with hypertryptasemia and MC alterations. Our data suggest that MS as well as MC alterations may contribute to bone fragility in addition to other osteoporotic-related disorders, such as male hypogonadism, diabetes mellitus, kidney stones, inflammatory bowel diseases, and pregnancy.

Finally, MC-related disorders emerged as a significant cause of secondary OP accounting for about 7% of cases and should be considered in patients with prevalent vertebral impairment, in terms of both BMD and fractures.

Admittedly, the study suffered from some limits: (1) it was a retrospective analysis; (2) it is likely that patients with evident causes of secondary OP did not receive a tryptase assessment, leading to an underestimated prevalence of the MC-related disorders in osteoporotic patients; (3) the study design did not allow to establish a pathogenic role of MC-related disorders in osteoporosis and bone fragility. Nonetheless, the present data may suggest further investigation about the role of tryptase and/or mast cell proliferation in the modulation of bone metabolism.

In conclusion, hypertryptasemia is a frequent finding in unexplained severe osteoporotic patients and bone marrow SM represents a cause of secondary OP in up to 1.3% of cases. We suggest of assessing serum tryptase levels in patients with bone fragility, particularly in the presence of spine BMD impairment and multiple vertebral fractures, even in the absence of classical signs and symptoms of MC activation usually reported in MS.

Data Availability

Clinical data are collected in Osteoregistry, which is a property of IRCCS Istituto Ortopedico Galeazzi.

Conflicts of Interest

Giulia Carosi, Gregorio Guabello, Matteo Longhi, Federica Grifoni, Elena Passeri, and Sabrina Corbetta declare that they have no conflict of interest.

Acknowledgments

The study was partially supported by Italian Ministry of Health (L4126) and by Gruppo San Donato Foundation (Progetto 5x1000 2016 “Osteoregistry”).

References

- [1] M. Rossini, S. Adami, F. Bertoldo et al., “Guidelines for the diagnosis, prevention and management of osteoporosis,” *Rheumatismo*, vol. 68, no. 1, pp. 1–39, 2016.
- [2] P. M. Camacho, S. M. Petak, N. Binkley et al., “American Association of Clinical Endocrinologists and American College of Endocrinology clinical practice guidelines for the diagnosis and treatment of postmenopausal osteoporosis — 2016,” *Endocrine Practice*, vol. 22, Supplement 4, pp. 1–42, 2016.
- [3] J. A. Kanis, C. Cooper, R. Rizzoli, J. Y. Reginster, and on behalf of the Scientific Advisory Board of the European Society for Clinical and Economic Aspects of Osteoporosis (ESCEO) and the Committees of Scientific Advisors and National

- Societies of the International Osteoporosis Foundation (IOF), "European guidance for the diagnosis and management of osteoporosis in postmenopausal women," *Osteoporosis International*, vol. 30, no. 1, pp. 3–44, 2019.
- [4] A. Pardanani, "Systemic mastocytosis in adults: 2019 update on diagnosis, risk stratification and management," *American Journal of Hematology*, vol. 94, pp. 363–377, 2018.
- [5] P. Valent, C. Akin, and D. D. Metcalfe, "Mastocytosis: 2016 updated WHO classification and novel emerging treatment concepts," *Blood*, vol. 129, no. 11, pp. 1420–1427, 2017.
- [6] S. S. Cohen, S. Skovbo, H. Vestergaard et al., "Epidemiology of systemic mastocytosis in Denmark," *British Journal of Haematology*, vol. 166, no. 4, pp. 521–528, 2014.
- [7] S. Merante, V. V. Ferretti, C. Elena et al., "The Italian Mastocytosis Registry: 6-year experience from a hospital-based registry," *Future Oncology*, vol. 14, no. 26, pp. 2713–2723, 2018.
- [8] H. P. Horny, D. D. Metcalfe, C. Akin et al., "Mastocytosis," in *WHO classification of tumors of hematopoietic and lymphoid tissues*, S. H. Swerdlow, Ed., pp. 62–69, International Agency for Research and Cancer (IARC), Lyon, France, 2017.
- [9] D. A. Arber, A. Orazi, R. Hasserjian et al., "The 2016 revision to the World Health Organization classification of myeloid neoplasms and acute leukemia," *Blood*, vol. 127, no. 20, pp. 2391–2405, 2016.
- [10] L. Pieri, P. Bonadonna, C. Elena et al., "Clinical presentation and management practice of systemic mastocytosis. A survey on 460 Italian patients," *American Journal of Hematology*, vol. 91, no. 7, pp. 692–699, 2016.
- [11] M. Rossini, R. Zanotti, P. Bonadonna et al., "Bone mineral density, bone turnover markers and fractures in patients with indolent systemic mastocytosis," *Bone*, vol. 49, no. 4, pp. 880–885, 2011.
- [12] M. Rossini, R. Zanotti, O. Viapiana et al., "Bone involvement and osteoporosis in mastocytosis," *Immunology and Allergy Clinics of North America*, vol. 34, no. 2, pp. 383–396, 2014.
- [13] E. Veer, W. Goot, J. G. R. Monchy, H. C. Kluin-Nelemans, and J. J. Doormaal, "High prevalence of fractures and osteoporosis in patients with indolent systemic mastocytosis," *Allergy*, vol. 67, no. 3, pp. 431–438, 2012.
- [14] J. A. Kanis, "Assessment of fracture risk and its application to screening for postmenopausal osteoporosis: synopsis of a WHO report. WHO Study Group," *Osteoporosis International*, vol. 4, no. 6, pp. 368–381, 1994.
- [15] M. Rossini, R. Zanotti, G. Orsolini et al., "Prevalence, pathogenesis, and treatment options for mastocytosis-related osteoporosis," *Osteoporosis International*, vol. 27, no. 8, pp. 2411–2421, 2016.
- [16] L. B. Schwartz, T. R. Bradford, C. Rouse et al., "Development of a new, more sensitive immunoassay for human tryptase: use in systemic anaphylaxis," *Journal of Clinical Immunology*, vol. 14, no. 3, pp. 190–204, 1994.
- [17] I. Maric and X. Sun, "Advances in diagnosis of mastocytosis and hypereosinophilic syndrome," *Seminars in Hematology*, vol. 56, no. 1, pp. 22–29, 2019.
- [18] N. Alpay Kanitez, B. Erer, Ö. Doğan et al., "Osteoporosis and osteopathy markers in patients with mastocytosis," *Turkish Journal of Haematology*, vol. 32, no. 1, pp. 43–50, 2015.
- [19] Á. Acosta-Mérida and S. Ojeda-Bruno, "Multiple vertebral fractures as the first manifestation of systemic mastocytosis," *Osteoporosis International*, vol. 30, no. 5, pp. 1121–1124, 2019.
- [20] R. H. Dellings and M. Werner, "Histological characteristics and prevalence of secondary osteoporosis in systemic mastocytosis. A retrospective analysis of 158 cases," *Pathologie*, vol. 22, no. 2, pp. 132–140, 2001.
- [21] P. Spinnato, A. Bazzocchi, G. Facchini et al., "Vertebral fractures of unknown origin: role of computed tomography-guided biopsy," *International Journal of Spine Surgery*, vol. 12, no. 6, pp. 673–679, 2018.
- [22] A. Y. S. Lee, "Elevated serum tryptase in non-anaphylaxis cases: a concise review," *International Archives of Allergy and Immunology*, vol. 181, no. 5, pp. 357–364, 2020.
- [23] J. J. Lyons, "Hereditary alpha tryptasemia: genotyping and associated clinical features," *Immunology and Allergy Clinics of North America*, vol. 38, no. 3, pp. 483–495, 2018.
- [24] G. Greiner, B. Sprinzl, A. Górská et al., "Hereditary alpha tryptasemia is a valid genetic biomarker for severe mediator-related symptoms in mastocytosis," *Blood*, 2020.
- [25] J. J. Lyons, J. Chovanec, M. P. O'Connell et al., "Heritable risk for severe anaphylaxis associated with increased α -tryptase-encoding germline copy number at TPSAB1," *Journal of Allergy and Clinical Immunology*, 2020.
- [26] S. Broesby-Olsen, D. K. Farkas, H. Vestergaard et al., "Risk of solid cancer, cardiovascular disease, anaphylaxis, osteoporosis and fractures in patients with systemic mastocytosis: a nationwide population-based study," *American Journal of Hematology*, vol. 91, no. 11, pp. 1069–1075, 2016.
- [27] Y. Degboé, M. Eischen, D. Nigon et al., "Prevalence and risk factors for fragility fracture in systemic mastocytosis," *Bone*, vol. 105, pp. 219–225, 2017.
- [28] Y. Degboé, M. Eischen, P. A. Apoil et al., "Higher prevalence of vertebral fractures in systemic mastocytosis, but not in cutaneous mastocytosis and idiopathic mast cell activation syndrome," *Osteoporosis International*, vol. 30, no. 6, pp. 1235–1241, 2019.
- [29] L. W. Greene, K. Asadipooya, P. F. Corradi, and C. Akin, "Endocrine manifestations of systemic mastocytosis in bone," *Reviews in Endocrine & Metabolic Disorders*, vol. 17, no. 3, pp. 419–431, 2016.

Research Article

CD4⁺ T Cell Profile and Activation Response in Sickle Cell Disease Patients with Osteonecrosis

Paula B. Daltro ¹, Tiago O. Ribeiro,¹ Gildásio C. Daltro ², Roberto J. Meyer ¹,
and Vitor Fortuna ¹

¹Health Science Institute, Federal University of Bahia, Salvador, BA 40110-100, Brazil

²Prof. Edgar Santos Hospital Complex, HUPES, Federal University of Bahia, Salvador, BA 40110-060, Brazil

Correspondence should be addressed to Vitor Fortuna; vfort@ufba.br

Received 31 July 2020; Revised 10 September 2020; Accepted 25 September 2020; Published 9 October 2020

Academic Editor: Drenka Trivanović

Copyright © 2020 Paula B. Daltro et al. This is an open access article distributed under the Creative Commons Attribution License, which permits unrestricted use, distribution, and reproduction in any medium, provided the original work is properly cited.

Recent evidence suggests that abnormalities involving CD4⁺T lymphocytes are associated with the pathophysiology of osteonecrosis (ON); however, few studies have addressed the CD4⁺T cells in ON related to sickle cell disease (SCD/ON). In addition, T cells producing multiple cytokines simultaneously are often present in the inflammatory milieu and may be implicated in the immune response observed in SCD/ON. In the present study, we aimed to characterize the functional status of CD4⁺T cells in SCD by simultaneously determining the frequency of IFN- γ ⁺, IL-4⁺, and IL-17⁺ CD4⁺T in cell cultures under exogenous stimuli. Peripheral blood mononuclear cells (PB-MNCs) from 9 steady-state SCD patients, 15 SCD/ON patients, and 19 healthy controls had functional status of CD4⁺T cells analyzed. Bone marrow mononuclear cells (BM-MNCs) from 24 SCD/ON patients (SCD BM) and 18 patients with ON not related to SCD (non-SCD BM) were also analyzed. We found that PB-MNC of SCD patients with or without ON presented significantly reduced TCD4⁺, TCD8⁺, and TCD4⁺ naïve cell frequencies and increased frequency of circulating CD4⁺T cells able to simultaneously produce IFN- γ ⁺/IL4⁺ and IL-17⁺/IL4⁺ compared to healthy controls. Conversely, the polyclonal stimulation of BM-MNC induced an increased frequency of CD4⁺IFN- γ ⁺ and CD4⁺IL-17⁺ in SCD BM compared to non-SCD BM. The increased proportion of CD4⁺ T cells able to produce a broad spectrum of proinflammatory cytokines after a strong stimulus indicates that the immune system in SCD/ON patients presents an expressive pool of partially differentiated cells ready to take on effector function. It is possible that this increased subpopulation may extend to inflammatory sites of target organs and may contribute to the maintenance of inflammation and the pathophysiology of osteonecrosis in sickle cell disease.

1. Introduction

Sickle cell disease (SCD) is caused by a point mutation in the β -globin gene (HBB), resulting in the production of hemoglobin S (HbS). The abnormal hemoglobin polymerizes upon deoxygenation and produces deformed red blood cells (RBCs). This primary pathophysiological alteration has many downstream effects including the production of several inflammatory molecules and responses that ultimately lead to hemolysis and vasoocclusion of microvessels [1]. Repeated microvascular occlusion, tissue hypoxia, and cytokine production perpetuate the chronic inflammatory state with a pivotal role in the vaso-occlusive crisis (VOC) and painful

episodes, the major cause of hospitalization in SCD patients [2]. Impaired leucocyte function, defective humoral, and cell-mediated immunities underlie the immunocompromised state of patients with SCD [3–5]. In addition to driving the vaso-occlusive processes, inflammatory responses are associated with numerous complications of the disease including osteonecrosis [6, 7].

Osteonecrosis is a long-term debilitating complication of SCD, representing an important cause of morbidity in SCD patients [8]. Osteonecrosis commonly affects the hip but may concurrently involve other joints, including the knee, shoulder, ankle, and spine [9, 10]. SCD patients usually start with silent bone lesions. If left untreated, the disorder

gradually progresses and the majority of SCD patients will experience structural bone deterioration, collapse of the joint, and degenerative arthritis [11].

Recent studies have demonstrated that inflammatory processes are associated with the development and progression of osteonecrosis. Abnormal immune response, imbalanced immune cell subpopulations, and higher plasma levels of inflammatory cytokines in patients with osteonecrosis suggest that inflammation plays a crucial role in this disorder [12–14]. Moreover, chemokines and cytokines released by necrotic cells recruit inflammatory cells, inducing local and systemic immune response in patients with osteonecrosis [15–17]. However, whether these inflammatory processes are also involved in SCD osteonecrosis has rarely been investigated.

To date, a few preliminary works have suggested alterations of the adaptive immune system and related cytokines in the development or progression of osteonecrosis in SCD patients [18]. Mukisi-Mukaza and coworkers described non-specific granulomatous inflammatory reaction with a significant presence of lymphocytes in SCD osteonecrotic lesions [19]. Recently, Alagbe et al. demonstrated that SCD patients during bone infarction crisis have elevated TNF- α , IL-8, and ET-1 levels, which are critical mediators of inflammation, bone remodeling, and pain [20]. In addition, increased IL-6 levels, a pleiotropic cytokine produced during inflammatory response, were present in SCD patients with osteonecrosis in comparison to healthy SCD patients [6].

This study is aimed at investigating the possible association of T cell population in the pathophysiology of osteonecrosis that affects patients with sickle cell disease. We analyze peripheral blood and bone marrow aspirate for hematological aspects and peripheral blood mononuclear cells for CD4⁺, CD8⁺, CD45RA and CD45RO markers. We also investigated TCD4⁺-producing intracellular cytokines IFN- γ , IL-4, and IL-17 in PB-MNC and BM-MNC to better understand T cell response in osteonecrosis from SCD pathogenesis.

2. Materials and Methods

2.1. Participants. The institutional review board of the Health Science Institute (Federal University of Bahia-Salvador, Bahia-Brazil, protocol no. 67238317.0.0000.5662) approved this study. Written informed consent was obtained from all participants.

Between January 2017 and August 2019, peripheral blood (PB) was obtained from forty-three participants, both sexes, aged 10–55 years, and allocated in three groups: steady-state SCD patients (SCD, $N = 9$), SCD patients affected by ON (SCD/ON, $N = 15$), and healthy subjects (control $N = 19$). After enrollment, sociodemographic data and clinical information were collected. Exclusion criteria for these PB participants were recent viral infection, diabetes, autoimmune disease, immunodeficiency, pregnancy, obesity, presence of neoplastic disease, steroid treatment, acute pain/bone crisis, and hydroxyurea use. Sickle cell disease patients that experienced recurrent painful crises, displayed ulcers, or received

blood transfusion at least three months before were also excluded.

Bone marrow (BM) aspirates were obtained from forty-two consecutive participants who underwent osteonecrosis treatment with autologous BM graft surgery, between August 2017 and September 2019. Enrolled participants, both sexes, aged 9–57 years, were allocated in two groups: participants affected by SCD and osteonecrosis (SCD, $N = 24$) and participants affected by osteonecrosis not related to SCD (non-SCD, $N = 18$). Inclusion criteria were precollapse ON, radiological diagnosis according to Ficat stage 0–IIA, and scoring at least 20 points on the pain and daily life activities questionnaire. The exclusion criteria were participants with Ficat stage III or higher, current or previous bone infection at the limb affected by necrosis, acute recurrent painful crises, recent viral infection, immunosuppressive drug therapy, a history of previous surgery on the same injured limb, pregnancy, and presence of neoplastic disease.

2.2. Peripheral Blood and Bone Marrow Collection. Peripheral blood (PB) samples were collected from the antecubital vein using heparin anticoagulant tubes (VACUETTE® Blood Collection Tubes–16/100). The bone marrow (BM) was harvested under general anesthesia from the posterior iliac crest of patients diagnosed with osteonecrosis. The bone marrow was aspirated in 20 mL heparinized plastic syringe. An automated analyzer (ABX Horiba/Pentra80) was used for the quantitative evaluation of hematological parameters.

2.3. Mononuclear Cell (MNC) Preparation. Peripheral blood (PB) and bone marrow aspirate (BMA) mononuclear cell (PB-MNC and BM-MNC, respectively) isolation was done using density gradient Ficoll-Paque™ (GE Healthcare) as described by the manufacturer.

2.4. Lymphocyte Subset Immunophenotyping Analysis. Immunophenotyping analysis was performed on PB-MNC and BM-MNC for the expression of cell surface antigens using direct four-color analysis with fluorescein isothiocyanate- (FITC-) conjugated, phycoerythrin- (PE-) conjugated, APC-conjugated, and peridinin chlorophyll protein complex- (PerCP-) conjugated monoclonal antibodies. Lymphocyte subsets were determined using BD Tritest CD3/CD4/CD8 and Multitest CD3/CD4/CD45RA/CD45RO (BD Biosciences, Brazil). In brief, approximately 250 thousand cells were labeled with 10 μ L of the fluorescent cocktail. After 30 min of incubation in the dark at room temperature, non-specific binding was removed and cells were washed and analyzed immediately on a flow cytometer (BD FACS Calibur Flow Cytometer, BD Biosciences, Brazil), by selecting the appropriate area on the dot plot from the forward (FSC) and side scatter (SSC) histogram. The percentage of lymphocytes labeled with the investigated antigen was considered in the positive selection area.

2.5. Hematopoietic Progenitor Stem Cells (CD34⁺CD45^{low}) Analysis. The frequency of hematopoietic stem cells (HSCs) and progenitor cells can be considered by CD34⁺CD45^{low} cell analysis [21]. For this purpose, BMA was submitted to CD34⁺CD45^{low} staining and analysis. Antibody reagent

TABLE 1: Demographic and hematologic profiles for peripheral blood, from the control, SCD, and SCD/ON groups.

| | Control | SCD | SCD/ON | <i>p</i> value | | |
|-----------------------------|---------------------|--------------------|--------------------|-----------------|--------------------|----------------|
| | | | | Control vs. SCD | Control vs. SCD/ON | SCD vs. SCD/ON |
| <i>N</i> (%) | 19 (44.2) | 9 (20.9) | 15 (34.9) | | | |
| Age (y) | 31 (18-49) | 30 (19-47) | 31 (18-55) | | | |
| Male (%) | 52.63 | 88.88 | 46.66 | | | |
| WBC ($10^3/\text{mm}^3$) | 6.9 (3.5-9.3) | 7.4 (4.5-13.3) | 9.6 (5.0-13.1) | 0.182 | 0.0008*** | 0.546 |
| Lym (%) | 37.1 (9.5-54.5) | 40.5 (24.2-57.8) | 32.8 (26.2-38.7) | 0.443 | 0.272 | 0.083 |
| RBC ($10^6/\text{mm}^3$) | 5.4 (3.3-7.8) | 2.9 (2.5-5.1) | 3.7 (2.3-5.5) | 0.003** | 0.002** | 0.469 |
| Hgb (g/dL) | 14.6 (9.2-21.0) | 10.9 (8.4-13.5) | 11.8 (8.6-16.2) | 0.009** | 0.050* | 0.289 |
| Hct (%) | 44.6 (28.4-69.3) | 31.3 (23.2-41.0) | 33.3 (18.2-50.8) | 0.007** | 0.002** | 0.666 |
| MCV (fL) | 86.2 (76.7-91.0) | 93.6 (79.9-101.4) | 91.2 (79.2-117.5) | 0.010* | 0.165 | 0.228 |
| MCH (pg) | 27.3 (18.9-34.4) | 32.2 (23.7-37.0) | 31.6 (27.4-37.3) | 0.035* | 0.013* | 0.253 |
| RDW (%) ^a | 13.4 (11.8-17.3) | 18.3 (17.0-19.4) | 14.5 (11.4-18.0) | <0.0001**** | 0.1007 | 0.0001*** |
| Plat ($10^3/\mu\text{L}$) | 196.0 (107.0-472.0) | 241.0 (68.0-451.0) | 257.5 (55.0-532.0) | 0.950 | 0.370 | 0.931 |

Results are presented as median (min–max), except where noted otherwise. WBC: white blood cell; Lym: lymphocytes; RBC: red blood cells; Hgb: hemoglobin; Hct: hematocrit; MCV: mean corpuscular volume; MCH: mean corpuscular hemoglobin; RDW: red cell distribution width; and Plat: platelets. Significance values are presented as * $p < 0.05$, ** $p < 0.005$, *** $p < 0.0005$, and **** $p < 0.00005$.

cocktail containing, anti-CD34 antibody (PE, Clone 581, mouse IgG1 κ , Exbio), anti-CD45 antibody (FITC, Clone 2D1, mouse IgG1 κ , Exbio), and 7-aminoactinomycin-D (7-AAD, BD Pharmingen) was added in 5 mL round-bottom tubes, immediately prior to use, one hundred microliters of BMA sample was added to each tube and incubated for 20 minutes in the dark at room temperature. Red blood cells (RBCs) were lysed (Excelllyse Easy; Exbio) followed by 10 minutes of incubation in the dark at room temperature. Flow cytometry data was acquired on a flow cytometer (BD FACS Calibur Flow Cytometer, BD Biosciences, Brazil), and analysis was performed using the Cell Quest software (BD Biosciences).

2.6. Intracellular Cytokine Profile Characterization of CD4⁺ T Cells. Intracellular cytokine profile was performed on PB-MNCs and BM-MNCs using the Human Th1/Th2/Th17 intracellular phenotyping kit (BD Biosciences, Brazil), according to the manufacturer’s instructions. Approximately 1 million mononuclear cells/mL was incubated in RPMI 1640 (Sigma Aldrich, Brazil) medium, supplemented with 10% fetal calf serum, and stimulated for 5 hours with 50 ng/mL phorbol ester (PMA) and 1 $\mu\text{g}/\text{mL}$ calcium ionophore (Ionomycin), in the presence of the BD GolgiStop™ Protein Transport Inhibitor. Nonstimulated cells were included as a control during the assay. After incubation, cells were washed, fixated, permeabilized, and stained with antibody cocktail containing, Human CD4 PerCP-Cy5.5 (clone: SK3); Human IL-17A PE (clone: N49-653); Human IFN-GMA FITC (clone: B27), and Human IL-4 APC (clone: MP4-25D2).

2.7. Statistical Analysis. Data were evaluated using descriptive statistics (mean, standard deviation, minimum, maximum, median, frequency, and ratio). The results were expressed as the mean (SD) for quantitative variables with normal distributions. The parameters of total and differential blood cell

count according to distribution plots and analysis of variance homogeneity were presented as the median and the range (min–max). Student’s *t*-test was used for intergroup comparison of normally distributed data. Comparison among more than two groups were carried out based on one-way ANOVA and post hoc Dunnett’s test or Kruskal–Wallis tests. *p* values of < 0.05 were considered statistically significant. Statistical analysis was done using SPSS statistics (version 26) and GraphPad Prism (version 8) software.

3. Results

3.1. Patients with SCD Affected by Osteonecrosis Have Lower Hemoglobin and Higher WBC Count at Baseline Compared to Healthy Control Patients. The baseline demographic and PB hematological values are shown on Table 1. Demographic data was comparable among the groups, and no significant difference was observed. In comparison to the control group, patients with SCD and SCD/ON had a significantly lower median total red blood cell count (RBC) (5.4 (range 3.3–7.8) vs. 2.9 (range 2.5–5.1) and 3.7 (range 2.3–5.5) $\times 10^6/\text{mm}^3$, $p = 0.005$), lower hematocrit (2.9 (range 2.5–5.1), 3.7 (range 2.3–5.5) vs. 5.4 (3.3–7.8) $\times 10^6/\text{mm}^3$, $p = 0.01$ and $p = 0.005$), lower mean hemoglobin content (2.9 (range 2.5–5.1), 3.7 (range 2.3–5.5) vs. 5.4 (3.3–7.8) $\times 10^6/\text{mm}^3$, $p = 0.001$ and 0.05), and higher mean corpuscular hemoglobin (MCH) (2.9 (range 2.5–5.1), 3.7 (range 2.3–5.5) vs. 5.4 (3.3–7.8) $\times 10^6/\text{mm}^3$, $p = 0.05$) (Table 1). We also observed a significantly higher mean white blood cell count (WBC) in SCD/ON patients compared to the control group (9.6 (range 5.0–13.1) vs. 6.9 (3.5–9.3) $\times 10^3/\text{mm}^3$, $p = 0.0008$). A similar trend to increased WBC count was noted in SCD patients but failed to reach statistical significance (7.4 (range 4.5–13.3) vs. 6.9 (3.5–9.3) $\times 10^3/\text{mm}^3$, $p = 0.182$). While there was a relatively higher mean corpuscular volume (MCV) for

TABLE 2: Demographic and hematology profiles for the bone marrow aspirate, from the SCD and non-SCD groups.

| | Non-SCD BM (N = 18) | SCD BM (N = 24) | p value |
|---|---------------------|--------------------|---------|
| Age (y) | 36 (16-59) | 25.7 (9-57) | |
| Male (%) | 61.1 | 50 | |
| WBC ($\times 10^3/\text{mm}^3$) | 7.8 (5.0-24.5) | 12.8 (6.2-31.9) | 0.081 |
| Lym (%) | 34.5 (21.9-48.4) | 36.9 (5.2-55.4) | 0.450 |
| RBC ($\times 10^6/\text{mm}^3$) | 4.0 (2.1-6.3) | 3.1 (1.7-5.2) | 0.005** |
| Hgb (g/dL) | 12.8 (7.1-17.8) | 10.3 (6.7-13.5) | 0.026* |
| Hct (%) | 36.3 (19.9-57.2) | 31.7 (18.0-45.0) | 0.058 |
| MCV (fL) | 88.9 (78.2-95.1) | 103.9 (71.0-135.5) | 0.001** |
| MCH (pg) | 32.2 (23.3-37.9) | 35.6 (25.7-46.1) | 0.217 |
| RDW (%) | 12.5 (10.2-16.3) | 14.8 (10.9-19.4) | 0.001** |
| Plat ($10^3/\mu\text{L}$) | 8.0 (6.5-10.2) | 8.7 (7.8-9.8) | 0.037* |
| CD34 ⁺ CD45 ^{low} (%) | 0.6 (1.3-0.2) | 0.5 (1.2-0.2) | 0.401 |

^aResults are presented as median (min-max), except where noted otherwise. WBC: white blood cell; Lym: lymphocytes; RBC: red blood cells; Hgb: hemoglobin; Hct: hematocrit; MCV: mean corpuscular volume; MCH: mean corpuscular hemoglobin; RDW: red cell distribution width; and Plat: platelets. Significance values are presented as *p*; **p* < 0.05, ***p* < 0.005, ****p* < 0.0005, and *****p* < 0.00005.

TABLE 3: Lymphocyte frequencies (%) in PB-MNC.

| | Control | SCD | SCD/ON | Control vs. SCD | p value Control vs. SCD/ON | SCD vs. SCD/ON |
|--------------------------------------|------------------|-----------------|------------------|-----------------|-------------------------------|----------------|
| TCD4 ⁺ | 42.0 (19.2-61.6) | 21.4 (5.7-47.5) | 30.0 (8.4-59.7) | 0.0074** | 0.0442* | 0.2854 |
| TCD8 ⁺ | 24.0 (14.1-38.7) | 12.5 (4.8-23.7) | 14.6 (2.6-23.9) | 0.0085** | 0.0020** | 0.5962 |
| TCD4 ⁺ /45RO ⁺ | 21.6 (4.8-41.3) | 10.8 (4.3-16.1) | 15.5 (4.6-25.6) | 0.0154* | 0.1541 | 0.1892 |
| TCD4 ⁺ /45RA ⁺ | 40.3 (20.8-59.4) | 10.8 (2.3-28.6) | 12.60 (2.4-25.0) | 0.0003*** | <0.0001**** | 0.8749 |

All values are presented in median. Significance values are presented as **p* < 0.05, ***p* < 0.005, ****p* < 0.0005, and *****p* < 0.00005.

patients with SCD compared to the control group (9.6 (range 5.0-13.1) vs. 6.9 (3.5 – 9.3) $\times 10^3/\text{mm}^3$, *p* = 0.0008), there were no significant differences (NS) in total lymphocyte and platelet counts among the groups. The lack of significant difference in many baseline characteristics indicates similarities between the cohort of patients with SCD and SCD/ON evaluated here. In addition, these results demonstrate a need for better PB characterization of patients with SCD affected by osteonecrosis.

Bone marrow aspirated from 24 SCD patients affected by osteonecrosis (SCD BM) and 18 patients with osteonecrosis not related to SCD (non-SCD BM) were also analyzed. There were no significant differences in the distribution of age, disease duration, stages, and the values of index of femoral head collapse among the different groups of patients. While WBC cell count from SCD BM (*n* = 24) and non-SCD BM (*n* = 18) was similar (12.8 (range 6.2-31.9) vs. 7.8 (range 5.0 – 24.5) $\times 10^3/\text{mm}^3$), RBC (12.8 (range 6.2-31.9) vs. 7.8 (range 5.0 – 24.5) $\times 10^3/\text{mm}^3$, *p* = 0.01), and hemoglobin content (12.8 (range 6.2-31.9) vs. 7.8 (range 5.0 – 24.5) $\times 10^3/\text{mm}^3$, *p* = 0.05) from SCD BM were significantly lower (Table 2). In contrast, SCD BM had significantly higher mean MCV (12.8 (range 6.2-31.9) vs. 7.8 (range 5.0 – 24.5) $\times 10^3/\text{mm}^3$, *p* = 0.005), higher mean RDW (12.8 (range 6.2-31.9) vs. 7.8 (range 5.0 – 24.5) $\times 10^3/\text{mm}^3$, *p* = 0.005), and higher median

platelet counts (12.8 (range 6.2-31.9) vs. 7.8 (range 5.0 – 24.5) $\times 10^3/\text{mm}^3$, *p* = 0.05) compared to non-SCD BM. The frequency of CD34⁺CD45^{low} was not significantly different between SCD BM and non-SCD BM (Table 2).

3.2. SCD Patients Have a Lower Proportion of TCD4⁺ and TCD8⁺ Cells Compared to Healthy Control Patients. Previous research has described alterations of lymphocyte phenotype and function in SCD patients, especially deregulated adaptive cell behavior, imbalanced T cell subsets, and alloimmunization [3, 18, 22, 23] To determine the frequencies of the major T cell subsets, we applied the staining panel to freshly isolated peripheral blood mononuclear cells (PB-MNC) from SCD, SCD/ON, and healthy control patients. Table 3 and Figure 1 show the frequency for TCD4⁺ (T helper) and TCD8⁺ (T cytotoxic) coexpressing the CD3 marker. Compared with healthy controls, SCD and SCD/ON patients had a significantly lower median distribution of TCD4⁺ (41.98% (range 19.24-61.57) vs. 21.37% (range 5.67-47.5) and 30.04% (range 8.37-59.66), *p* = 0.01 and 0.05, respectively) and TCD8⁺ (24.02% (range 14.15-38.69) vs. 12.47% (range 4.83-23.77) and 14.57% (range 2.65-23.9), *p* = 0.01 and 0.005, respectively) cell subpopulations. There were no significant differences in these subsets between the SCD and SCD/ON groups. Figures 1(g) and 1(h) show TCD4⁺

effector cells (CD4⁺45RO⁺) and TCD4⁺ naïve cells (CD4⁺CD45RA⁺) frequencies in the control, SCD, and SCD/ON groups.

Frequencies of CD45RA⁺ within CD4⁺ T cell subpopulations were significantly higher in the control patients relative to both SCD (40.31% (range 20.79-59.84) vs. 10.78% (range 2.34-28.6), $p = 0.0005$) and SCD/ON (40.31% (range 20.79-59.84) vs. 12.60% (range 2.37-25.02), $p = 0.0001$) patients. Only SCD subjects had significantly lower median effector T cell proportions than the control subjects (21.62% (range 4.84-41.26) vs. 10.84% (range 4.33-16.08), $p = 0.05$). In sum, we found similar frequencies of major T cell subsets in the peripheral blood of SCD patients with or without osteonecrosis. Except for effector T cells in SCD/ON, control patients had significantly higher frequencies of T cell subsets in PB-MNCs in comparison to SCD, irrespective to the presence of osteonecrosis.

Because many of the T lymphocytes migrate to the bone marrow and partly return later to the blood [24], we also analyzed the frequency of T cell subsets in the bone marrow aspirate of SCD patients affected by osteonecrosis (SCD BM) and patients with osteonecrosis not related to SCD (non-SCD BM). Table 4 and Figure 2 show the distribution for the various lymphocyte subsets investigated in BM-MNC. We noted a higher frequency of TCD4⁺ and TCD8⁺ in non-SCD BM compared with SCD BM (32.01% (range 19.09-46.3) vs. 24.28% (range 5.41-47.82) and 23.20% (range 13.14-31.58) vs. 16.18% (range 6.4-31.68), $p = 0.05$ and $p = 0.01$, respectively). There were no significant differences in the frequency of other T subsets between groups.

3.3. Increased Frequency of IL4⁺TCD4⁺ Cells and Bifunctional IFN- γ ⁺/IL4⁺ and IL-17⁺/IL4⁺CD4⁺T Cells in SCD and SCD/ON Compared to Healthy Control Patients. Next, we investigated functionally polarized TCD4⁺ cell subsets in SCD, SCD/ON, and healthy control patients. This was accomplished by simultaneously determining intracellular IFN- γ ⁺ (representing Th1-like), IL4⁺ (representing Th2-like), and IL-17⁺ (representing Th17-like) expressions by flow cytometry after *in vitro* stimulation. Based on the distinctive patterns of intracellular cytokine expression, the percentage of mono- and bifunctional cells were assessed among the TCD4⁺ population. The spontaneous cytokine production of nonstimulated cells was minimal, and no significant differences were observed in the frequencies of TCD4⁺-expressing IFN- γ , IL4, and IL-17 between groups (data not shown).

After *in vitro* stimulation with PMA/ionomycin (PMA/Io) (polyclonal stimulation), a significantly higher frequency of IL4⁺TCD4⁺ cells in SCD and SCD/ON were detected in comparison to the control (0.19% (range 0.01-0.55) vs. 2.54% (range 1.98-4.41) and 0.19% (range 0.01-0.55) vs. 2.08% (range 0.57-4.15)) ($p = 0.0016$ and $p = 0.0017$, respectively) (Figure 3). When IFN- γ ⁺ were analyzed, PB-MNC from the SCD and SCD/ON groups contained higher proportion of IFN- γ ⁺ cells compared to the healthy control group; however, differences failed to reach statistical significance ($p = 0.0593$ and $p = 0.1605$, respectively) (Figure 3). Accordingly, the bifunctional IFN- γ ⁺IL4⁺TCD4⁺ cells in

SCD (1.72% (range 0.58-3.92)) and SCD/ON (1.57% (range 0.64-2.69)) were significantly higher compared to the control group (0.14% (range 0.00-0.48)) ($p = 0.0264$; $p = 0.0006$, respectively). In comparison to the healthy controls (0.02% (range 0.00-0.09)), significantly higher frequencies of bifunctional IL17⁺IL4⁺TCD4⁺ cells were noted in the SCD and SCD/ON groups (0.32% (range 0.10-0.47); 0.13% (range 0.00-0.35)) ($p = 0.0094$ and $p = 0.0162$, respectively) (Figure 3(g)). The frequency of bifunctional TCD4⁺ cells coexpressing IL17⁺ and IL4⁺ was significantly higher in SCD compared to the SCD/ON group ($p = 0.0425$). The increase in IL-4⁺TCD4⁺ subset frequency suggests a shift of CD4⁺ T cell response, corresponding to a Th2 phenotype.

We also investigated functional polarization of TCD4⁺ cell subsets in SCD and non-SCD BM based on intracellular cytokines IFN- γ , IL-4, and IL-17 expressions (Figure 4). The production of these cytokines was minimal in nonstimulated BM-MNC cultures (data not shown). When stimulated with PMA/ionomycin, the frequency of monofunctional IFN- γ ⁺TCD4⁺ cells (Figure 4(a)) and IL-17⁺TCD4⁺ cells (Figure 4(c)) was increased in SCD BM compared to non-SCD BM (13.31% (range 0.55-33.68) vs. 5.45% (range 2.97-7.36)) ($p = 0.027$, $p < 0.0001$), respectively). There was no difference in the relative frequency of IL-4⁺TCD4⁺ cells or bifunctional cells between SCD BM and non-SCD BM patients in culture-stimulated PMA/Io. The T cell immune response towards a cytokine secretion phenotype after stimulation indicated that the immune system of SCD patients has partially differentiated cells ready to assume Th1 and Th17 effector functions.

4. Discussion

Several SCD studies have reported evidences of abnormal immune cell counts and dysfunctional T lymphocyte response, but none of these previous works have investigated the immunological profile of SCD patients with osteonecrosis. In this small cross-sectional study, we demonstrated that lower frequency of circulating CD4⁺, CD8⁺, and naïve T lymphocyte subsets were directly associated with SCD disease but not with osteonecrosis. After *in vitro* stimulation of PBMC, the percentage of IL4⁺TCD4⁺ cells coexpressing either IFN- γ ⁺ or IL-17⁺ were significant higher in SCD and SCD/ON patients in comparison to control subjects. More importantly, the frequencies of IFN- γ ⁺-producing and IL-17⁺-producing CD4⁺T cells in stimulated BM-MNCs were significantly higher in SCD/ON patients than controls patients with osteonecrosis not related to SCD. These results indicate that there are differences in peripheral and bone marrow T cell subsets in SCD patients with osteonecrosis that are able to assume a phenotype of cytokine secretion after stimulation. The changes observed on T cell responses could extend to inflammatory sites of bone complications, thereby contributing to the maintenance of inflammation and the pathophysiology of osteonecrosis. Given that previous studies have shown strong association between proinflammatory cytokines and osteonecrosis in SCD patients [6], our findings corroborate previous observations and support the notion that T cell may participate

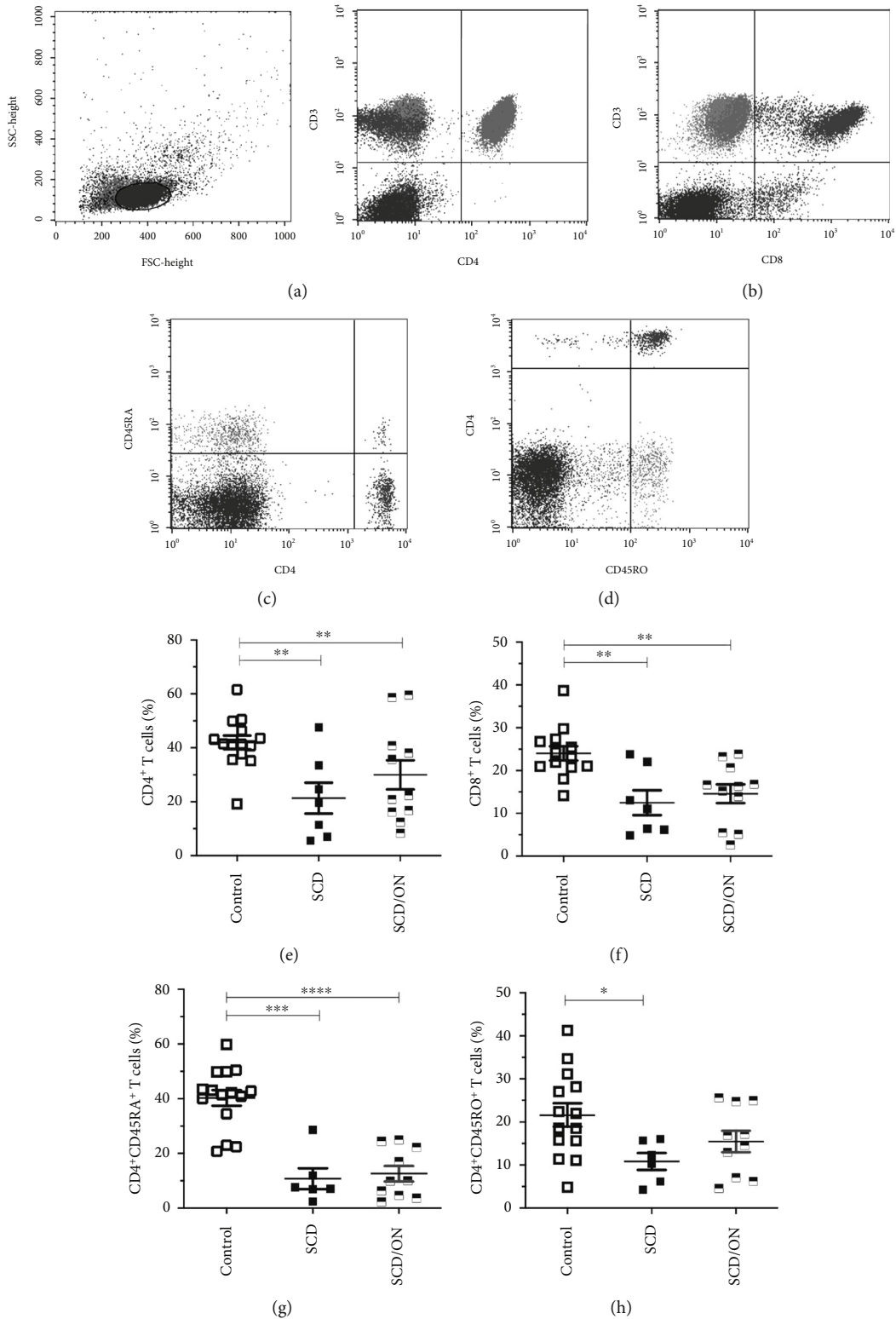


FIGURE 1: Relative frequency of major T cell populations in peripheral blood mononuclear cells from healthy donors (control), steady-state SCD, and SCD with osteonecrosis (SCD/ON) patients. Representative dot plots illustrate the strategy of gating for major T cell subsets defined by CD3+CD4+ (a), CD3+CD8+ (b), CD4+/45RA+ (c), and TCD4+/45RO+ (d) surface expressions in PBMC. All gates were based on isotype-matched control staining. Cumulative data showing the frequencies of total TCD4+ (e), total TCD8+ (f), TCD4+CD45RA+ (g), and TCD4+CD45RO+ (h) subpopulations within live-gated single cells. Each symbol represents an individual subject. Horizontal lines represent mean and standard error. * $p < 0.05$, ** $p < 0.005$, *** $p < 0.0005$, and **** $p < 0.00005$.

TABLE 4: Lymphocyte frequencies (%) in BM-MNC.

| | Non-SCD BM | SCD BM | <i>p</i> value |
|------------------------|---------------------|--------------------|----------------|
| TCD4 ⁺ | 32.0 (19.09-46.3) | 24.28 (5.41-47.82) | 0.0332* |
| TCD8 ⁺ | 23.20 (13.14-31.58) | 16.18 (6.4-31.68) | 0.0065** |
| TCD4/45RO ⁺ | 19.81 (12.61-30.27) | 17.00 (4.94-43.4) | 0.3965 |
| TCD4/45RA ⁺ | 7.68 (3.47-24.52) | 8.57 (2.01-17.68) | 0.5065 |

All values are presented in mean. Significance values are presented as **p* < 0.05, ***p* < 0.005, ****p* < 0.0005, and *****p* < 0.00005.

in the development of abnormal immune response and chronic inflammation in SCD patients with osteonecrosis.

In this context, we observed that the percentage of circulating CD4⁺, CD8⁺, and naïve TCD4⁺ cells were significantly reduced in SCD and SCD/ON patients. We also observed decreased percentage of CD4⁺ and CD8⁺ in the bone marrow of patient with osteonecrosis related to SCD in comparison to non-SCD patients. Many studies have correlated mild lymphopenia, elevated inflammation biomarkers, and poor outcomes in patients with SCD [4, 25]. It is worth nothing that the proportions of CD4⁺ T cells, naïve CD4⁺ T cells, memory CD4⁺ T cells, memory CD8⁺ T cells, and CD4/CD8 ratio were profoundly reduced in the presence of splenic-associated abnormalities [26] or during vaso-occlusive crisis [22]. In fact, reduced peripheral CD4⁺ and Treg frequencies, as well as coexisting levels of both high and low Th1- and Th2-type cytokines in chronically transfused patients, suggested an underlying inflammatory state in SCD [27]. Together with reports of lymphopenia and reduced peripheral T cell levels in SCD patients [5, 18, 22], these findings suggest that T cells are attracted away from the blood and into the target site of inflammation. Recently, Nickel et al. described normalization of most CD4⁺T subpopulations and memory CD8⁺ T cells in SCD patients receiving immunosuppressant therapy to halt progression of chronic inflammation [28]. It must be pointed out that our SCD and SCD/ON patients were not under medication and they presented severe SCD biomarkers significantly different from the healthy control group. Overall, our results suggest that the decreased frequency of T cell subsets might be directly related to an underlying inflammatory state in SCD rather than osteonecrosis status.

In our study, there was an increased relative frequency of CD4⁺ T lymphocytes producing IL-4, IL-4/IL-17, or IL-4/INF- γ in samples from SCD and SCD/ON patients in comparison to healthy controls after stimulation with PMA/ionomycin. This finding corroborates previous reports that show an increased frequency of Th2 lymphocytes and elevated serum levels of IL-4 in SCD patients [22, 29]. The analysis of intracellular cytokine expression allowed a flexible identification of functional subtypes of T cells in contrast with the traditional classification defined by surface markers. Our finding suggests that SCD and SCD/ON patients show an increased subset of circulating T helper cells able to produce a broad spectrum of pro- and anti-inflammatory cytokines after a strong stimulus, such as PMA/ionomycin. In contrast, a significantly higher frequency of IL-17⁺, CD4⁺, and INF- γ CD4⁺ was observed in bone marrow T lymphocytes. There

were no differences in the relative frequencies of IL4⁺CD4⁺ and bifunctional CD4⁺ T cells in the bone marrow of SCD BM patients compared with non-SCD BM patients. These results suggest that Th1 cells and Th17 are the main types of cellular immunity in the bone marrow of SCD patients, meaning that these increased T subsets in the bone marrow may contribute to the immune disorders in SCD patients with osteonecrosis. Recently, CD4⁺ T cells from steady-state SCD patients exhibit hallmarks of terminal T cell exhaustion and migration defects, including the expression of CTLA-4 and reduced expression of CCR7 [4]. Of relevance, emerging evidences have pointed toward RBC as dynamic reservoirs of cytokines that may affect immune function in SCD patients. Karsten et al. have shown that RBCs can store and release cytokines into the plasma, such as IFN- γ , IL-1 β , IL-18, TNF- α , and several chemokines, including IL-8 and RANTES, suggesting that in hemolytic conditions, such as sickle cell disease, RBC may play downstream effects on neighboring cells and may have a critical role in modulating T cell behavior, including different subsets of T cells [30]. Indeed, IL6 and IL-10 frequently produced by SCD patients could also be associated with the alterations in immune profile and functions [6], although the reason for these particular phenotypes is not fully understood.

Bone homeostasis is regulated by the immune system [31–34]. In our study, we demonstrated that polyclonal stimulation of BM-MNC induced an increased frequency of CD4⁺IFN- γ ⁺ and CD4⁺IL-17⁺ in SCD BM compared to non-SCD BM patients. Previous studies have shown that activated T cells play an important role in bone health and disease. Especially, Th17 cells have a great influence on bone metabolism by secreting characteristic soluble factor that induces osteoclastogenesis [35]. In contrast, effector T cell production of IFN- γ strongly suppresses bone resorption by interfering with the RANKL/RANK signaling pathway [36]. It has been shown that increased serum levels of IL-17A and IFN- γ are present in patients with steroid-related osteonecrosis [37]. All together, these results suggest that Th17 and Th1 cells may have a role in the pathogenesis of osteonecrosis in sickle cell disease. The combined analysis of the data herein presented, together with the existing information in the literature, provides clues to a better understanding of the pathophysiology of osteonecrosis related to SCD and opens perspectives to the development of alternative therapies for this disease.

It is conceivable that personalized cytokine blocking therapy specifically designed according to the predominant profile of functional T cells will be effective in helping restore the immunologic balance in each SCD patient. IL-17-producing and IFN- γ -producing T lymphocytes seem to play a prominent role in pathophysiology of osteonecrosis related to SCD and may represent a potential target for therapy. In fact, it is possible that cytokine-targeted and personalized therapy may contribute to improving the balance of effector immune response, avoiding or minimizing the damage caused by the unbalanced immune response.

Our study has some limitations. First, this study was cross-sectional and thus only involved a single timepoint for each of the enrolled patients. A prospective longitudinal

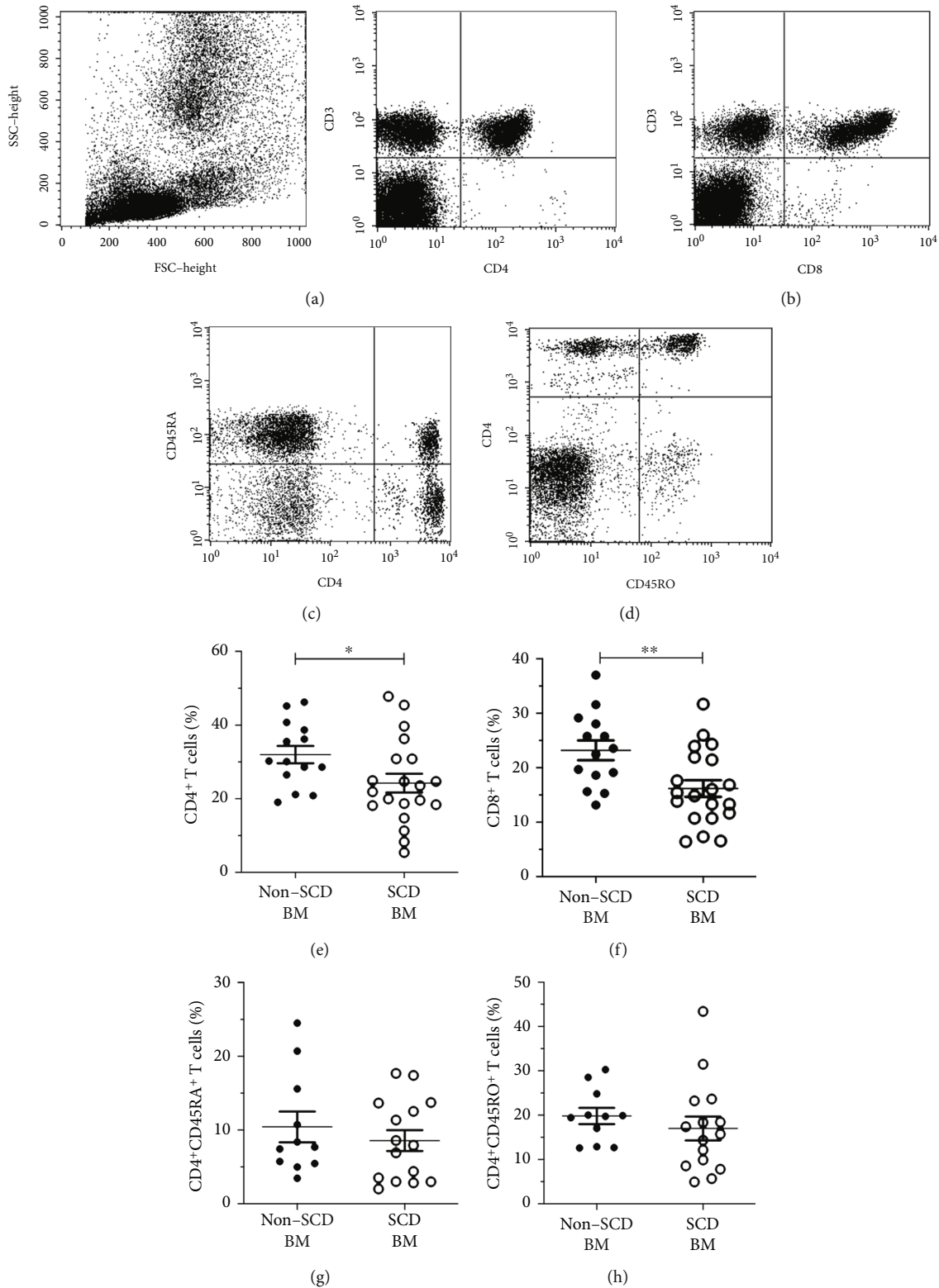


FIGURE 2: Relative frequency of major T cell populations in bone marrow mononuclear cells (BM-MNC) from SCD patients with osteonecrosis (SCD BM) and patients with osteonecrosis not related to SCD (non-SCD BM). Representative dot plots illustrate the strategy of gating for major T cell subsets defined by $CD3^+CD4^+$ (a), $CD3^+CD8^+$ (b), $CD4^+/45RA^+$ (c), and $CD4^+/45RO^+$ (d) surface expressions in BM-MNC. All gates were based on isotype-matched control staining. $CD4^+$ and $CD8^+$ cells are lower in SCD BM. Cumulative data showing the frequencies of total $CD4^+$ (e), total $CD8^+$ (f), $CD4^+CD45RA^+$ (g), and $CD4^+CD45RO^+$ (h) subpopulations within live-gated single cells. Each symbol represents an individual subject. Horizontal lines represent mean and standard error. * $p < 0.05$; ** $p < 0.005$.

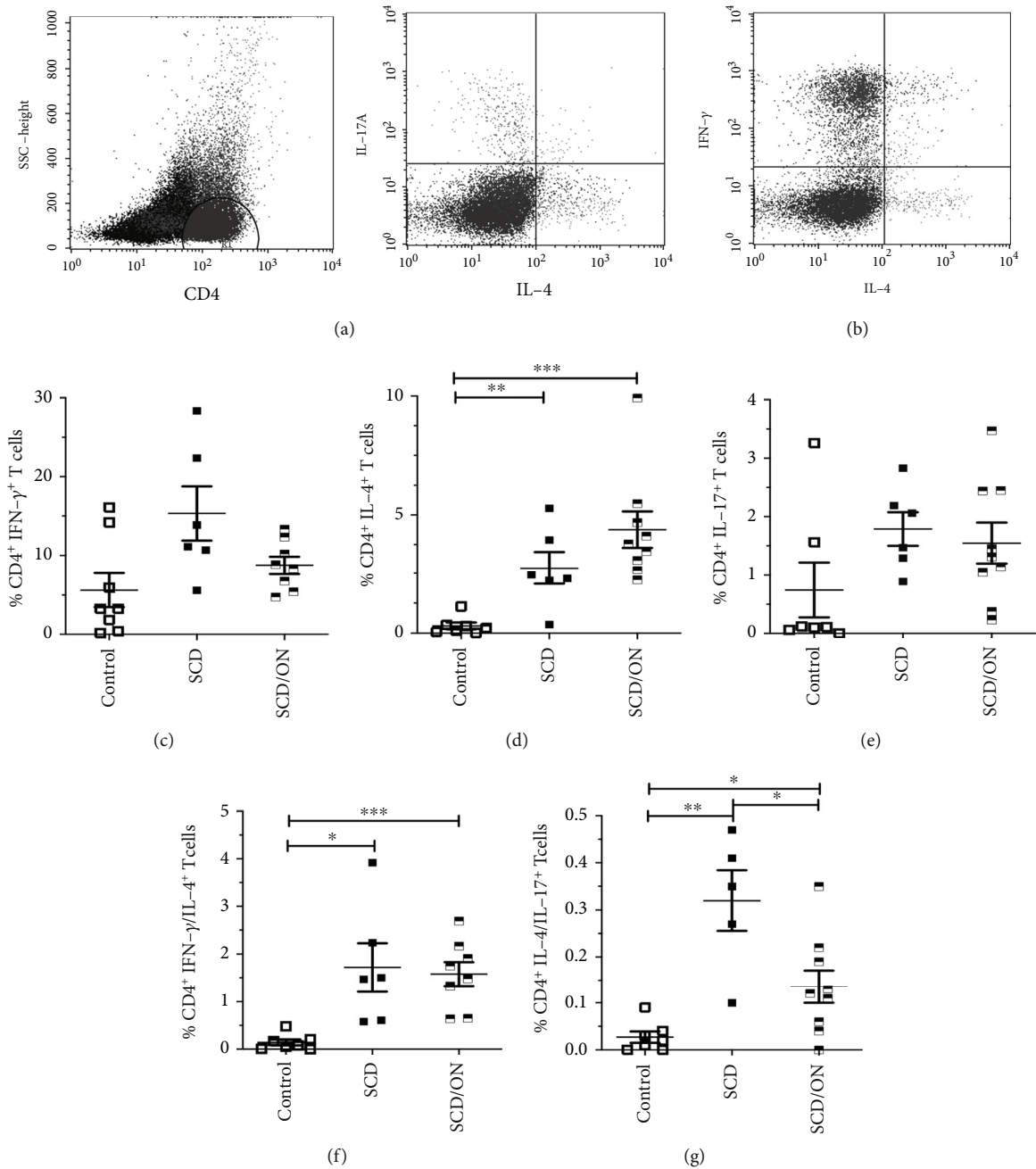


FIGURE 3: Increased frequency of IL4⁺CD4⁺ T cells and bifunctional IFN- γ ⁺/ IL4⁺ and IL-17⁺/ IL4⁺CD4⁺ T cells in SCD and SCD/ON compared to healthy controls. Peripheral blood mononuclear cells from healthy donors (control), steady-state SCD, and SCD with osteonecrosis (SCD/ON) patients were culture stimulated with PMA/Io and stained for intracellular cytokine production. Representative dot plots illustrate intracellular staining for IFN- γ ⁺/IL-4⁺ (a) and IL-4⁺/IL-17⁺ (b) in TCD4⁺ cells after stimulation. Relative frequency of IFN- γ ⁺ (c), IL-4⁺ (d), IL-17⁺ (e), bifunctional IFN- γ ⁺/IL-4⁺ (f), and IL-4⁺/IL-17⁺ TCD4⁺ (g) cells producing cytokines in relation to total TCD4⁺ cells in culture. Each symbol represents an individual subject. Horizontal lines represent mean and standard error. * $p < 0.05$, ** $p < 0.005$, and *** $p < 0.0005$.

study is necessary to fully evaluate the causal relationship between osteonecrosis onset or progression and the T cell subset changes in SCD patients. Second, although the changes in lymphocyte subset numbers and the functional status of many of the CD4⁺ T cells were investigated, it cannot be assumed to reflect functional immune deviation. To overcome this limitation, antigen-specific tests of immune

activation will be important to add to further *in vitro* studies. Finally, increasing sample size should improve statistic power and reproducibility on repeated measured outcomes. Future studies that include more SCD patients both at steady state as well as with osteonecrosis would shed light on the impact of this complication on the immune manifestations of SCD.

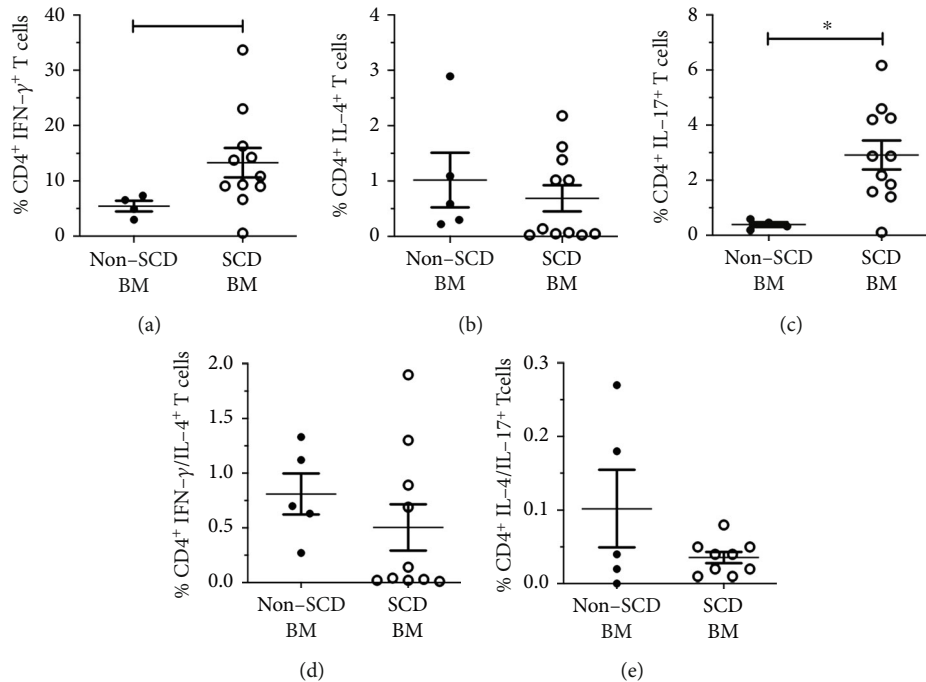


FIGURE 4: Increased frequency of IFN- γ^+ CD4 $^+$ T and IL-17 $^+$ CD4 $^+$ T cells in SCD BM compared to non-SCD BM patients. Bone marrow mononuclear cells (BM-MNC) from SCD patients with osteonecrosis (SCD BM) and patients with osteonecrosis not related to SCD (non-SCD BM) were culture stimulated with PMA/Io and stained for intracellular cytokine production. Relative frequency of IFN- γ^+ (a), IL-4 $^+$ (b), IL-17 $^+$ (c), bifunctional IFN- γ^+ /IL-4 $^+$ (d), and IL-4 $^+$ /IL-17 $^+$ TCD4 $^+$ (e) cells producing cytokines in relation to total TCD4 $^+$ cells in culture. Each symbol represents an individual subject. Horizontal lines represent mean and standard error. * $p < 0.05$, ** $p < 0.005$, and *** $p < 0.0005$.

5. Conclusion

In conclusion, this study has described that SCD patients with or without ON presented significantly reduced TCD4 $^+$, TCD8 $^+$, and TCD4 $^+$ naïve cell frequencies in PB-MNC and increased frequency of circulating CD4 $^+$ T cells able to simultaneously produce IFN- γ^+ /IL4 $^+$ and IL-17 $^+$ /IL4 $^+$ compared to healthy controls. Conversely, there was an increased frequency of either IFN- γ^+ or IL-17 $^+$ CD4 $^+$ T cells in stimulated BM-MNC of SCD patients with osteonecrosis. This finding suggests that the bone marrow of patients with SCD show an increased subset of T helper cells able to produce a broad spectrum of proinflammatory cytokines after a strong stimulus, such as PMA/Io. This increased CD4 $^+$ T subset may extend to inflammatory sites of target organs and may contribute to the immune disorders in SCD patients with osteonecrosis.

Data Availability

The data used to support the findings of this study are available from the corresponding author upon request.

Disclosure

The funders had no role in the study design and data collection and analysis.

Conflicts of Interest

The authors declare that there is no conflict of interest regarding the publication of this article.

Acknowledgments

We would like to acknowledge the surgery orthopedic team member Dr. Thiago Faleiro from the Prof. Edgar Santos Hospital Complex, Federal University of Bahia, Bahia, Brazil, for the collection of bone marrow samples. This study was financially supported by the Brazilian Ministry of Health, the Brazilian National Research Council (CNPq) grant 443137/2016-1 to VF, Research Support Foundation of the State of Bahia (FAPESB), and cofunded by the Coordenação de Aperfeiçoamento de Pessoal de Nível Superior–Brasil (CAPES)–Finance Code 001 (scholarship to PBD and TOR).

References

- [1] G. J. Kato, F. B. Piel, C. D. Reid et al., “Sickle cell disease,” *Nature Reviews Disease Primers*, vol. 4, no. 1, article 18010, 2018.
- [2] E. Nader, M. Romana, and P. Connes, “The red blood cell—inflammation vicious circle in sickle cell disease,” *Frontiers in Immunology*, vol. 11, p. 454, 2020.
- [3] E. Balandya, T. Reynolds, S. Obaro, and J. Makani, “Alteration of lymphocyte phenotype and function in sickle cell anemia:

- Implications for vaccine responses,” *American Journal of Hematology*, vol. 91, no. 9, pp. 938–946, 2016.
- [4] B. Vingert, M. Tamagne, M. Desmarests et al., “Partial dysfunction of Treg activation in sickle cell disease,” *American Journal of Hematology*, vol. 89, no. 3, pp. 261–266, 2014.
- [5] J. T. C. de Azevedo and K. C. R. Malmegrim, “Immune mechanisms involved in sickle cell disease pathogenesis: current knowledge and perspectives,” *Immunology Letters*, vol. 224, pp. 1–11, 2020.
- [6] I. F. Domingos, D. A. Pereira-Martins, M. J. V. C. Sobreira et al., “High levels of proinflammatory cytokines IL-6 and IL-8 are associated with a poor clinical outcome in sickle cell anemia,” *Annals of Hematology*, vol. 99, no. 5, pp. 947–953, 2020.
- [7] P. Vicari, S. A. Adegoke, D. R. Mazzotti, R. D. Caçado, M. A. E. Nogutti, and M. S. Figueiredo, “Interleukin-1 β and interleukin-6 gene polymorphisms are associated with manifestations of sickle cell anemia,” *Blood Cells, Molecules, and Diseases*, vol. 54, no. 3, pp. 244–249, 2015.
- [8] K. L. Vanderhave, C. A. Perkins, B. Scannell, and B. K. Brighton, “Orthopaedic manifestations of sickle cell disease,” *Journal of the American Academy of Orthopaedic Surgeons*, vol. 26, no. 3, pp. 94–101, 2018.
- [9] C. H. Flouzat-Lachaniet, X. Roussignol, A. Poignard, M. M. Mukasa, O. Manicom, and P. Hernigou, “Multifocal joint osteonecrosis in sickle cell disease,” *The Open Orthopaedics Journal*, vol. 3, no. 1, pp. 32–35, 2009.
- [10] G. Daltro, B. A. Franco, T. B. Faleiro, D. A. V. Rosário, P. B. Daltro, and V. Fortuna, “Osteonecrosis in sickle cell disease patients from Bahia, Brazil: a cross-sectional study,” *International Orthopaedics*, vol. 42, no. 7, pp. 1527–1534, 2018.
- [11] P. Hernigou, A. Habibi, D. Bachir, and F. Galacteros, “The natural history of asymptomatic osteonecrosis of the femoral head in adults with sickle cell disease,” *The Journal of Bone and Joint Surgery-American Volume*, vol. 88, no. 12, pp. 2565–2572, 2006.
- [12] B. Kaymaz, K. Büyükdogan, N. Kaymaz et al., “Neutrophil to lymphocyte ratio may be a predictive marker of poor prognosis in Legg-Calvé-Perthes disease,” *Hip International*, vol. 26, no. 6, pp. 598–601, 2016.
- [13] D. Zou, K. Zhang, Y. Yang et al., “Th17 and IL-17 exhibit higher levels in osteonecrosis of the femoral head and have a positive correlation with severity of pain Th17,” *Endokrynologia Polska*, vol. 69, no. 3, pp. 283–290, 2018.
- [14] J. Ma, J. Ge, F. Gao et al., “The role of immune regulatory cells in nontraumatic osteonecrosis of the femoral head: a retrospective clinical study,” *BioMed Research International*, vol. 2019, Article ID 1302015, 7 pages, 2019.
- [15] J. Lechner, S. Schuett, and V. von Baehr, “Aseptic-avascular osteonecrosis: local ‘silent inflammation’ in the jawbone and RANTES/CCL5 overexpression,” *Clinical, Cosmetic and Investigational Dentistry*, vol. 9, pp. 99–109, 2017.
- [16] J. Ma, W. Guo, Z. Li, B. Wang, S. Li, and P. Wang, “Hip osteonecrosis is associated with increased plasma IL-33 level,” *Mediators of Inflammation*, vol. 2017, Article ID 1732638, 6 pages, 2017.
- [17] J. Tao, B. Dong, L. X. Yang, K. Q. Xu, S. Ma, and J. Lu, “TGF- β 1 expression in adults with non-traumatic osteonecrosis of the femoral head,” *Molecular Medicine Reports*, vol. 16, no. 6, pp. 9539–9544, 2017.
- [18] M. J. B. M. Rêgo, R. R. da Silva, M. C. Pereira et al., “Evaluation of CD4+CD25+FoxP3+ T cell populations, IL-10 production, and their correlation with clinical and biochemical parameters in sickle cell anemia patients with leg ulcers,” *Cytokine*, vol. 75, no. 2, pp. 310–315, 2015.
- [19] M. Mukisi-Mukaza, A. Gomez-Brouchet, M. Donkerwolcke, M. Hinsenkamp, and F. Burny, “Histopathology of aseptic necrosis of the femoral head in sickle cell disease,” *International Orthopaedics*, vol. 35, no. 8, pp. 1145–1150, 2011.
- [20] A. E. Alagbe, J. A. Olaniyi, and O. W. Aworanti, “Adult sickle cell anaemia patients in bone pain crisis have elevated proinflammatory cytokines,” *Mediterranean Journal of Hematology and Infectious Diseases*, vol. 10, no. 1, article e2018017, 2017.
- [21] A. Leonard, A. Bonifacino, V. M. Dominical et al., “Bone marrow characterization in sickle cell disease: inflammation and stress erythropoiesis lead to suboptimal CD34 recovery,” *British Journal of Haematology*, vol. 186, no. 2, pp. 286–299, 2019.
- [22] B. O. P. Musa, G. C. Onyemelukwe, J. O. Hambolu, A. I. Maman, and A. H. Isa, “Pattern of serum cytokine expression and T-cell subsets in sickle cell disease patients in vaso-occlusive crisis,” *Clinical and Vaccine Immunology*, vol. 17, no. 4, pp. 602–608, 2010.
- [23] B. Vingert, M. Tamagne, A. Habibi et al., “Phenotypic differences of CD4+T cells in response to red blood cell immunization in transfused sickle cell disease patients,” *European Journal of Immunology*, vol. 45, no. 6, pp. 1868–1879, 2015.
- [24] R. Pabst, “The bone marrow is not only a primary lymphoid organ: the critical role for T lymphocyte migration and housing of long-term memory plasma cells,” *European Journal of Immunology*, vol. 48, no. 7, pp. 1096–1100, 2018.
- [25] N. P. Garcia, A. L. S. Júnior, G. A. S. Soares et al., “Sickle cell anemia patients display an intricate cellular and serum biomarker network highlighted by TCD4+CD69+ lymphocytes, IL-17/MIP-1 β , IL-12/VEGF, and IL-10/IP-10 axis,” *Journal of Immunology Research*, vol. 2020, Article ID 4585704, 22 pages, 2020.
- [26] K. G. Koffi, D. Sawadogo, M. Meite et al., “Reduced levels of T-cell subsets CD4+ and CD8+ in homozygous sickle cell anaemia patients with splenic defects,” *The Hematology Journal*, vol. 4, no. 5, pp. 363–365, 2003.
- [27] W. Bao, H. Zhong, X. Li et al., “Immune regulation in chronically transfused allo-antibody responder and nonresponder patients with sickle cell disease and β -thalassemia major,” *American Journal of Hematology*, vol. 86, no. 12, pp. 1001–1006, 2011.
- [28] R. S. Nickel, J. T. Horan, R. M. Fasano et al., “Immunophenotypic parameters and RBC alloimmunization in children with sickle cell disease on chronic transfusion,” *American Journal of Hematology*, vol. 90, no. 12, pp. 1135–1141, 2015.
- [29] A. Pathare, S. al Kindi, A. A. Alnaqdy, S. Daar, H. Knox-Macaulay, and D. Dennison, “Cytokine profile of sickle cell disease in Oman,” *American Journal of Hematology*, vol. 77, no. 4, pp. 323–328, 2004.
- [30] E. Karsten, E. Breen, and B. R. Herbert, “Red blood cells are dynamic reservoirs of cytokines,” *Scientific Reports*, vol. 8, no. 1, pp. 3101–3113, 2018.
- [31] Y. Liu, L. Wang, T. Kikuri et al., “Mesenchymal stem cell-based tissue regeneration is governed by recipient T lymphocytes via IFN- γ and TNF- α ,” *Nature Medicine*, vol. 17, no. 12, pp. 1594–1601, 2011.

- [32] M. N. Weitzmann and R. Pacifici, "The role of T lymphocytes in bone metabolism," *Immunological Reviews*, vol. 208, no. 1, pp. 154–168, 2005.
- [33] M. Croes, F. C. Öner, D. van Neerven et al., "Proinflammatory T cells and IL-17 stimulate osteoblast differentiation," *Bone*, vol. 84, pp. 262–270, 2016.
- [34] M. C. Phipps, Y. H. Huang, R. Yamaguchi et al., "In vivo monitoring of activated macrophages and neutrophils in response to ischemic osteonecrosis in a mouse model," *Journal of Orthopaedic Research*, vol. 34, no. 2, pp. 307–313, 2016.
- [35] C. Guder, S. Gravius, C. Burger, D. C. Wirtz, and F. A. Schildberg, "Osteoimmunology: a current update of the interplay between bone and the immune system," *Frontiers in Immunology*, vol. 11, p. 58, 2020.
- [36] H. Takayanagi, K. Ogasawara, S. Hida et al., "T-cell-mediated regulation of osteoclastogenesis by signalling cross-talk between RANKL and IFN- γ ," *Nature*, vol. 408, no. 6812, pp. 600–605, 2000.
- [37] H. Zhang, F. Xiao, Y. Liu, D. Zhao, Y. Shan, and Y. Jiang, "A higher frequency of peripheral blood activated B cells in patients with non-traumatic osteonecrosis of the femoral head," *International Immunopharmacology*, vol. 20, no. 1, pp. 95–100, 2014.